Dario Schalla

Fourth generation neutrinos and neutrino induced hadron production in the resonance region

Fourth generation neutrinos and neutrino induced hadron production in the resonance region

Dissertation
zur Erlangung des Grades eines
Doktors der Naturwissenschaften
der Fakultät Physik
der Technischen Universität Dortmund

technische universität
dortmund

vorgelegt von
Dario Schalla

Januar 2013

1. Gutachter: Prof. Dr. H. Päs
2. Gutachter: Prof. Dr. E. A. Paschos
Tag der mündlichen Prüfung: 1. März 2013
Vorsitzender des Promotionsausschusses: Prof. Dr. T. Weis

All work presented in this document is the author's own work, unless stated otherwise. This includes passages written by the author as well as results which have previously been published in the following articles:

- A. Lenz, H. Pas, and D. Schalla, *Fourth Generation Majorana Neutrinos*, *Phys. Rev. D 85,* **075025** (2012) arXiv:1104.2465.
- S. Hollenberg, H. Pas, and D. Schalla, *Baryon asymmetry of the universe and new neutrino states*, arXiv:1110.0948.
- E. Paschos and D. Schalla, *Neutrino production of hadrons at low energy and in the small Q^2 region*, *Phys.Rev.* **D84** (2011) 013004, arXiv:1102.4466.
- E. Paschos and D. Schalla, *Pion production by neutrinos in the delta resonance region and possible application to CP searches*, arXiv:1209.4219.
- E. Paschos and D. Schalla, *Neutrino-induced pion production at low energies and in the small Q^2 region*, arXiv:1212.4662.

Been Dazed and Confused for so long it's not true.

– Led Zeppelin [1]

Zusammenfassung

Wir untersuchen zwei Aspekte der Neutrinophysik. Zunächst betrachten wir die Erweiterung des Standardmodells durch eine vierte Generation von Fermionen. Wir erlauben eine endliche Mischung des zusätzlichen Neutrinos, welches möglichst allgemein mit Majoranamasse gehalten wird, und leiten durch dessen Beitrag zum neutrinolosen Doppelbetazerfall Beschränkungen für die Größe der Majoranamasse her. Dies legt fest, dass das Neutrino ein pseudo-Dirac Teilchen sein muss. Die Auswirkungen auf die Leptonenzahl verletzende Prozesse werden diskutiert. Nach einer Beschränkung der Elemente der Mischungsmatrix durch radiative Zerfälle geladener Leptonen präsentieren wir ein Model mit Extradimensionen, welches die horizontale Hierarchie der Neutrinomassen abschwächt. Anschließend untersuchen wir die Konsequenzen des Neutrinos für die Baryogenese, wo eine ähnliche Grenze für die Majoranamasse abgeleitet wird, indem der Auswascheffekt für Baryon- oder Leptonenasymmetrien abgeschätzt wird. Das zweite Thema ist die Produktion von Pionen durch Neutrino-Nukleon Wechselwirkungen durch die Erzeugung von Resonanzen. Für diesen Prozeß werden verschiedene Wirkungsquerschnitte, inklusive nuklearer Korrekturen und Pionenspektren, berechnet und eine Anwendung für CP Suchen vorgeschlagen.

Abstract

We investigate two aspects in neutrino physics. First, we consider the extension of the standard model by a fourth fermion generation. Allowing finite mixing of the additional neutrino, which is kept most general with a Majorana mass term, constraints on the size of its Majorana mass are derived by its contribution in neutrinoless double beta decay. This determines the neutrino to be a pseudo-Dirac particle and implications for lepton number violating processes are discussed. After constraining the mixing matrix elements by radiative charged lepton decays we present an extradimensional model for softening the horizontal neutrino mass hierarchy. Then we study the consequences of the neutrino in baryogenesis, where a similar bound on the Majorana mass is obtained by estimating the washout effect on any baryon- or lepton-asymmetry. The second topic is the production of pions by neutrino-nucleon interactions via resonances. For this process various cross sections, including nuclear corrections and pion spectra, are calculated and possible applications to CP searches are proposed.

Contents

1. Introduction

The two topics covered in this dissertation, namely fourth generation Majorana neutrinos and pion production by neutrino-nucleon interactions, belong to the large field of neutrino physics that now has come from its *Golden Age* of first discoveries of new fundamental neutrino properties to its *Precision Era*, where observables get determined more and more accurate allowing first tests of neutrino models and model building in general. However, neutrinos still remain a puzzle in elementary particle physics, although there has been large progress since its first years of postulation and discovery.

In 1914 Chadwick found the electron energy spectrum in the beta decay of radium to be continuous [2]. As the only known elementary particles constituting the atom were the proton and the electron at this time, a discrete spectrum for the emitted electron was expected and had already been observed in nuclear alpha and gamma decays. The observed continuous spectrum hinted at either a violation of the conservation of energy, or shortcomings of the nuclear theory. However, another possible explanation was given by Wolfgang Pauli in his famous, but informal, letter to the *Gruppe der Radioaktiven* [3, 4]. He proposed the existence of an additional particle, called *neutron*, that should be a spin-$\frac{1}{2}$ particle, electrically neutral and very light. Later, Fermi renamed this particle to *neutrino* [5, 6], after the massive neutron had been found to be a constituent of nuclei by Chadwick in 1932 [7, 8]. It took decades before, in 1956, Cowan and Reines finally detected the free neutrino [9].

Up to this time there was only one kind of neutrino ν and its antiparticle $\overline{\nu}$. The decay of the muon $\mu^- \to e^- \overline{\nu} \nu$ raised the question why the two final state neutrinos do not annihilate. In 1959 Pontecorvo proposed that the two neutrinos are different particles [10] and associated them with the two lepton flavors. The muon neutrino was experimentally discovered in 1962 by Schwartz, Lederman and Steinberger [11]. Finally, in 1975, the third charged lepton generation, the tau, was detected by Perl [12] and, consequently, the tau neutrino got postulated and, finally, discovered in 2000 by the DONUT* collaboration [13].

No further generations have been observed, directly or indirectly, so far.

*For explicit names of experiments and collaborations see list of acronyms.

However, a fourth generation of fermions is not excluded and its discovery would yield new insights into the underlying theories of elementary particle physics.

In 1998 the Super-K collaboration announced the first evidence of neutrino oscillations [14]. This experiment measures the flux of electron- and muon neutrinos produced in hadronic showers caused by cosmic rays in the upper atmosphere. This is done by observing charged current neutrino interactions with nuclei within the underground detector. It was found that the number of detected neutrinos was smaller than theoretical predicted. However, this deficit can be explained when considering one neutrino flavor oscillating into another flavor that cannot be measured. This is only possible if there is a mass difference between these two flavors, indicating the fist evidence of nonzero neutrino masses. Two years later, the missing neutrinos actually were identified with the tau neutrino [15].

Besides atmospheric neutrino oscillations, the interactions of neutrinos originating from the sun were measured at the SNO. In 2001 evidence of non-electron flavor neutrinos in these solar neutrinos was announced [16] and confirmed in 2002 [17,18].

The KamLAND, in 2004, was the first detector to measure anti-electron neutrino disappearance [19] in neutrinos coming from nuclear reactors. This evidence combined with the solar data yielded the first precise determination of neutrino oscillation parameters like the mass difference of the neutrinos and their mixing angle.

After these experiments, that consisted of only one detector, the era of long-baseline experiments began. For this type the neutrino source is either a reactor or an accelerator. As the oscillation probability depends on the neutrino energy and the propagated distance, it became necessary to measure the neutrino fluxes of the same source at different distances, confirming the theory of neutrino oscillations to a high degree. Today there are many long baseline experiments working on precision measurements of oscillation observables such as mixing angles and mass differences: MINOS, NOνA, MINERνA, K2K, T2K, OPERA, MiniBooNE, SciBooNE and many more.

For a long time one particular mixing angle, θ_{13}, had not been measured and its bounds were compatible with zero. However, the two recent experiments Daya Bay [20] and later on RENO [21] were finally able to determine the last missing value of all mixing angles.

In addition to these parameters, open questions in neutrino experimental physics remain, for example the absolute mass scale, which is tackled by nuclear beta decay experiments such as KATRIN and neutrinoless double beta decay experiments such as GERDA and NEMO. The latter experiments are also capable of answering the question whether neutrinos are their own antiparticles or not.

This dissertation addresses two issues in the framework of neutrino physics depicted above.

In chapter 2 the basic idea of an additional sequential fermion generation is introduced. Here, after a brief definition of notation and underlying theoretical principles, the broad landscape of fourth generation fermions is summarized. Thereby, special emphasis is laid on the neutral lepton for which we point out existing constraints from various analyses.

Chapter 3 deals with the special case of Majorana neutrinos. Herein the effect of nonvanishing mixing of the fourth generation with the first three generations is studied and compared with experimental data, implying constraints on the Majorana mass of this neutrino. Additionally, the phenomenological impact of these constraints is discussed as well as a model is presented which sheds light on the neutrino mass hierarchy between the first three and the fourth generation.

A similar constraint for Majorana neutrinos is obtained in chapter 4. Independently from the analysis in chapter 3, we find the same statement by investigating the evolution of the baryon asymmetry of the universe with additional neutrinos, for example a fourth generation or sterile neutrinos, introducing their potentially dangerous lepton number violating effects.

The second topic of this dissertation is the determination of the cross section for pion production by neutrinos that scatter on a nuclear target. This reaction is crucial for long baseline experiments in order to determine the neutrino fluxes accurately. As neutrino physics has entered an era of precision measurements, the errors within theoretical models have to be lowered to find deviations from the simple three flavor oscillation scenario, such as active-sterile oscillations or a violation of charge and partity symmetry. The reaction considered is dominated by the production of the delta resonance. Therefore, in chapter 5, a model for low momentum transfers is derived, that enhances existing form factor based models by introducing a parameter-free cross section for the axial current contribution. For this model, isospin rotations and nuclear effects within the target are discussed as well as expected spectra of the produced pions. Also an application for searches of the charge and parity violating phase in the lepton sector is proposed

In chapter 6 we conclude and summarize the findings of this dissertation.

2. A fourth fermion generation

Theoretical particle physics has flourished since the standard model (SM) has been established in terms of the Glashow-Weinberg-Salam model [22] and by today there are countless extensions of the SM, such as supersymmetry and theories with an extended gauge or scalar sector. However elaborate such theories are, they suffer from the fact, that numerous new parameters have to be introduced for explaining the new particle masses as well as new interactions. Besides these theories, one of the most simplest and straight forward extensions of the standard model is still alive but seldom considered: an additional, sequential fourth fermion generation. By this we mean the that the common standard model with three generations (SM3) is accompanied by a fourth generation without any change of the gauge sector and keeping the particle multiplets ordered as usual.

Thus we define the fermion content of the standard model with four generations (SM4) as follows:

$$\begin{aligned}
&\text{1st generation}: && \begin{pmatrix} u \\ d \end{pmatrix}_L, && u_R, && d_R, && \begin{pmatrix} \nu_e \\ e^- \end{pmatrix}_L, && e^-_R, && \nu_{e,R} \\
&\text{2nd generation}: && \begin{pmatrix} c \\ s \end{pmatrix}_L, && c_R, && s_R, && \begin{pmatrix} \nu_\mu \\ \mu^- \end{pmatrix}_L, && \mu^-_R, && \nu_{\mu,R} \\
&\text{3rd generation}: && \begin{pmatrix} t \\ b \end{pmatrix}_L, && t_R, && b_R, && \begin{pmatrix} \nu_\tau \\ \tau^- \end{pmatrix}_L, && \tau^-_R, && \nu_{\tau,R} \\
&\text{4th generation}: && \begin{pmatrix} t' \\ b' \end{pmatrix}_L, && t'_R, && b'_R, && \begin{pmatrix} \nu_4 \\ l^-_4 \end{pmatrix}_L, && l^-_{4,R}, && \nu_{4,R}.
\end{aligned} \tag{2.1}$$

Here we also introduced one right handed neutrino for each generation in order to construct Majorana neutrinos and keeping the model as general as possible.

In fact, the SM4 has become rather popular, see e. g. [23–25]. Especially several issues in flavor physics of the SM3 can be cured or at least softened by the SM4 (see, for example, [26–31] and [32,33] for some early work).

For example, the SM3 fails to describe both the B_d and B_s mixings

by 3.8 standard deviations [34], although the Cabibbo-Kobayashi-Maskawa (CKM) picture [35, 36] has been shown enormous success in particle physics.

Furthermore, a measurement of the D0 collaboration [37, 38] of the dimuon asymmetry which was a factor of 42 larger than the SM3 result [39, 40] with a statistical significance of 3.2 standard deviations could be enhanced by the SM4, although not completely explained [31].

In the following sections we will briefly address several topics involving a fourth fermion generation by surveying the landscape of SM4 physics.

2.1 Invisible Z decay width

The most stringent bound on the number of neutrino generations N_ν is given by the decay width of the Z boson measured at the Standford Linear Collider (SLC) and Large Electron-Positron storage ring (LEP). A combined analysis [41] of all collaborations involved at these measurements addressed the issue of neutrino generations as follows. The Z particle is produced as a resonance in electron-positron collisions. The width Γ_Z of its subsequent decay is given by

$$\Gamma_Z = \Gamma_{\ell\ell} + \Gamma_{\nu\nu} + \Gamma_{had}, \tag{2.2}$$

where $\Gamma_{\ell\ell}$ is the partial decay width to charged lepton pairs and Γ_{had} the partial decay width to hadronic final states. Assuming lepton universality these two parts are known. The solely free parameter is the number of neutrino generations within the partial decay width $\Gamma_{\nu\nu}$, the invisible decay width of the Z, meaning the production of neutrino pairs. Figure 2.1 shows the experimental data in comparison with the theoretical predictions of two, three and four neutrino generations. The best fit of the data is given for

$$N_\nu = 2.984 \pm 0.008 \tag{2.3}$$

neutrino generations. However stringent this constraint appears, there is still the possibility for further neutrino generations. At the decay of the Z boson only particles with an invariant mass smaller than the mass of the Z can be created. For neutrino pair production this means that only neutrinos with a mass smaller than half the Z boson mass m_Z contribute to the decay width. If there is a neutrino with a mass m_N large enough to obey

$$m_N > \frac{m_Z}{2} \approx 45.6\,\mathrm{GeV} \tag{2.4}$$

it would be still in agreement with this data.

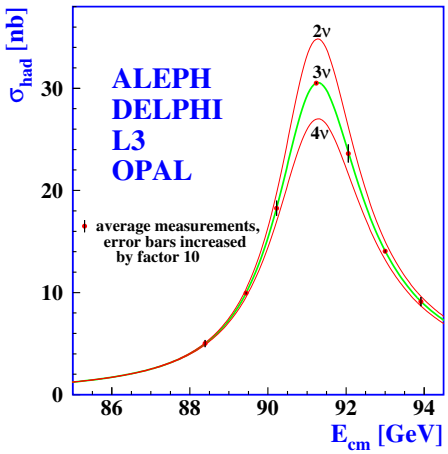

Figure 2.1: Fit of the Z boson decay width for two, three and four light neutrino generations. Taken from [41].

2.2 Higgs mass and DSB

As the LHC experiments ATLAS and CMS have announced [42,43] the discovery of a new boson with $m_h \sim 125\,\text{GeV}$ being compatible with the long sought Higgs boson, some of the advantages of the four generation (4G) scenario turned into conflicts. Before this discovery there was some tension of the Higgs mass bounds that were softened in a 4G framework [44–48].

Considering the simplest scenario with one Higgs particle, the new discovery prefers the SM3 in terms of an p-value analysis [49] due to its small mass. The SM4 remains compatible albeit unlikely. However, the SM4 now prefers the two Higgs doublet model [50].

The reason is that in such theories electroweak symmetry breaking (EWSB) is driven by the condensation of the fourth generation quarks [51, 52]. Such scalar condensates of heavy fermions, including all fourth generation fermions as well as the heavy top quark, result in a multiple composite Higgs spectrum [53,54]. The lightest composite Higgs can be associated with the observed boson and additional can be pushed outside of experimental reach. If the heavy Higgses decouple the theory effectively reduces to a two Higgs doublet model [55].

For further details on these strong dynamic effects see [56,57] and on the development of dynamical symmetry breaking (DSB) scenarios [54,58–65].

2.3 Electroweak and flavor constraints

A great effort has been made to trace the fourth generation fermions in existing electroweak precision [44,45,66–72] and flavor data [73–78]. Especially the quark sector has gotten heavily constrained. We will exemplify

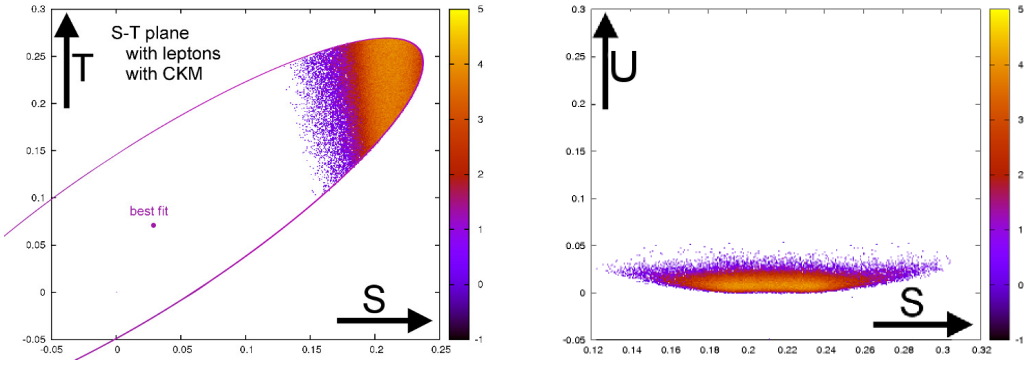

(a) *S-T* plane (b) *S-U* plane

Figure 2.2: Fits of electroweak parameters taken from [71]. The Higgs mass was assumed to be 117 GeV.

these studies by sketching the findings of [71].

First, the current experimental bounds on charged weak decays and flavor changing neutral currents (FCNC) are used to determine CKM matrix elements. In contrast to the SM3 CKM matrix, the introduction of an additional generation also introduces three new mixing angles and two new charge and parity (CP) phases into the CKM matrix.

Second, the oblique electroweak parameters U, S and T, the Peskin-Takeuchi parameters [79,80], are investigated. They measure the impact of new physics by its contributions to radiative corrections of gauge bosons. For the SM3 they are all chosen to be zero and beyond the standard model physics in general is only allowed to cause slight deviations from this to reproduce the SM3 as the effective theory observed and remarkably confirmed. The parameters themselves are defined as combinations of weak gauge boson self energies and are, therefore, directly linked with gauge couplings. In figure 2.2 we show again two fits of these parameters from [71].

After adding constraints from FCNCs, the results for the new mixing angles are:

$$\theta_{14} < 0.0535 \tag{2.5}$$
$$\theta_{24} < 0.121 \tag{2.6}$$
$$\theta_{34} < 0.35. \tag{2.7}$$

Analyses investigating the 4G mass spectrum are depending on the underlying Higgs model. A recent analysis [81] determined the probability densities in both one Higgs and two Higgs models. The mass splitting between the 4G quarks is found to be less than the mass of the W boson. For the two Higgs model smaller values are preferred. In figure 2.3 we show the density plots of [81] for the now preferred two Higgs model. Interest-

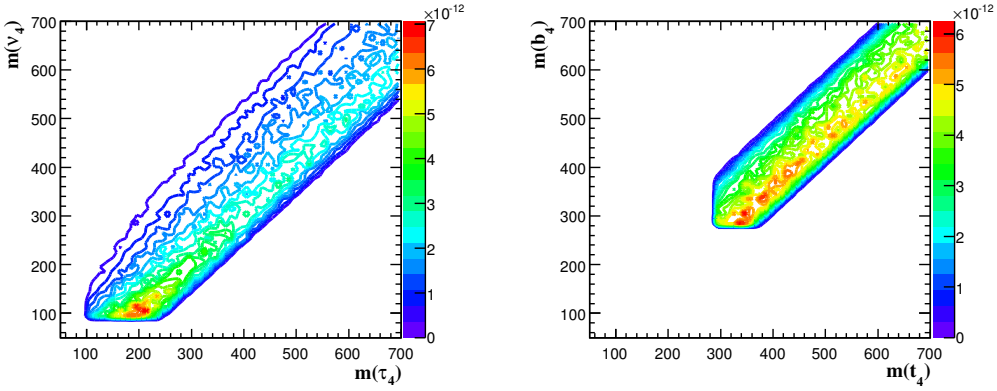

Figure 2.3: Density distributions for 4G fermion masses taken from [81].

ingly the charged lepton τ_4 probability peaks near the experimental bound, making it the best candidate for discovery.

2.4 CP violation and EWPT

The introduction of a fourth fermion generation offers also enhancements in the field of CP violation in the quark sector [82, 83]. A CP violation can, principally, explain electroweak baryogenesis. However, the measure of CP violation within the SM3 is too small to explain the observed baryon to photon ratio in our universe. To explain the enhancement by the SM4 we repeat the argumentation of [83]. As measure for CP violation in the SM3 we take the Jarlskog invariant CP violation measure given by:

$$J_{\mathrm{SM3}} = \left(m_t^2 - m_u^2\right)\left(m_t^2 - m_c^2\right)\left(m_c^2 - m_u^2\right) \times \left(m_b^2 - m_d^2\right)\left(m_b^2 - m_s^2\right)\left(m_s^2 - m_d^2\right) \times A_{\mathrm{SM3}} \quad (2.8)$$

with $A_{\mathrm{SM3}} \approx 3 \cdot 10^{-5}$. The baryon to photon ratio is of the order of 10^{-9}. For comparison, one has to normalize the Jarlskog invariant by the temperature of the electroweak phase transition (EWPT):

$$R_{\mathrm{SM3}} = \frac{J_{\mathrm{SM3}}}{T_{\mathrm{EW}}^{12}} \approx 10^{-20} \quad (2.9)$$

which is ten to eleven orders of magnitude too small. The resulting number is so small because of the small quark masses compared to $T_{\mathrm{EW}} \sim 100\,\mathrm{GeV}$. At this point the difference arises when considering the SM4, which intro-

duces two new heavy quarks into the Jarlskog invariant:

$$J_{\mathrm{SM4}} = \left(m_{t'}^2 - m_c^2\right)\left(m_{t'}^2 - m_t^2\right)\left(m_t^2 - m_c^2\right) \times \left(m_{b'}^2 - m_s^2\right)\left(m_{b'}^2 - m_b^2\right)\left(m_b^2 - m_s^2\right) \times A_{\mathrm{SM4}}. \quad (2.10)$$

The larger quark masses can increase the ratio R_{SM3} by approximately 15 orders of magnitude and thus permitting CP violation which is capable of generating the observed baryon to photon ratio and, therefore, a successful baryogenesis.

In addition also the strength of the phase transition might be increased in a SM4 framework [84–86] which is also enhancing electroweak baryogenesis scenarios by creating the necessary out-of-equilibrium condition.

2.5 Gauge coupling unification

One of the advantages of SM4 in the pre-Higgs era was the potential of gauge coupling unification without supersymmetry. Despite a problem with arising Landau poles below the scale of grand unified theories (GUT) and, therefore, nonpertubative Yukawa couplings, the introduction of heavy fermions can lead to a successful gauge coupling unification [87]. However, this analysis assumed a large Higgs mass of $m_H > 174\,\mathrm{GeV}$ and may change in respect of the boson discovery at the LHC. Especially, the Landau poles are now at higher energies, curing the basic difficulty of this topic. The evolution of the couplings with the discovered boson mass has not been carried out, yet.

2.6 Lepton sector

In contrast to the quark sector, the lepton sector of the SM4 has gained more interest in the last years [88–97]. The particle data group (PDG) [98] gives the following experimental bounds on the fourth generation charged lepton mass m_{ℓ_4}:

$$m_{\ell_4} > 100.8\,\mathrm{GeV}\ \text{(charged lepton)} \quad (2.11)$$

$$m_{\ell_4} > 102.6\,\mathrm{GeV}\ \text{(stable charged heavy lepton)}. \quad (2.12)$$

For the fourth generation neutrino mass m_4 it gives:

$$m_4 > 45\,\mathrm{GeV}\,(39.5\,\mathrm{GeV})\ \text{(stable Dirac (Majorana) neutrino)} \quad (2.13)$$

$$m_4 > 90.3\,\mathrm{GeV}\,(80.5\,\mathrm{GeV})\ \text{(unstable Dirac (Majorana) neutrino)}. \quad (2.14)$$

Dirac type neutrinos differ slightly from Majorana type neutrinos due to different couplings to the SM3. Stable neutrinos can be lighter because if

they do not decay within the detectors they cannot be identified. We will use the bound for stable neutrinos in the next chapter, which coincides with the invisible Z decay width of section 2.1.

The analysis [71] mentioned above also gives bounds on the mass splittings of the leptons:

$$\left|m_{\ell_4} - m_4\right| < 140\,\text{GeV}. \tag{2.15}$$

In typical seesaw models (see section 3.4 for details), the Dirac mass of the additional neutrino m_{D4} gives the upper bound of the light neutrino mass eigenstate. In order to stay within the perturbative regime the Dirac mass shall not exceed the electroweak scale. Therefore, taking into account the bound from equation (2.4), the Dirac mass is given in the range

$$45\,\text{GeV} \leq m_{D4} \leq 1000\,\text{GeV}. \tag{2.16}$$

Radiative contributions to the light neutrinos induced by the additional fourth generation neutrino may exceed the mass bounds on neutrinos from cosmology, tritium beta decay and neutrinoless double beta decay. The two-loop contribution (see figure 2.4) has more stringent bounds by cosmology than by neutrinoless double beta decay as discussed in the next chapter. For a discussion of fourth generation induced loop effects on light neutrinos we refer to [99, 100] and the recent papers [96, 101]. We will restrict ourselves to neutrinoless double beta decay, as the cosmological bound suffers from large systematic uncertainties.

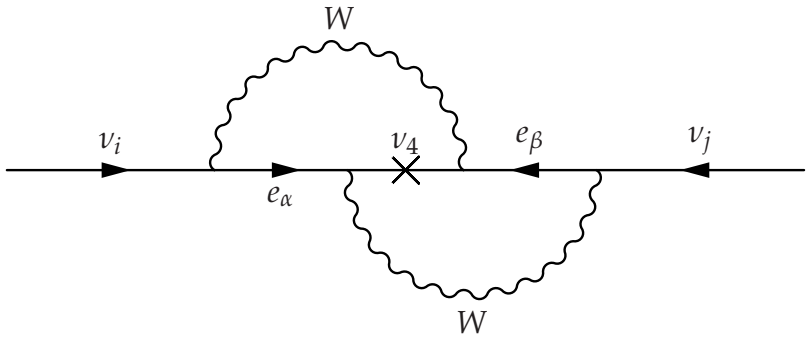

Figure 2.4: Feynman diagram of the radiative two-loop contribution to the light neutrino masses.

One of the basic assumption of the analyses in the following chapters concerns the mixing of the fourth generation neutrino to the SM3. We start by a partial fit of the Pontecorvo-Maki-Nakagawa-Sakata (PMNS) mixing matrix to a set of experimental data in the SM4 framework, which provides a hint for a nonzero admixture of a fourth generation neutrino to the

electron at 2σ confidence level [102]. The bounds on the additional PMNS matrix elements are:

$$U = \begin{pmatrix} * & * & * & \begin{smallmatrix} <0.089 \\ >0.021 \end{smallmatrix} \\ * & * & * & < 0.029 \\ * & * & * & < 0.085 \\ < 0.115 & < 0.115 & < 0.115 & \begin{smallmatrix} <0.9998 \\ >0.9934 \end{smallmatrix} \end{pmatrix}. \tag{2.17}$$

These bounds have changed due to new experimental data since the original publication [102] and the matrix element U_{e4} is now compatible with zero at 2σ-level [103]. However, the central value is now at $U_{e4} = 0.044$ with $0.015 < U_{e4} < 0.060$ at 1σ-level. Therefore, our assumption of finite mixing U_{e4} remains well motivated. As the new fit values are not published or elsewhere validated we use the results of [102] given in equation (2.17). The following chapter studies the implications of this nonvanishing matrix element and does not rely on the exact value of this mixing element as it provides order of magnitude estimations. Small changes of the value do not lead to significant changes of the results and conclusions.

3. Constraining the fourth generation neutrino

In this chapter several bounds on the possible Majorana nature of a fourth sequential generation will be derived. As mentioned in the previous section, a fit [102] of the neutrino mixing matrix to electroweak observables leads to the following bound on the mixing element U_{e4}:

$$0.021 < U_{e4} < 0.089. \tag{3.1}$$

Note, that this bound changes with new experimental data. For example, the new bound on radiative charged lepton decays reduces the level of significance. However, the central value at $U_{e4} = 0.044$ remains larger than zero within the 1σ significance level ($0.015 < U_{e4} < 0.060$) [103]. As this new estimate is not validated, we will use the published bounds given in equation (3.1) for our analysis. The exact value of the mixing matrix element is not of importance as the results do not change significantly with small deviations. We will assume this nonzero mixing and consider its implications on the Majorana mass of the fourth generation neutrino by investigating its lepton number violating effects.

The findings of this chapter have been published as [104]

A. Lenz, H. Päs and D. Schalla
Fourth Generation Majorana Neutrinos
Physical Review D85 (2012) 075025, arXiv:1104.2465

and, in an earlier version, in the conference prodceedings [105] of the 16th International Symposium on Particles, Strings and Cosmology 2010 (PASCOS2010) in València, Spain

A. Lenz, H. Päs and D. Schalla
Constraints on fourth generation Majorana neutrinos
Journal of Physics: Conference Series 259 (2010) 012096, arXiv:1010.3883 .

3.1 Neutrinoless double beta decay

The radioactive beta decay of a neutron $n \to pe^-\overline{\nu}_e$ is a common process that is a direct consequence of the Fermi theory of weak interactions. The

simultaneous decay of two seperate neutrons within a single nucleus is called double beta decay. As the single beta decay generally occurs more frequent, the double beta decay signal cannot be measured in most cases. However, for some nuclei the single beta decay is forbidden but the double beta decay allowed. For example for germanium-76, the single beta decay to arsenic-76 is energetically forbidden, but the direct decay to selenium-76 allowed and, therefore, principally measurable. In the SM, there are two types of double beta decays that differ in the number of emitted neutrinos.

The first and more frequent occurring possibility is the independent decay of two neutrons into two protons, two electrons and two anti-electron neutrinos in the final state. This is the two neutrino double beta decay ($2\nu\beta\beta$) whose Feynman diagram is shown in figure 3.1(a). Due to the evading neutrinos the final electrons are distributed in a broad spectrum. For instance, the EXO Collaboration has measured the $2\nu\beta\beta$ half-life time of ^{136}Xe to be $T_{1/2} = 2.11 \cdot 10^{21}$ yr [106]. As it is allowed in the SM, it does not yield any specific new information on neutrino properties but can help to determine and check hadronic models for obtaining nuclear matrix elements (NME) that are crucial for calculating double beta decay half-life. Part of the information contained in the NMEs for $2\nu\beta\beta$ can be related to the second type of double beta decay [107, 108].

In this second process, namely neutrinoless double beta decay ($0\nu\beta\beta$) depicted in figure 3.1(b), there are no final state neutrinos. Instead of escaping, the neutrino emitted within the decay of one neutron is also interacting with the second neutron thus becoming an intermediate state. As in this case no energy is carried away as missing energy, the final state energy spectrum is a discrete line. Connecting the two vertices with one neutrino requires a flip of its spin which is only possible if the neutrino has nonzero mass. Furthermore, it has been shown [109] that in gauge theories any mechanism that can mediate the $0\nu\beta\beta$ must contain a Majorana mass term.

The light neutrino exchange, depicted in figure 3.1(b), is the only SM allowed $0\nu\beta\beta$ mechanism and therefore, if observed, would imply neutrinos to be Majorana particles. Models with an enlarged particle content such as supersymmetry or majoron models, are, in principle, capable of triggering $0\nu\beta\beta$ but will not be discussed here.

The typical half-life time of $0\nu\beta\beta$ is even larger than that of $2\nu\beta\beta$ and it has not been detected, yet. It is not allowed in the SM as a Majorana mass for the neutrinos is required. The best lower bound of the half-life time for the neutrinoless double beta decay of germanium-76 is given by the IGEX collaboration [110]:

$$T_{1/2}^{\mathrm{Ge}} > 1.57 \cdot 10^{25}\,\mathrm{yr}. \tag{3.2}$$

First, we consider this process without neutrino mixing and thus only with one mass eigenstate m in the propagator. Following the calculation

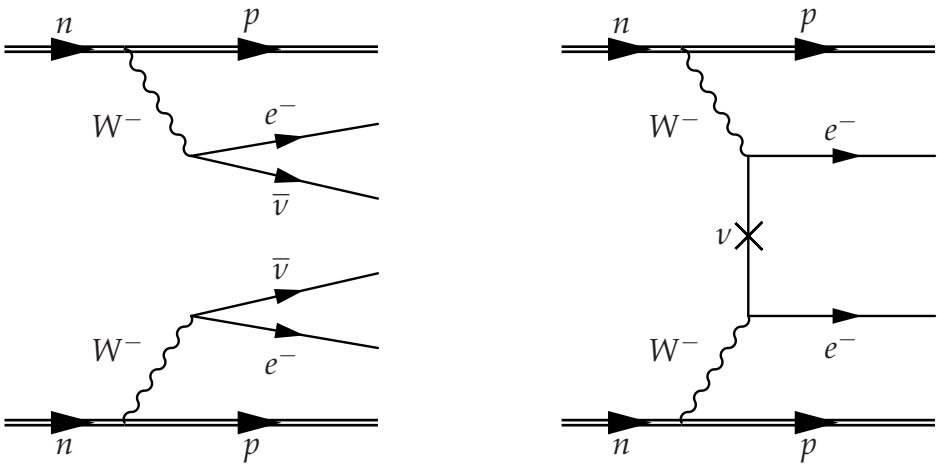

(a) $2\nu\beta\beta$ (b) $0\nu\beta\beta$

Figure 3.1: Feynman diagrams of double beta decay processes.

of the half-life time as sketched in [111], the leptonic tensor $M_{\mu\lambda}$ of the process in figure 3.1(b) is given by

$$M_{\mu\lambda} = \varphi^* \overline{u}_e \gamma_\mu \frac{1}{2}(1-\gamma_5) \frac{\not{q} + m}{q^2 - m^2} \gamma_\lambda \frac{1}{2}(1+\gamma_5) v_e. \tag{3.3}$$

Here φ is the phase factor of the propagator. The $\not{q}$ part vanishes due to Dirac algebra. The momentum transfer q of the neutrino is of the order of the typical Fermi momentum of the nucleus $q \sim \mathcal{O}(100\,\mathrm{MeV})$. As the neutrino masses considered in this simple case are all below 1 eV, the relevant observable is

$$M_{\mu\lambda} \propto \frac{m}{q^2 - m^2} \overset{q^2 \gg m^2}{\longrightarrow} M_{\mu\lambda} \propto m. \tag{3.4}$$

This provides a probe for the absolute neutrino mass.

Including neutrino mixing and using the notation of [112] the contribution of light neutrinos to the inverse $0\nu\beta\beta$ half-life time is then given by

$$\left[T^{0\nu\beta\beta}_{1/2}\right]^{-1} = \left(\frac{\langle m_\nu \rangle}{m_e}\right)^2 C^{LL}_{mm}, \tag{3.5}$$

where C^{LL}_{mm} is the combination of the NME and a phase space factor. Here the subscript m denotes the mass mediation and the superscript L the light neutrino contribution for both vertices. Those factors were calculated in [113, 114]. The observable $\langle m_\nu \rangle$, defined as

$$\langle m_\nu \rangle = \sum_\alpha U^2_{e\alpha} m^\nu_\alpha, \tag{3.6}$$

is the effective light neutrino mass including neutrino mixing. The electron neutrino produced at each vertex is a flavor eigenstate and consists of a superposition of all three light neutrino mass eigenstates. Each eigenstate m_α enters the calculation with the appropriate PMNS mixing matrix element $U_{e\alpha}$, where $\alpha = 1,2,3$ is the index of light ($m < 100\,\mathrm{MeV}$) neutrino mass eigenstates.

Considering the half-life bound in equation (3.2) this yields an effective neutrino mass of

$$\langle m_\nu \rangle \leq 3.7\,\mathrm{eV}. \tag{3.7}$$

Introducing a fourth generation with an additional Majorana neutrino changes this picture in a significant way: Not only the light neutrinos, but also the additional 4G heavy neutrino can mediate $0\nu\beta\beta$. As shown in the previous chapter, a fourth generation neutrino must be heavier than half of the Z-boson mass to avoid detection in the invisible Z-decay width. Thus for a heavy neutrino the matrix element in equation (3.4) is proportional to the inverse neutrino mass:

$$M_{\mu\lambda} \propto \frac{m}{q^2 - m^2} \overset{q^2 \ll m^2}{\longrightarrow} M_{\mu\lambda} \propto \frac{1}{m}. \tag{3.8}$$

Therefore, a second observable, the effective heavy neutrino mass, contributes also to the inverse half-life:

$$\left[T^{0\nu\beta\beta}_{1/2}\right]^{-1} = \left(\frac{\langle m_\nu \rangle}{m_e}\right)^2 C^{LL}_{mm} + \left(\frac{m_p}{\langle m_N \rangle}\right)^2 C^{NN}_{mm} + \left(\frac{\langle m_\nu \rangle}{m_e}\right)\left(\frac{m_p}{\langle m_N \rangle}\right) C^{NL}_{mm} \tag{3.9}$$

with

$$\langle m_N \rangle^{-1} = \sum_\beta U^2_{e\beta} (m^N_\beta)^{-1}, \tag{3.10}$$

where β counts all heavy ($> \mathcal{O}(100\,\mathrm{GeV})$) neutrino mass eigenstates. Note the presence of an interference term of light and heavy vertices.

The light neutrinos produce a long half-life ($\sim m^\nu_\alpha$) due to their masses being small. In contrast, the heavy neutrinos produce a long half-life ($\sim 1/m^N_\beta$) by being heavy. For the case of intermediate (MeV) scale neutrinos see [115], where a careful treatment of the fermion propagator leads to altered neutrino potentials. However, as there cannot be an active neutrino state in this intermediate regime, we can clearly associate the mass eigenstates to either light or heavy.

Assuming now a mixing of the fourth generation to the electron as indicated by [102] with the bounds of equation (3.1) and neglecting contributions of the light neutrinos ($\langle m_\nu \rangle = 0$) we are able to calculate the resulting

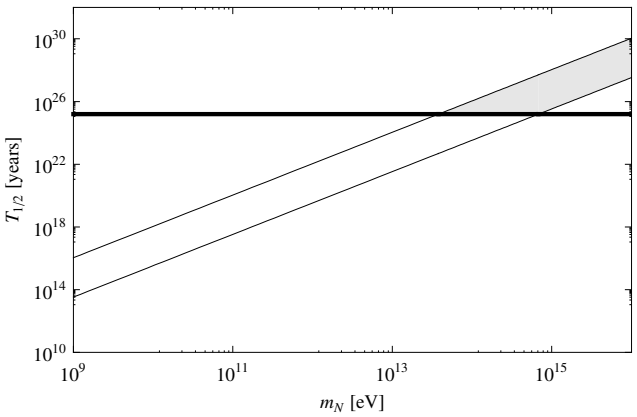

Figure 3.2: Contribution of a single heavy neutrino to the $0\nu\beta\beta$ half-life (thin lines) within the mixing region given by equation (3.1) and the IGEX lower bound (thick line). The gray area indicates the allowed region.

half-life as a function of the heavy neutrino mass eigenstate m_4. Figure 3.2 shows this dependence in comparison with the experimental bound given by the IGEX experiment.

Thereby, using the mixing elements from equation (3.1), we find the following mass bounds on the fourth heavy mass eigenstate m_4:

$$U_{e4}^{max} = 0.089 \;\Rightarrow\; m_4 \geq 6.8 \cdot 10^5\,\mathrm{GeV} \tag{3.11}$$

$$U_{e4}^{min} = 0.021 \;\Rightarrow\; m_4 \geq 3.8 \cdot 10^4\,\mathrm{GeV}. \tag{3.12}$$

The mass is found to be larger than $\mathcal{O}(10\,\mathrm{TeV})$ which is in contradiction to equation (2.16) that constrains the light additional mass eigenstate to be less than 1 TeV.

This $0\nu\beta\beta$ bound can be loosened by considering the contribution of the light neutrinos canceling the heavy neutrino contribution due to relative phases. To investigate the impact of such phases (α, β) we introduce the following notation:

$$\langle m_\nu \rangle \Rightarrow \mathrm{e}^{i\alpha} \langle m_\nu \rangle \tag{3.13}$$

$$\langle m_N \rangle^{-1} \Rightarrow \mathrm{e}^{i\beta} \langle m_N \rangle^{-1}. \tag{3.14}$$

The cancellation is maximal for opposite phases and large light neutrino masses. Thus for light neutrino masses we use a quasi-degenerate spectrum with the maximum neutrino mass limit given by the large scale structure (LSS) of the universe given by [116]:

$$\sum m_\nu < 0.66\,\mathrm{eV} \tag{3.15}$$

and consider mass splittings as obtained by neutrino oscillation experiments [117]. This partial cancellation of the $0\nu\beta\beta$ amplitude yields the

following reduced mass bounds to be compared with equation (3.11):

$$U_{e4}^{max} = 0.089 \;\Rightarrow\; m_4 \geq 4.5 \cdot 10^5\,\text{GeV} \tag{3.16}$$

$$U_{e4}^{min} = 0.021 \;\Rightarrow\; m_4 \geq 2.5 \cdot 10^4\,\text{GeV}. \tag{3.17}$$

The light neutrino contribution is capable of reducing the mass bound within one order of magnitude, whereas several orders of magnitude are required to match the desired mass range.

In general, there are three possibilities to save the idea of a fourth generation neutrino:

1. At least the fourth generation does not possess a Majorana mass term that may trigger $0\nu\beta\beta$. All neutrinos being Dirac particles would rule out several attractive features such as the seesaw mechanism for the light neutrino mass suppression and leptogenesis as an explanation for the baryon asymmetry of the universe. The 4G neutrino being the only Dirac particle would be an unnatural choice and against the idea of the sequential 4G scenario.

2. Some other, yet unknown, physics or particle contributes to $0\nu\beta\beta$ and cancels the heavy neutrino contribution. For a successful cancellation the new physics must be fine tuned to exactly match the heavy neutrino contribution without producing a signal on its own.

3. The heavy fourth generation neutrino is a pseudo-Dirac particle.

We will elaborate on the last alternative, as it is the simplest scenario without any further beyond the standard model physics. It also keeps the neutrino properties as general as possible by allowing a Majorana mass term.

A pseudo-Dirac neutrino [118,119] is the special case, where the Majorana mass of the neutrino is much smaller than its Dirac mass. Following the definitions of [120] we start with the one generation mass matrix $\mathcal{M}_\nu$ and its rotation by the rotation matrix $\mathcal{O}$ to the diagonal matrix $\mathcal{M}_d$:

$$\mathcal{M}_\nu = \mathcal{O}\mathcal{M}_d\mathcal{S}\mathcal{O}. \tag{3.18}$$

Here $\mathcal{S}$ is a diagonal matrix containing the entries $s_i = \pm 1$ (assuming CP invariance) with $i = 1,2$ that ensures positive masses for the neutrinos. With an arbitrary choice of the rotation matrix this equation reads

$$\begin{pmatrix} 0 & m_D \\ m_D & M_R \end{pmatrix} = \begin{pmatrix} \cos\theta & \sin\theta \\ -\sin\theta & \cos\theta \end{pmatrix} \begin{pmatrix} m & 0 \\ 0 & M \end{pmatrix} \begin{pmatrix} s_1 & 0 \\ 0 & s_2 \end{pmatrix} \begin{pmatrix} \cos\theta & -\sin\theta \\ \sin\theta & \cos\theta \end{pmatrix} \tag{3.19}$$

where m (M) is the smaller (larger) mass eigenstate and, m_D the Dirac and M_R the right-handed Majorana mass. Note, that we neglect a possible left-handed Majorana mass, because we want to retain the idea of the seesaw

mechanism. The first matrix in this equation is the mass matrix in flavor space in the basis given by equation (3.53). It will be further explained in section 3.4.

The corresponding mixing angle θ between the two mass eigenstates is given by

$$\tan 2\theta = \frac{2m_D}{M_R}. \tag{3.20}$$

In general, both mass eigenstates propagate in $0\nu\beta\beta$ with their respective mixing and the leptonic tensor for the matrix element for $0\nu\beta\beta$ contains the term

$$\mathcal{M} \propto \frac{m}{q^2 - m^2} \cos^2\theta - \frac{M}{q^2 - M^2} \sin^2\theta. \tag{3.21}$$

The minus sign indicates that the two mass eigenstates have opposite creation phases.

In the common seesaw case [121–124], where $m_D \ll M_R$, the mixing is small:

$$m_D \ll M_R \qquad \Rightarrow \qquad \tan 2\theta \to 0 \qquad \theta \to 0. \tag{3.22}$$

As a result the heavy mass eigenstate M is almost decoupled and can be neglected in many cases. Only the light mass eigenstate m contributes to $0\nu\beta\beta$ which was used in equation (3.5). They are found to be

$$m = \frac{1}{2}\left(\sqrt{4m_D^2 + M_R^2} - M_R\right) \approx \frac{m_D^2}{M_R} \tag{3.23}$$

$$M = \frac{1}{2}\left(\sqrt{4m_D^2 + M_R^2} + M_R\right) \approx M_R + \frac{m_D^2}{M_R}. \tag{3.24}$$

In contrast to this, the pseudo-Dirac case $m_D \gg M_R$ leads to the mixing angle

$$m_D \gg M_R \qquad \Rightarrow \qquad \tan 2\theta \to \infty \qquad \theta \to \frac{\pi}{4} \tag{3.25}$$

yielding maximal mixing between the two mass eigenvalues

$$m = \frac{1}{2}\left(\sqrt{4m_D^2 + M_R^2} - M_R\right) \approx m_D - \frac{M_R}{2} \tag{3.26}$$

$$M = \frac{1}{2}\left(\sqrt{4m_D^2 + M_R^2} + M_R\right) \approx m_D + \frac{M_R}{2}. \tag{3.27}$$

The two corresponding eigenstates form one object and the matrix element reads

$$\mathcal{M} \propto \frac{1}{2}\left(\frac{m}{q^2 - m^2} - \frac{M}{q^2 - M^2}\right). \tag{3.28}$$

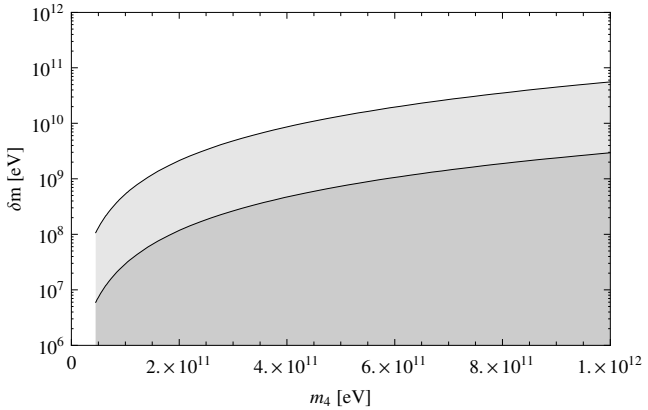

Figure 3.3: Maximal mass splitting δm for heavy pseudo-Dirac neutrinos. The upper (lower) curve corresponds to the lower (upper) bound on U_{e4} according to equation (3.1). The shaded area represents the allowed parameter space.

For a deeper discussion of the seesaw type-I mass model see section 3.4.

For the heavy fourth generation this modifies the half-life time for $0\nu\beta\beta$ to

$$\left[T_{1/2}^{0\nu\beta\beta}\right]^{-1} = \frac{1}{4}\left(\frac{m_p}{\langle m_4\rangle} - \frac{m_p}{\langle M_4\rangle}\right)^2 C_{mm}^{NN}. \tag{3.29}$$

Therefore, the contributions of the two different mass eigenstates partly cancel each other suppressing the cross section. The important quantity is the mass splitting δm of the two eigenstates

$$\delta m \equiv M - m = M_R. \tag{3.30}$$

For the Dirac case with vanishing Majorana mass the two terms in equation (3.29) cancel each other exactly affirming that this process is forbidden for Dirac neutrinos. Thus for small Majorana masses it is possible to avoid a signal in $0\nu\beta\beta$ due to a cancellation of the contribution of the two mass eigenstates m and M, even if the mass eigenstates themselves are in a mass region as required by equation (2.16). The Majorana mass may not exceed a certain value depending on the assumed PMNS matrix element and the neutrino mass itself. These allowed Majorana masses for neutrinos fulfilling equation (2.16) are shown in figure 3.3.

For the case $U_{e4} = 0.021$ we find the limits

$$m_4 = 45\,\text{GeV} \quad \Rightarrow \quad \delta m = 0.107\,\text{GeV} \tag{3.31}$$

$$m_4 = 1000\,\text{GeV} \quad \Rightarrow \quad \delta m = 56\,\text{GeV}. \tag{3.32}$$

As the ratio $\delta m/m_4$ is of the order of 10^{-3} to 10^{-2} the approximation of maximal mixing and the pseudo-Dirac nature is valid.

3.2 Like-sign dilepton production

The constraint on the Majorana mass of a fourth generation neutrino derived in the previous section has implications for any lepton number violating (LNV) processes triggered by this neutrino. Usually processes involving heavy neutrino propagators are derived with the assumption of only one mass eigenstate participating. We will exemplify the impact of the pseudo-Dirac nature by investigating the cross section of like-sign dilepton production (LSD) at hadron colliders:

$$pp \to \ell_1^+ \ell_2^+ X. \tag{3.33}$$

LSD is the analog of $0\nu\beta\beta$ at hadron colliders and thus contains the identical neutrino propagator as can be seen in its Feynman diagrams in figure 3.4.

According to [125] the cross section of LSD production mediated by a single heavy mass eigenstate is given by:

$$\sigma_{single}\left(pp \to \ell_1^+ \ell_2^+ X\right) = \frac{G_F^4 m_W^6}{8\pi^5}\left(1 - \frac{1}{2}\delta_{\ell_1\ell_2}\right)\left|U_{\ell_1 4} U_{\ell_2 4}\right|^2 F\left(E, m_4\right), \tag{3.34}$$

where $F\left(E, m_4\right)$ is a function of beam energy and the heavy neutrino mass but does not depend on mixing variables. It also contains the neutrino propagator in form of the subprocess $W^+W^+ \to \ell_1^+ \ell_2^+$, which has been taken from [126]. This unmodified cross section is illustrated in figure 3.5 for dielectron production mediated by a heavy Majorana neutrino obeying the U_{e4} bound of equation (3.1). In our computation we use Martin-Stirling-Thorne-Watt (MSTW) parton distributions [127].

In contrast to $0\nu\beta\beta$, where the average momentum is much smaller than the heavy neutrino mass, at hadron colliders the neutrino mass is smaller than the average energy. Thus the approximate propagator for pseudo-Dirac neutrinos is now proportional to its mass (see equation (3.4)).

Therefore, we will modify the cross section σ_{single} by introducing a pseudo-Dirac correction factor Δ_{pD} to obtain the pseudo-Dirac LSD cross

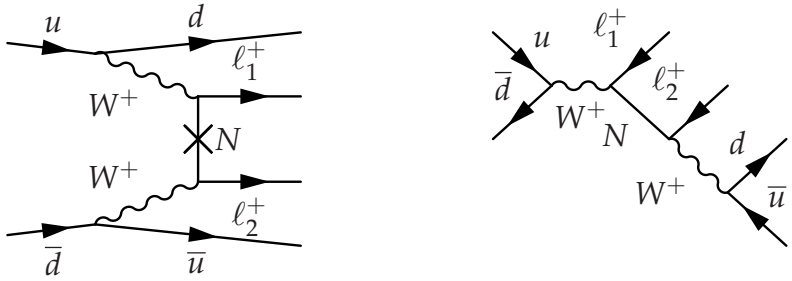

Figure 3.4: Feynman diagrams of LSD production.

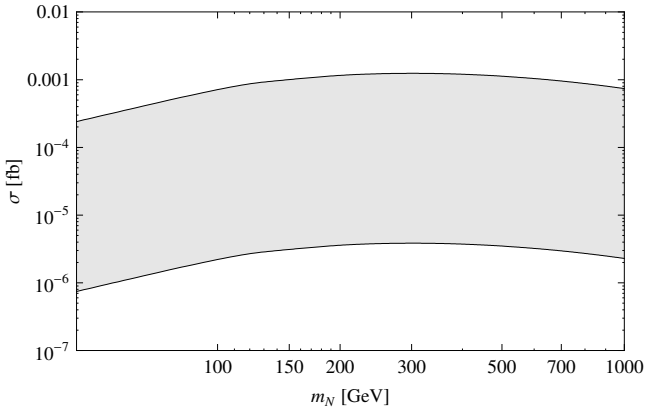

Figure 3.5: Cross section for like-sign dielectron production by an electroweak scale Majorana neutrino without $0\nu\beta\beta$ constraints. The shaded area corresponds to the allowed values of U_{e4} according to equation (3.1).

section:

$$\sigma = \Delta_{pD} \cdot \sigma_{single} \left(pp \to \ell_1^+ \ell_2^+ X \right). \tag{3.35}$$

This correction factor is given by

$$\Delta_{pD} = \frac{1}{4} \frac{1}{m_4^2} (M_4 - m_4)^2 = \frac{1}{4} \left(\frac{\delta m}{m_4} \right)^2. \tag{3.36}$$

As a consequence, the LSD cross section is considerably smaller than in the single neutrino case, which can be seen in figure 3.6. As the flavors of the final state leptons enter the cross section in equation (3.34) only by an overall factor, the various flavor combinations can easily be obtained by choosing the appropriate flavor factor $\left| U_{\ell_1 4} U_{\ell_2 4} \right|^2$ for the cross section. These factors are given in table 3.1.

The suppression and the resulting smallness of the LSD cross sections exhibits the impact of the pseudo-Dirac nature of a neutrino species on any LNV process. Although the mass eigenstates themselves can be comparable large, the magnitude of the Majorana mass is crucial. Thus the Majorana nature can only be constrained but not strictly excluded.

3.3 Radiative lepton decays

The bound on U_{e4} in equation (3.1) obtained in [102] is dominated by experimental constraints on radiative, lepton flavor violating, charged lepton decays, particularly the radiative decay of the muon. We will scrutinize these reactions in this section.

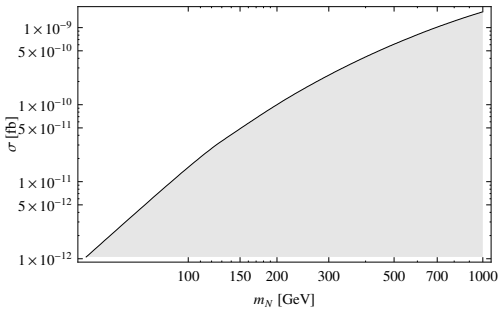

(a) Cross section for like-sign dielectron production.

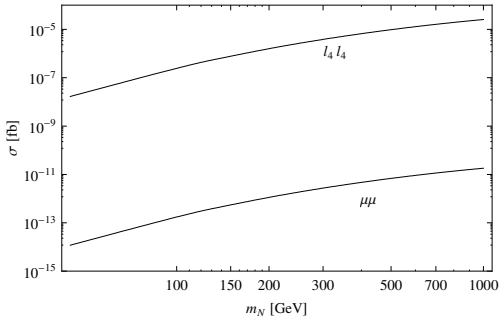

(b) Cross section for like-sign dimuon and like-sign two fourth generation charged lepton production.

Figure 3.6: Upper bound on the cross section for like-sign dilepton production triggered by an electroweak scale pseudo-Dirac neutrino fulfilling $0\nu\beta\beta$ constraints.

final state	flavor factor $[10^{-5}]$
$l_4 l_4$	49960
$e l_4$	791.78
τl_4	722.21
μl_4	84.07
$e\tau$	5.72
ee	3.14
$\tau\tau$	2.61
$e\mu$	0.67
$\mu\tau$	0.61
$\mu\mu$	0.04

Table 3.1: Flavor factor $\left|U_{\ell_1 4} U_{\ell_2 4}\right|^2$ of the LSD production cross section shown in figure 3.6. The states are sorted by their flavor factor.

The processes (see figure 3.7) and the experimental bounds on their branching ratios [128,129] are

$$BR(\mu \to e\gamma) < 2.4 \cdot 10^{-12} \tag{3.37}$$

$$BR(\tau \to \mu\gamma) < 4.4 \cdot 10^{-8} \tag{3.38}$$

$$BR(\tau \to e\gamma) < 3.3 \cdot 10^{-8}. \tag{3.39}$$

The corresponding amplitude for the decay of a charged lepton ℓ into the charged lepton ℓ' is given by [130]

$$T_\alpha = U_{\ell\alpha} U_{\ell'\alpha} F\left(\frac{m_\alpha^2}{m_W^2}\right) \tag{3.40}$$

where $F(x_\alpha)$ is

$$F(x_\alpha) = 2(x_\alpha + 2) I^{(3)}(x_\alpha) - 2(2x_\alpha - 1) I^{(2)}(x_\alpha) + 2x_\alpha I^{(1)}(x_\alpha) + 1 \tag{3.41}$$

with $x_\alpha \equiv \frac{m_\alpha^2}{m_W^2}$ and

$$I^{(n)}(x_\alpha) = \int_0^1 \mathrm{d}z \frac{z^n}{z + (1-z)x_\alpha}. \tag{3.42}$$

Thus the decay width can be written as

$$\Gamma_{\ell \to \ell'\gamma} = \frac{1}{2} \frac{G_F^2 m_\ell^5}{(32\pi^2)^2} \alpha_W \sum_\alpha |U_{\ell\alpha} U_{\ell'\alpha}|^2 F_{eff}^2(x_\alpha). \tag{3.43}$$

Here we define

$$F_{eff}(x_\alpha) = F(x_\alpha) - F(0) \tag{3.44}$$

due to the unitarity cancellation

$$\sum_\alpha U_{\ell\alpha} U_{\ell'\alpha} = 0 \tag{3.45}$$

of the constant term in $F(x_\alpha)$ in equation (3.43).

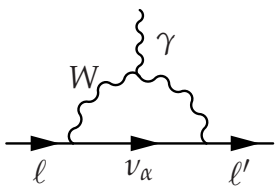

Figure 3.7: Feynman diagram of the radiative decay of a lepton.

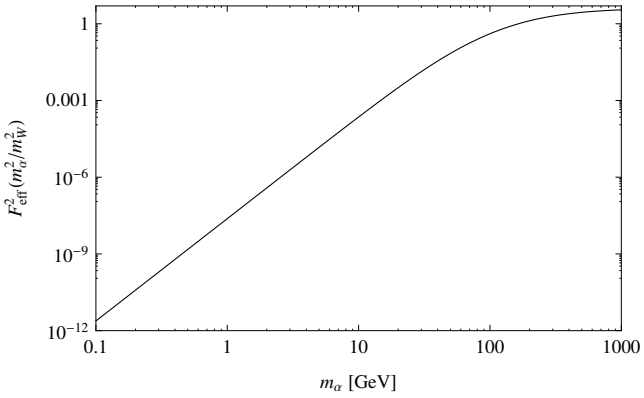

Figure 3.8: F^2_{eff} as a function of the mass of the exchanged neutrino.

Note, that this process is allowed for both Majorana and Dirac neutrinos. As the neutrino mass in the analysis [102] was fixed to 45 GeV we will first focus on the mass dependence of the decay width, which enters equation (3.43) in form of the factor $F^2_{eff}(x_\alpha)$. The mass dependence of this factor is shown in figure 3.8. For the first three, light neutrinos the decay width is suppressed by the smallness of the mass eigenstate and a resulting small F_{eff}. The quantity $|U_{\ell\alpha}U_{\ell'\alpha}|^2$ can, therefore, be large, allowing large PMNS matrix elements. For a fourth generation this is not the case as can be seen in figure 3.8. Consequently, the smallness of the decay width has to be a result of a small mixing between the lepton flavors. However, only the product of two PMNS matrix elements is observable, yielding no absolute bounds but an allowed region in the $U_{\ell\alpha}$-$U_{\ell'\alpha}$ parameter space. For instance, a larger neutrino mass does not imply a more stringent bound on U_{e4} as the matrix element $U_{\mu 4}$ can be arbitrary small. This is shown in figure 3.9 for various neutrino masses. Within the required mass range $45\,\text{GeV} \leq m_4 \leq 1\,\text{TeV}$ the bounds vary only within one order of magnitude.

The decays of the tauon have much weaker experimental bounds and do not give any additional constraints.

3.4 Fourth generation neutrino mass model with extra dimensions

Even with todays knowledge of neutrino oscillation parameters and huge experimental effort, the theory of massive neutrinos still remains a mystery challenging model building. The charged fermions typically acquire their masses via the Higgs mechanism as they are pure Dirac particles. The

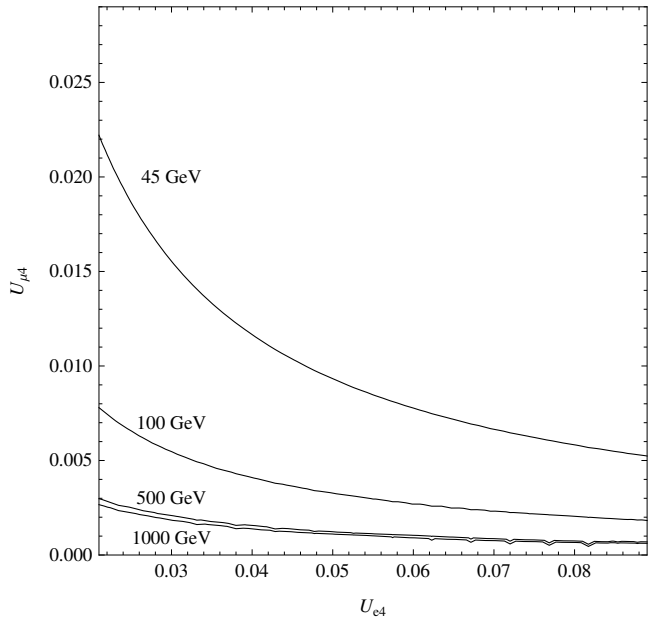

Figure 3.9: Constraint on the $U_{\mu 4} - U_{e4}$ parameter space obtained from the bound on the branching ratio for $\mu \to e\gamma$. The lower left is the allowed region. The boundaries of the intervals plotted are given by the allowed values $U_{\mu 4} - U_{e4}$ with $m_4 = 45\,\mathrm{GeV}$ according to equation (3.1).

Lagrangian for the fermion masses is given by:

$$-\mathcal{L}_{\mathrm{Dirac}} = y_\ell \overline{L}^i \phi^i \ell_R + \text{h. c.}, \tag{3.46}$$

where L is the left handed lepton doublet, ℓ_R the right handed lepton singled, ϕ the Higgs doublet and y_ℓ the Yukawa coupling. After electroweak symmetry breaking, the Higgs doublet acquires the vacuum expectation value

$$v \approx 246\,\mathrm{GeV}$$

and the mass term now reads

$$-\mathcal{L}_{\mathrm{Dirac}} = y_\ell v \overline{\ell}_L \ell_R + \text{h.c.} \tag{3.47}$$

For instance, this yields a Yukawa coupling for the electron of

$$y_e \approx 2 \cdot 10^{-6}. \tag{3.48}$$

The quarks acquire their masses in the same way, yielding for the top quark

$$y_t \approx 0.7. \tag{3.49}$$

All remaining fermions have Yukawa couplings within this range. For now we consider also neutrinos as Dirac particles and use 1 eV as their order of magnitude. The corresponding Yukawa coupling would be

$$y_\nu \sim 10^{-12}. \tag{3.50}$$

This large hierarchy is illustrated in the left column of figure 3.10. Here the masses of the third generation fermions are illustrated on an exponential axis. Again, we choose the scale of the neutrino mass to be maximal given by the LSS constraint on the sum of light neutrino species. While the charged fermions have masses converging to order one Yukawa couplings, the neutrino is nine orders of magnitude lighter causing a huge gap in the fermion mass spectrum which appears unnatural. This shortcoming of the Dirac type neutrino mass model has been cured by the seesaw mechanism [121–124], which employs the interplay between the Dirac mass Lagrangian of the form

$$\mathcal{L}_{\text{Dirac}} = m_D \left(\overline{\nu}_R \nu_L + \overline{\nu}_L^c \nu_R^c\right) + \text{h.c.} \tag{3.51}$$

and the additional Majorana mass Term

$$\mathcal{L}_{\text{Majorana}} = M_R \left(\overline{\nu}_R^c \nu_R\right) + \text{h.c.} \tag{3.52}$$

Here we restrict ourselves to one generation only. For more generations the neutrino states get generation indices and the masses become mass matrices. These Lagrangians add up to the complete mass Lagrangian, that can be efficiently written as the matrix equation:

$$-\mathcal{L}_{\text{mass}} = \frac{1}{2} \begin{pmatrix} \overline{\nu}_L^c & \overline{\nu}_R \end{pmatrix} \begin{pmatrix} 0 & m_D \\ m_D & M_R \end{pmatrix} \begin{pmatrix} \nu_L \\ \nu_R^c \end{pmatrix} + \text{h.c.} \tag{3.53}$$

As the matrix, that connects the neutrino flavor and mass eigenstates, is not diagonal, these mass and flavor eigenstates are not identical. The neutrino mass eigenstates are the eigenstates of this matrix and the neutrino masses its eigenvalues:

$$m = \frac{1}{2}\left(\sqrt{4m_D^2 + M_R^2} - M_R\right) \tag{3.54}$$

$$M = \frac{1}{2}\left(\sqrt{4m_D^2 + M_R^2} + M_R\right). \tag{3.55}$$

The type-I seesaw model generates small neutrino masses by introducing large Majorana masses ($M_R \gg m_D$). This leads to the mass eigenvalues

$$m_i \approx \frac{m_D^2}{M_R} \tag{3.56}$$

$$M_i \approx M_R - \frac{m_D^2}{M_R}. \tag{3.57}$$

Typically, the Majorana mass is chosen at the grand unified scale and the Dirac mass is comparable to the charged fermions with order one Yukawa couplings. This leads to a mass spectrum as shown in the left column of figure 3.10, explaining the gap in the hierarchy of the fermion masses.

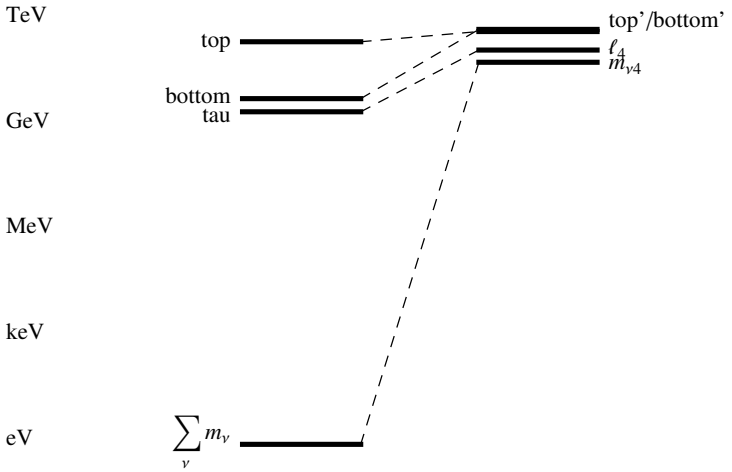

Figure 3.10: Sketch of the mass hierarchies of third generation fermions compared to the lower bounds on a fourth generation. As the third generation neutrino mass we show the upper bound of the sum of all light neutrinos given by LSS. For discussion see the text.

One would expect a similar spectrum for a fourth generation. With each generation the charged fermions get larger Yukawa couplings and, therefore, larger masses. As in the seesaw model the Majorana mass is similar for the first three generations, it is reasonable to assume the same for the fourth generation. Thus the fourth generation mass spectrum is expected to show a similar gap between the neutrino and charged fermions as in the third generation. However, as already pointed out in section 2.1, the neutrino must be significantly heavier. In figure 3.10 the right column gives the lower bounds on the fourth generation fermion mass spectrum as discussed in section 2. Whereas the charged fermion masses agree with the above statement, the neutrino mass changes dramatically compared to the third generation. Although it does not necessarily contradict the existence of a fourth generation, it is an open issue.

In section 3.1 stringent constraints on the size of the Majorana mass of a fourth generation neutrino have been derived. For simplicity we shall use the estimate of $M_R \sim 1\,\text{GeV}$ for the fourth generation. Therefore, if one relates the hierarchy with the Majorana mass, the hierarchy spans 16 orders of magnitude. There is either a large hierarchy in the Dirac masses or a large hierarchy in the Majorana masses. As the seesaw model has many useful applications and implications, for example leptogenesis and large Yukawa couplings, we will investigate a model that modifies the Majorana masses. Another advantage is that the Majorana masses are not affected by electroweak symmetry breaking scenarios. Hence we choose a natural hierarchy of the Yukawa couplings with equal spacings:

$$y_4 - y_3 = y_3 - y_2 = y_2 - y_1 = 0.25, \tag{3.58}$$

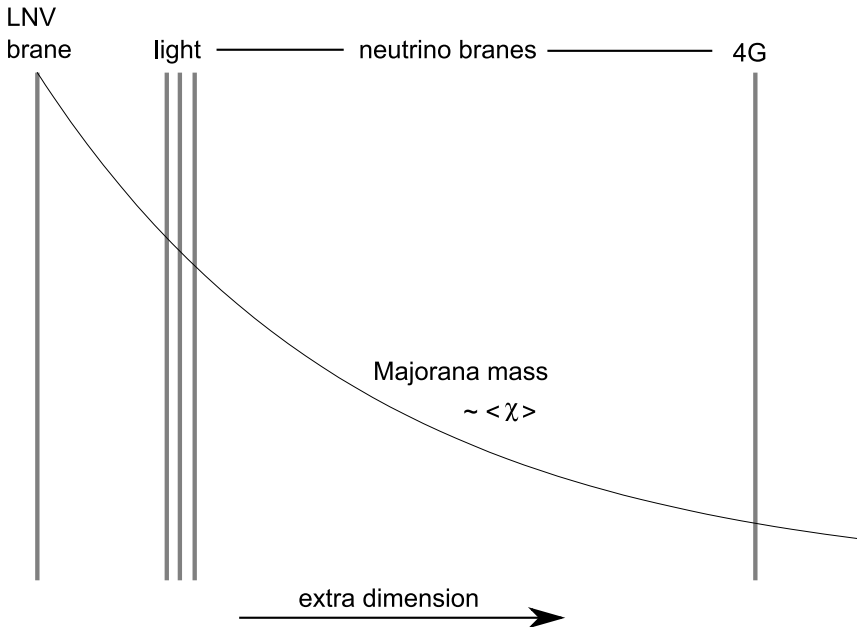

Figure 3.11: Evolution of the Majorana mass from the LNV brane along the extradimensional bulk to the branes where the neutrino generations are localized.

where the index indicates the neutrino generation. The fourth generation has a Yukawa couplings of $y_4 = 1$.

For the Majorana masses we use a model with extra dimensions that is capable of softening large hierarchies. We adopt a model by Arkani-Hamed and Dimopoulos [131] that introduces a brane in a distance r_0 along an extra dimension in addition to the SM. Approximate symmetries on our SM brane, such as LNV in our case, can be maximally broken on such a brane, which we will call LNV brane in our scenario. The information of LNV on this brane, Λ_{LNV}, gets transmitted along the extra dimension by a bulk field χ that overlaps with any other brane. However, the information carried by χ in terms of its vacuum expectation value $\langle\chi\rangle$ decreases with distance in the extra dimension as any interaction mediated by massive particles:

$$\langle\chi\rangle \propto \mathrm{e}^{-m_\chi r}. \tag{3.59}$$

Consequently, the LNV strength at distant branes is smaller than the initial scale Λ_{LNV}. As the decrease is exponential, large hierarchies can be explained by reasonable spacings along the extra dimension. In our scenario one right handed neutrino field for each generation is located between our SM brane and the LNV brane, thus receiving a different amount of LNV. This setup is sketched in figure 3.11.

The information of LNV is quantitatively given by the Majorana mass terms of the four neutrino generations, and thus an exponential ansatz for

i	α_i	m_i [GeV]	M_i [GeV]
4	~ 43.7	246	247
3	9.6	$5.0 \cdot 10^{-11}$	$6.7 \cdot 10^{14}$
2	8.7	$9.1 \cdot 10^{-12}$	$1.7 \cdot 10^{15}$
1	≤ 7.9	$\leq 4.1 \cdot 10^{-12}$	$\geq 3.7 \cdot 10^{15}$

Table 3.2: Localizations of the neutrino branes in the extradimensional bulk and corresponding mass eigenvalues for $\Lambda_{LNV} = 10^{19}\,\mathrm{GeV}$.

the Majorana masses along the extra dimension is chosen:

$$M_R(r) = \Lambda_{LNV} \mathrm{e}^{-r}. \tag{3.60}$$

Here r is the axis along the extra dimension.

The effective Majorana mass for the neutrino of generation i located at a distance α_i is

$$M_{Ri} = \Lambda_{LNV} \mathrm{e}^{-\alpha_i}. \tag{3.61}$$

Assuming normal hierarchy, the Majorana masses are then constrained by neutrino oscillation data (Δm^2_{12} and Δm^2_{13}) for the first three generations and by figure 3.3 for the fourth generation. The resulting localizations of the neutrino branes are listed in Table 3.2.

The positions of the neutrino branes soften the hierarchy of the neutrino Majorana masses in a significant way. Thus, in an extradimensional framework the huge gap between first three and fourth generation is considerably smaller. The seesaw mechanism applies for the first three generations and the fourth generation remains a pseudo-Dirac neutrino as requested.

3.5 Summary

In this chapter we revisited bounds on the masses and mixings of an additional fourth generation Majorana neutrino with the assumption of nonzero mixing to the electron neutrino. In section 3.1, such a neutrino was found not yet to be excluded by neutrinoless double beta decay, if its mass is of the order of hundreds GeV and the Majorana mass is small compared to its absolute mass. Therefore, it must be a pseudo-Dirac type neutrino, which is an object composed of two quasi-degenerate Majorana neutrinos. The implications of this pseudo-Dirac nature was exemplified in section 3.2 by showing the suppression of the lepton number violating process of like-sign dilepton production at hadron colliders. The difficulty to distinguish between pseudo-Dirac and pure Dirac neutrinos was shown. Turning to bounds on the neutrino mixing matrix elements we extended the initial

work [102] on the radiative decay of the muon by new experimental bounds and with variable neutrino mass. We found this reaction dominating the allowed parameter space in the $U_{\mu 4} - U_{e4}$ plane. The variation of neutrino mass has small impact on these bounds. It changes the values only slightly and keeps the order of magnitude of the mixing matrix elements stable. In section 3.4 we shed some light on possible solutions of the neutrino mass hierarchy problem. We considered the hierarchy settled in the Majorana sector and showed that in an extradimensional framework it can be strongly softened from 16 orders of magnitude to only one.

4. Baryon asymmetry of the universe and new neutrino species

Nowadays, additional neutrino states, such as the fourth generation $SU(2)$ doublet neutrino [88, 90, 104, 132] or additional $SU(2)$ singlet neutrinos are introduced for various reasons. The latter ones pose cures for several issues:

- neutrino oscillation anomalies observed in solar and reactor neutrino oscillations and the LSND and MiniBooNE experiments [133–135],
- warm dark matter candidates [136, 137],
- other attractive astrophysical properties such as the velocities of pulsars [138].

In the previous chapter we considered a complete sequential fourth neutrino generation and derived bounds on its Majorana masses. Independently from this analysis, we will investigate the impact of such a neutrino in the field of early universe cosmology in this chapter.

The findings have been published as [139]:

S. Hollenberg, H. Päs, D. Schalla
Baryon asymmetry of the universe and new neutrino states
arXiv:1110.0948 .

Here, we will also allow neutrinos to have Majorana mass. On the one hand, this preserves appealing features such as explaining the fermion mass hierarchies but on the other hand the introduction of LNV Majorana neutrinos poses a potential threat to the cosmology of the early universe, namely baryogenesis [140].

In the universe the number of baryons and antibaryons is not equal. All astrophysical structures observed are made of matter. Even if the universe started with an initial primordial baryon asymmetry, inflation would have diluted it, leaving no trace of any baryon asymmetry of the universe (BAU). Therefore, some mechanism had to generate the asymmetry dynamically

from initially zero to today's value of [141, 142]

$$\eta \equiv \frac{n_B - n_{\overline{B}}}{n_\gamma} = (6.1787 \pm 0.0015) \cdot 10^{-10}, \tag{4.1}$$

where n_B, $n_{\overline{B}}$, n_γ are the baryon, antibaryon and photon number density of the universe, respectively. The mechanism generating this asymmetry is called baryogenesis and there are numerous different models that aim to archive the observed BAU. However these models work in detail, there are three basic conditions that any model has to fulfill. These conditions were introduced by Sakharov [143] and read:

1. Baryon number violation,
2. C and CP violation,
3. out-of-equilibrium interactions.

Condition 1 can be fulfilled within the SM in terms of sphaleron processes [144]. These are nonperturbative processes in which a systems tunnels between two vacuum states with different baryon number. These transitions do not conserve baryon and lepton number separately but the combination $B - L$. In principle, sphalerons convert any lepton asymmetry into a baryon asymmetry and vice versa until they freeze out. Therefore, until the freeze out, asymmetries of lepton and baryon numbers are connected. As a consequence, it is possible to explain the BAU to be generated within the lepton sector. This is called the baryogenesis via leptogenesis scenario.

The violation of charge conjugation and combined chargeconjugation and parity symmetry as stated in condition 2 is also featured in the SM in terms of the weak interaction, provided the CP phase is nonzero. However, the SM3 does not provide the right amount of CP violation in order to explain the observed asymmetry (see section 2.4). In leptogenesis scenarios the source of CP violation lies within the leptonic sector by heavy right handed neutrino decays via Yukawa interactions.

In principle, condition 3 can be realized by the electroweak phase transition. However, in the SM3 the transition tends to be not a strongly first order phase transition that would be needed for a successful baryogenesis. As mentioned in section 2.4 the SM4 can improve this issue. In leptogenesis the departure from thermal equilibrium is given by the expansion of the universe. If the heavy neutrino decay lifetimes are shorter than the universe expands, the asymmetry is created at the time of nonequilibrium.

However, the following considerations do not depend on the specific type of baryogenesis model. Here we discuss the impact of an additional neutrino species on an pre-existing baryon asymmetry which may be created at a high temperature, for example the GUT scale. Additional neutrinos can potentially erase such an excess by their LNV interactions that

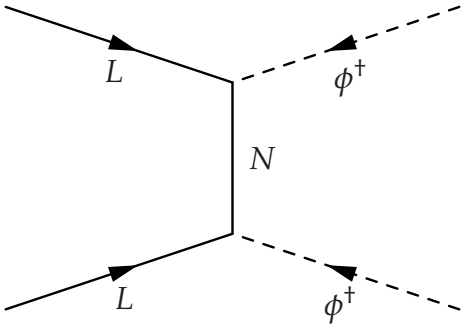

Figure 4.1: Feynman diagram of a typical $\Delta L = 2$ scattering process potentially capable of washing out any existing $B - L_\alpha$ asymmetries.

violate baryon number via sphaleron transitions. We will estimate this washout by $\Delta L = 2$ interactions [145, 146], which are elastic lepton Higgs scatterings as depicted in figure 4.1.

Moreover, light neutrino states, such as discussed in the previous chapter, freeze out at approximately their mass scale and, therefore, not during the large range from GUT scale temperatures to the EWPT. Consequently, the asymmetry must be protected for roughly 14 orders of magnitude, which is a problem regarding the Majorana nature of these states (for related works, see for example [147–149]).

As in the previous chapter, the additional neutrino will have an electroweak scale Dirac mass and be a pseudo-Dirac type neutrino. However, when considering the temperature regime mentioned above, the electroweak symmetry is restored and the Higgs vacuum expectation value vanishes. As the Dirac mass is proportional to the vacuum expectation value the Dirac mass also vanishes above the EWPT. In contrast, the Majorana mass is not affected by this and we shall assume it to be invariant. As already indicated in equation (3.20), the mixing angle between the two flavor eigenstates, at low energies being maximal for pseudo-Dirac neutrinos, is proportional to the Dirac mass and therefore becomes zero, too. The resulting bare mass eigenstates are zero and M_R. As a consequence, in the process shown in figure 4.1 only one neutrino propagates. Thus at temperatures above the electroweak phase transition pseudo-Dirac neutrinos behave exactly like light sterile neutrinos bearing only a Majorana mass. The bounds obtained in this chapter are valid for both $SU(2)$ doublet and singlet neutrinos.

As mentioned above, these processes give rise to lepton number violating scattering processes such as the scattering of lepton doublets l_L to Higgs particles ϕ, for example $l_L \phi \rightleftharpoons l_L^c \phi^c$. The washout by this scattering endangers a pre-existing asymmetry as long as they are in thermal equilibrium during the epoch between the GUT scale and the EWPT.

As such a depletion should not have taken place to, at least, some extent, these processes should either not come into thermal equilibrium or be weak enough not to dilute the pre-existing $B - L$ asymmetry at least down to the electroweak scale where the sphalerons freeze out.

First, we will stick to the strong and more conservative criterion of out-of-equilibrium scenario. A process takes place out-of-equilibrium at a temperature T if its decay width Γ is smaller than the Hubble constant H:

$$\Gamma(T) < H(T). \tag{4.2}$$

The Hubble constant is given by

$$H(T) = \sqrt{\frac{8\pi^3 g_*}{90}} \frac{T^2}{m_{\mathrm{Pl}}}, \tag{4.3}$$

where m_{Pl} the Planck mass and g_* the effective number of degrees of freedom.

In order to calculate the decay rate we must parameterize the thermally-averaged scattering cross section. As in most models the neutrinos considered are much heavier, for example have masses at the GUT scale, we must modify the propagator term compared to more common parameterizations [150]:

$$\langle \sigma |v| \rangle_\alpha \sim \kappa_\alpha^2 \frac{M_R^2}{\left(T^2 + \tilde{m}^2\right)^2} = \kappa_\alpha^2 \frac{1}{M_R^2} \frac{z^4}{\left(1 + \frac{z^2 \tilde{m}^2}{M_R^2}\right)^2}, \tag{4.4}$$

where $z \equiv \frac{M_R}{T}$. The index α denotes that the cross section affects the lepton flavor α in which the pre-existing asymmetry has been generated. κ_α denotes a generic coupling constant containing Yukawa couplings and neutrino mixing matrix elements which are model dependent. This cross section suffices the Dirac limit for $M_R \to 0$, in which the cross section should vanish as the Majorana mass is the only source of LNV. Thus for Dirac particles there is no washout as required.

In the denominator of equation (4.4), which originates from the fermion propagator of the exchanged neutrino, we use the thermal mass $\tilde{m}$ of the particle [142, 151]. As the neutrino couples to the primordial plasma via Yukawa interactions, it gains a mass proportional to its temperature. Thus we use the thermally corrected mass $\tilde{m}^2 \equiv m_0^2 + g^2 T^2$, where m_0 is the bare mass. This bare mass corresponds to the two mass eigenvalues and hence, above the electroweak phase transition, the bare mass of the light neutrino state can be taken to be zero and for the heavy state it is simply M_R. The interactions of the particles with the plasma come with a coupling strength g. As stated above the mixing angle between the neutrino states is zero for

temperatures above the electroweak threshold. Thus only the heavier of the two mass eigenstates, with a mass of

$$\tilde{m}^2 = M_R^2 + g^2 T^2 = M_R^2 \left(1 + \frac{g^2}{z^2}\right), \tag{4.5}$$

contributes to the cross section.

It can now be readily seen that in the limit $z \gg 1$ we recover the thermally-averaged cross section for GUT scale neutrino states given by

$$\langle \sigma |v| \rangle_\alpha \sim \kappa_\alpha^2 / M_R^2. \tag{4.6}$$

With the appropriate scattering cross section at hand, we can write down the relevant rate for the washout process:

$$\Gamma_\alpha(T) \sim n_\phi \langle \sigma |v| \rangle_\alpha. \tag{4.7}$$

Here Γ_α contains the number density $n_\phi \simeq 2\zeta(3) T^3/\pi^2$ of Higgses in which ζ is the Riemann zeta function.

The washout of lepton number L_α between GUT scale and electroweak scale can then be calculated straightforwardly via

$$\ln\left(\frac{L_\alpha(z_{\mathrm{EW}})}{L_\alpha(z_{\mathrm{GUT}})}\right) = -\frac{1}{H(z=1)} \int_{z_{\mathrm{GUT}}}^{z_{\mathrm{EW}}} \mathrm{d}z'\, z' n_\gamma \langle \sigma |v| \rangle_\alpha (z'), \tag{4.8}$$

where $n_\gamma \simeq n_\phi$ is the photon number density.

We understand that CP violating out-of-equilibrium decays of the new neutrino species prior to the electroweak phase transition could result in the generation of considerable additional lepton asymmetry hence alleviating its depletion in wash out processes. However, given the mass of the hypothetical new neutrino states of some hundred GeV, their freeze out occurs non-relativistically and thus roughly at the electroweak scale. We therefore find such effects to be marginal and neglect them in our analysis.

In figure 4.2 the behavior of the rates given above is illustrated for a certain set of parameters. As the washout is only effective in the regime where $\Gamma_\alpha \gtrsim H$ the integration limits in equation (4.8) are chosen accordingly. However, the effect of thermal masses only has minor impact on the scattering rate and hence does not alter the bounds on the Majorana mass significantly.

The result of the integration in equation (4.8) is shown in figure 4.3. For certain masses the scattering cannot come into thermal equilibrium until the electroweak scale and hence there cannot be any depletion of pre-existing lepton number. This is the case for Majorana masses less than

$$\left(\frac{M_R}{10\ \mathrm{keV}}\right)^2 \lesssim 0.9 \times \left(\frac{1+g^2}{\kappa_\alpha}\right)^2 \times \left(\frac{T_{\mathrm{EW}}}{246\ \mathrm{GeV}}\right)^3. \tag{4.9}$$

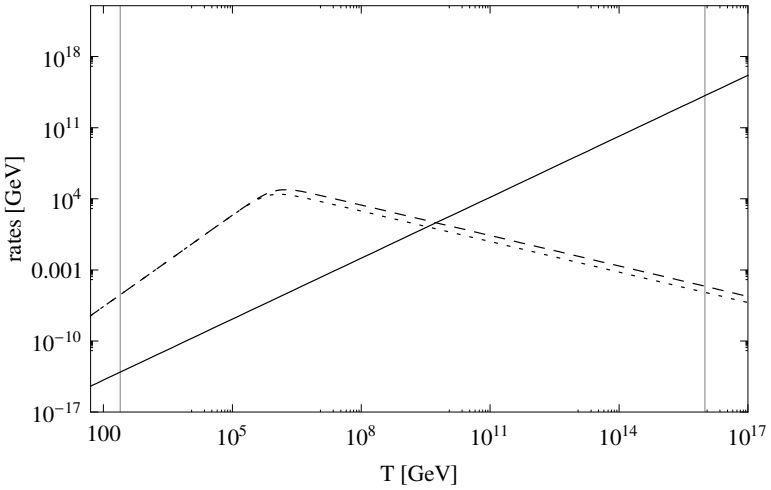

Figure 4.2: An illustrative plot of the rates involved in the freeze out of heavy additional Majorana neutrino states as a function of temperature. The solid line gives the Hubble rate $H(T)$, the dashed (dotted) line represents the scattering rate $\Gamma_\alpha(T)$ with $g = 0$ ($g = 1$). The vertical line to the left marks the electroweak threshold $T_{\rm EW} = 246$ GeV, the vertical line to the right marks the GUT threshold $T_{\rm GUT} = 10^{16}$ GeV. For illustrative purposes a Majorana mass of $M_R = 10^6$ GeV has been chosen.

Beyond this threshold lepton number violating scatterings can come into equilibrium and pre-existing lepton number gets diluted away exponentially as the neutrino mass increases. If, for instance, a drop in lepton number by one order of magnitude is considered compatible, the bound on the Majorana mass is relaxed to some $M_R \sim 25 - 50$ keV.

As this bound on the Majorana mass of the pseudo-Dirac pair corresponds to their mass splitting below the EWSB, the bounds obtained previously in section 3.1 from neutrinoless double beta decay searches are improved by at least three orders of magnitude. It has to be understood as a rough estimate, though, as it is subject to the exact values of Yukawa couplings and PMNS matrix elements describing the mixing of the flavor(s) in which the baryon asymmetry has been generated and the new neutrino states. Taking this into account the results obtained in this chapter apply for any additional Majorana neutrino species and constrain their Majorana mass to be in the keV range. This, in turn, implies that any additional species has to be of a pseudo-Dirac type by virtue of its small Majorana mass unless the baryon asymmetry is generated at or below the electroweak scale and/or flavor protected. Note, also, that the analysis presented here thus independently confirms our earlier findings in the context of a complete sequential fermion generation.

In summary we have discussed the washout of a pre-existing or GUT scale generated baryon asymmetry due to the presence of new neutrino

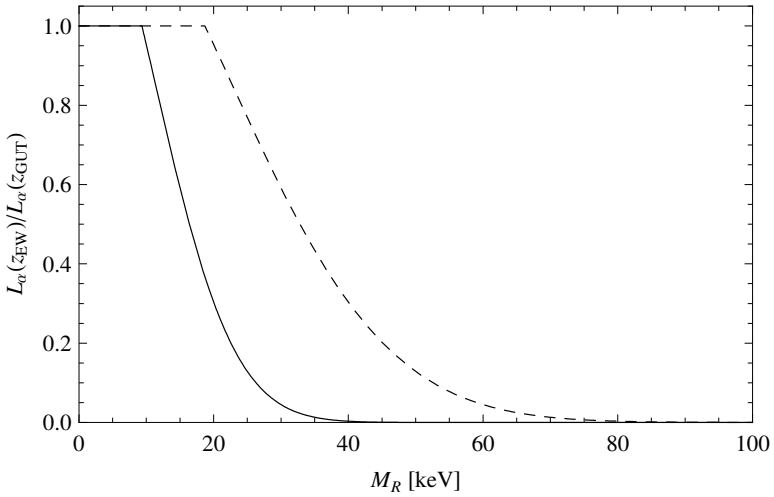

Figure 4.3: The ratio of the lepton asymmetry at the electroweak scale and the GUT scale as a function of the Majorana mass with $g = 0$ (solid) and $g = 1$ (dashed). The generic coupling has been chosen to be $\kappa_\alpha = 1$.

states. We find that pure Majorana neutrinos are limited to masses below the order of ten keV. Such light neutrino states have to be $SU(2)$ singlets to avoid the bound from the Z boson decay width. Weak scale pseudo-Dirac neutrinos are allowed only with tiny mass splittings of the order of ten keV. Thus a fourth generation neutrino being affected by the Z boson width bound has to be Dirac or pseudo-Dirac with very small lepton number violation.

This analysis constrains a potential fourth generation neutrino independently from the previous discussion of neutrinoless double beta decay but with a similar result. It points to the conclusion, that fourth generation neutrinos ought to be more Dirac than Majorana type, although a small Majorana admixture cannot yet be excluded.

5. Production of hadrons by neutrinos scattering off nuclei

Beyond the standard model physics in the neutrino sector such as additional generations or sterile singlet neutrinos are considerably attractive as the experimental constraints still remain soft, leaving space for various theoretical extensions. An important quantity regarding additional neutrino states is the PMNS matrix. Assuming unitarity and precise knowledge of its elements one could, in principle, determine missing oscillation probabilities favoring such states. Although a three flavor PMNS matrix compatible with unitarity does not rule out decoupled additional neutrino states, it constrains its parameters. The smaller the uncertainties of the matrix elements are the stricter the constraints get.

Some experiments measuring the PMNS matrix elements use neutrino beams with energies in the order of a few GeV and determine the exact flux of a nearby detector to be compared with the neutrino flux measured by a far away detector. Some experiments just use a single detector. However the specific setup may be, the neutrinos interact with the detector target via both charged and neutral currents and produce leptons and hadrons that subsequently produce detectable signals. From these final states, mostly pions, the fluxes have to be reconstructed. Thus a precise theoretical understanding of all neutrino-detector interaction channels is essential for determining the neutrino fluxes (see for example [152] for a recent review of neutino-nucleus interactions).

The energy dependence of the major charged current interaction channels is given in figure 5.1. The dominant neutrino induced process at low energies is charged current quasi-elastic scattering (CCQE)

$$\nu_\ell n \to \ell^- p, \tag{5.1}$$

where the neutrino scatters on the nucleons without the production of further particles.

The next dominant process for large energies is deep inelastic scattering (DIS)

$$\nu_\ell q \to \ell^- q'. \tag{5.2}$$

Here the neutrino interacts with a single quark and creates new hadronic final states.

The last two processes are important at intermediate energies. First, there is coherent pion production

$$\nu_\ell N \to \ell^- N \pi \tag{5.3}$$

which has the unique characteristic that the neutrino interacts with the entire nucleus without changing it. The exchanged boson produces a single pion in the field of the nucleus. Albeit its distinct signatures as low momentum transfers, its cross section is too small to be plotted in figure 5.1.

The second and more important process at intermediate neutrino energies is resonant single pion production (CC1π), for example

$$\nu_\ell n \to \ell^- \Delta^+ \to \ell^- n \pi^+ \tag{5.4}$$
$$\nu_\ell p \to \ell^- \Delta^{++} \to \ell^- p \pi^+ \tag{5.5}$$

where the neutrino excites the nucleons to a resonance, which decays and emitts a single pion. Figure 5.2 shows the Feynman diagram of the neutrino production of the Δ^{++} resonance, which will be the topic of this chapter. First we present the common ansatz for calculating the cross section in terms of structure functions and form factors. Then, we develop a new approach for calculating the cross section for small momentum transfers by the usage of the partially conserved axial-vector current (PCAC) that does not rely on additional parameters. Combining these two methods we compare the theoretical models with experimental data.

This improvement has been published as [153]

E. A. Paschos and D. Schalla
Neutrino production of hadrons at low energy and in the small Q2 region
Physical Review D84 (2011) 013004, arXiv:1102.4466 .

The calculation of isospin rotations, pion spectra, nuclear corrections and their application to *CP* searches was published in [154]

E. A. Paschos and D. Schalla
Pion production by neutrinos in the delta resonance region and possible application to CP searches
arXiv:1209.4219

as well as in [155]

E. A. Paschos and D. Schalla
Neutrino-induced pion production at low energies and in the small Q^2 region
arXiv:1212.4662 .

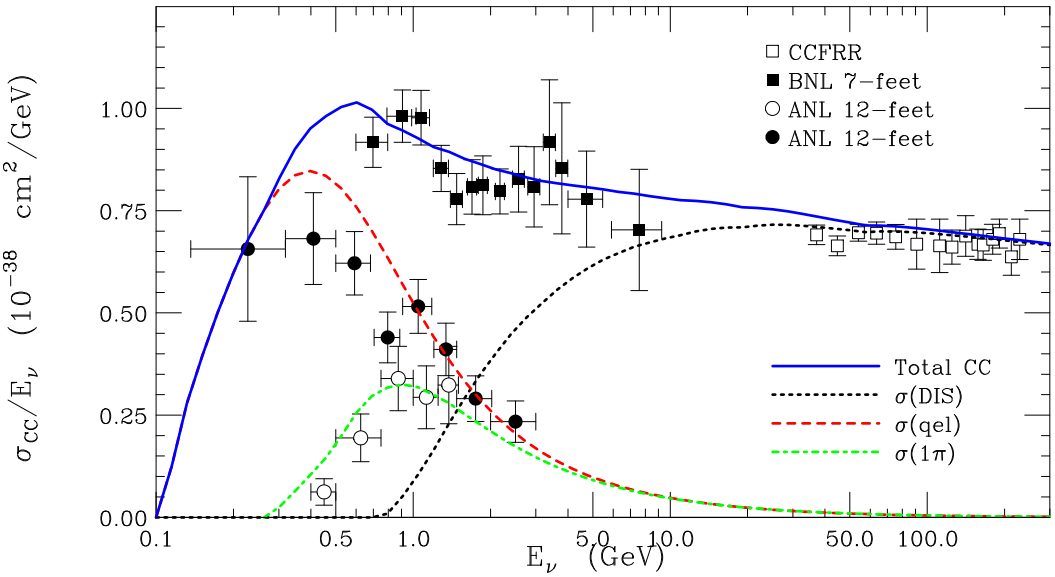

Figure 5.1: Contribution of each channel to the total charged current neutrino-nucleon cross section as a function of neutrino energy. This figure is taken from [156].

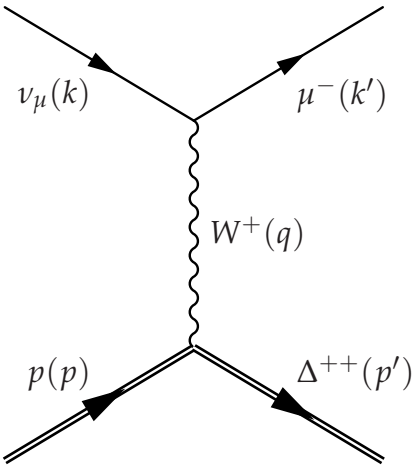

Figure 5.2: Feynman diagram corresponding to the production of the Δ^{++} resonance via charged current neutrino proton scattering.

5.1 Lalakulich-Paschos parametrization

The reaction we will restrict ourselves to is

$$\nu_\mu(k)p(p) \to \mu^-(k')\Delta^{++}(p') \tag{5.6}$$

and frequently used variables are

$$q \equiv k - k',\ Q^2 \equiv -q^2,\ W^2 = p'^2 \tag{5.7}$$

with Q^2 being the momentum transfer and W the invariant mass of the resonance.

In general we use the cross section and conventions defined in [157] as it is the most common and transparent ansatz for calculating resonance cross sections. An earlier approach is given in [158] which can be shown to be equal in the case of zero masses but lacks of clearness and thus became less used.

In the theory of [157], which will be sketched in this section, the differential cross section is decomposed into the product of a leptonic tensor $L_{\mu\nu}$ dotted with the hadronic tensor $\mathcal{W}^{\mu\nu}$:

$$\frac{\mathrm{d}\sigma}{\mathrm{d}Q^2\mathrm{d}W} = \frac{G_F^2|V_{ud}|^2}{16\pi}\frac{W}{m_N E^2}L_{\mu\nu}\mathcal{W}^{\mu\nu}. \tag{5.8}$$

The leptonic tensor is given by

$$T_{\mu\nu} = 4\left(k_\mu k'_\nu + k_\nu k'_\mu - g_{\mu\nu}(k\cdot k') - i\varepsilon_{\mu\nu\alpha\beta}k^\alpha k'^\beta\right). \tag{5.9}$$

The hadronic tensor is defined with six structure functions $\mathcal{W}_i$ with $i = 1 \ldots 6$ in a general Lorentz-invariant parametrization:

$$\begin{aligned}\mathcal{W}^{\mu\nu} =& -\mathcal{W}_1 g^{\mu\nu} + \frac{\mathcal{W}_2}{m_N^2}p^\mu p^\nu - i\varepsilon^{\mu\nu\sigma\lambda}p_\sigma q_\lambda\frac{\mathcal{W}_3}{2m_N^2}\\ &+ \frac{\mathcal{W}_4}{m_N^2}q^\mu q^\nu + \frac{\mathcal{W}_5}{m_N^2}\left(p^\mu q^\nu + q^\mu q^\nu\right) + i\frac{\mathcal{W}_6}{m_N^2}\left(p^\mu q^\nu - q^\mu p^\nu\right).\end{aligned} \tag{5.10}$$

The structure functions $\mathcal{W}_i$ contain the hadronic interactions within the nucleus including the excitation to resonants, for example the Δ^{++}. With this definition the cross section is given by

$$\begin{aligned}\frac{\mathrm{d}\sigma}{\mathrm{d}Q^2\mathrm{d}W} =& \frac{G_F^2|V_{ud}|^2}{4\pi}\frac{W}{m_N E^2}\left\{\mathcal{W}_1(Q^2+m_\mu^2)\right.\\ &+ \frac{\mathcal{W}_2}{m_N^2}\left[2(k\cdot p)(k'\cdot p) - \frac{m_N^2}{2}(Q^2+m_\mu^2)\right]\\ &- \frac{\mathcal{W}_3}{m_N^2}\left[Q^2(k\cdot p) - \frac{1}{2}(q\cdot q)\left(Q^2+m_\mu^2\right)\right]\\ &\left.- \frac{\mathcal{W}_4}{m_N^2}m_\mu^2\frac{Q^2+m_\mu^2}{2} - 2\frac{\mathcal{W}_5}{m_N^2}m_\mu^2(k\cdot p)\right\}.\end{aligned} \tag{5.11}$$

The structure functions $\mathcal{W}_i$ themselves depend on hadronic kinematics and several form factors (see appendix A of [157] for exact formulae). In general, there are three vector form factors C_i^V with $i = 3, 4, 5$ and four axial form factors C_i^A with $i = 3, 4, 5, 6$ whose functional form rely on empirical models fitted by experimental data. A recent analysis [159] proposes the following values and functional forms for the delta resonance:

$$C_3^V = \frac{2.13}{\left(1 + \frac{Q^2}{M_V^2}\right)^2} \frac{1}{1 + \frac{Q^2}{4M_V^2}} \tag{5.12}$$

$$C_4^V = \frac{-1.51}{\left(1 + \frac{Q^2}{M_V^2}\right)^2} \frac{1}{1 + \frac{Q^2}{4M_V^2}} \tag{5.13}$$

$$C_5^V = \frac{0.48}{\left(1 + \frac{Q^2}{M_V^2}\right)^2} \frac{1}{1 + \frac{Q^2}{0.776M_V^2}} \tag{5.14}$$

$$C_5^{A\Delta} = \frac{1.2}{\left(1 + \frac{Q^2}{M_A^2}\right)^2} \frac{1}{1 + \frac{Q^2}{3M_A^2}} \tag{5.15}$$

$$C_6^{A\Delta} = \frac{m_N^2}{Q^2 + m_\pi^2} C_5^{A\Delta} \tag{5.16}$$

with $M_V = 0.84\,\mathrm{GeV}$ and $M_A = 1.05\,\mathrm{GeV}$. The proportionality of the induced pseudoscalar C_6^A to C_5^A and the pion pole is a consequence of PCAC (see section 5.2). The superscript Δ denotes that the $Q^2 = 0$ value has been determined by the Goldberger-Treiman relation [160]

$$C_5^{A\Delta}(0) = \frac{f_\pi g_\Delta}{\sqrt{3}} \approx 1.2, \tag{5.17}$$

where $g_\Delta = 15.3\,\mathrm{GeV}^{-1}$ and $f_\pi = 0.97 m_\pi$ with m_π being the pion mass (see appendix A of [159] for derivation).

The remaining axial form factors have found to be in good agreement with:

$$C_3^A = 0 \qquad\qquad C_4^A = -\frac{C_5^A}{4}. \tag{5.18}$$

The dominant contributions to the cross section are given by C_3^V and C_5^A. The important structure functions are $\mathcal{W}_1$, $\mathcal{W}_2$ and $\mathcal{W}_3$. The contributions of $\mathcal{W}_4$ and $\mathcal{W}_5$ to the cross section are proportional to the muon mass squared and are therefore of minor importance (see equation (5.11)).The relative contributions of the individual structure functions and form factors to the total cross section are illustrated in figure 5.3 for $E_\nu = 1\,\mathrm{GeV}$. Note that $\mathcal{W}_1$ can be associated with $(C_3^V)^2$, $\mathcal{W}_2$ with $(C_5^A)^2$ and $\mathcal{W}_3$ with

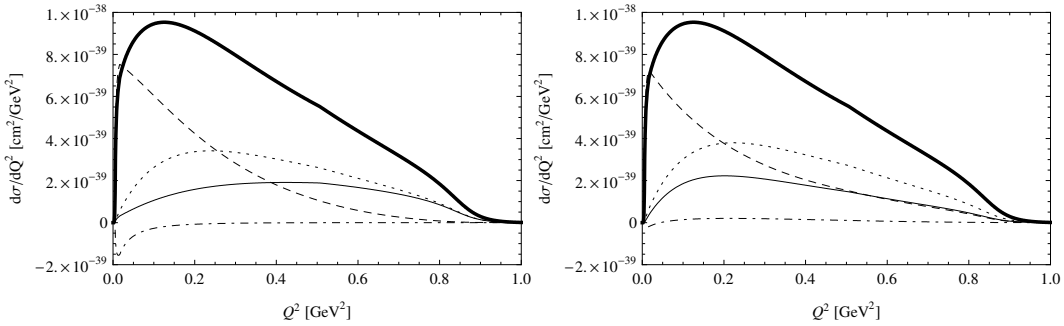

Figure 5.3: Relative contributions to the cross section of each individual structure function (left) and form factor (right) at $E = 1\,\mathrm{GeV}$ within the model [157]. The form factors used are from [159] (see equations (5.14) and (5.18)). Thick line: total cross section; thin line: $\mathcal{W}_1$ $((C_3^V)^2)$; dashed line: $\mathcal{W}_2$ $((C_5^A)^2)$; dotted line: $\mathcal{W}_3$ $(C_3^V C_5^A)$; dash-dotted line: remaining terms.

the vector-axialvector-interference term $C_3^V C_5^A$. The remaining structure functions and form factors give very small contributions.

The vector current form factors have been determined with good accuracy because the conserved vector current (CVC) hypothesis relates it directly to electroproduction data which is well measured. They have been determined in [159] and were applied in [161–163], for instance. The CVC has been used to calculate the hadronic structure as mentioned in the appendix of [159].

The axial vector form factors are different as they cannot be determined in the same way. They are usually assumed to have a modified dipole form and their parameters are fitted to match the data. In contrast to the vector current, the axial current and its matrix elements are not related to another observable quantity. There is only PCAC which gives relations at small values of Q^2. This is also the region where the axial contributions are most important. Therefore, it can be used to eliminate the difference between predictions of cross sections and experimental measurements [161,164].

In the next section, a method based on PCAC is developed, which avoids the necessity of form factors and hence, together with the CVC formalism for the vector current, increases the accuracy of the theory at small Q^2 with fewer free parameters.

5.2 PCAC approach

Calculating the cross section for small Q^2 is particularly cumbersome because many quantities such as momentum transfer Q^2, pion mass m_π and the mass of the muon m_μ are all of the same order of magnitude. The approach we will follow in this section was first derived in [165] and later applied in [166] for calculating coherent pion production by neutrinos. In

this method the leptonic current is expanded in four polarization vectors. Here we will neglect contributions of the two transverse polarizations as the amplitude for $Ap \to p\pi$ was found to be primarily longitudinal [167]. The remaining polarization vectors are the scalar polarization

$$\epsilon_l^\mu = \frac{q^\mu}{\sqrt{Q^2}} \tag{5.19}$$

and the helicity $\lambda = 0$ polarization

$$\epsilon_0^\mu = \frac{1}{\sqrt{Q^2}} \left(|\vec{q}|\,, \;\; 0, \;\; 0, \;\; q_0 \right). \tag{5.20}$$

The spin averaged absolute squared Matrix element consists of a leptonic ($T_{\mu\nu}$) and a hadronic ($\mathcal{W}^{\mu\nu}$) tensor:

$$\overline{|\mathcal{M}|^2} \propto T_{\mu\nu}\mathcal{W}^{\mu\nu}. \tag{5.21}$$

As the kinematics of the leptonic current is identical to the one in the previous section the leptonic tensor is has already been defined in equation (5.9).

Projecting this tensor onto the polarization vectors leads to the following density matrix elements:

$$\tilde{L}_{00} = \epsilon_{0\mu}^* T^{\mu\nu} \epsilon_{0\nu} = 2 \left[\frac{\left[Q^2(2E_\nu - \nu) - m_\mu^2 \right]^2}{Q^2\left(Q^2 + \nu^2\right)} - Q^2 - m_\mu^2 \right] \tag{5.22}$$

$$\tilde{L}_{ll} = \epsilon_{l\mu}^* T^{\mu\nu} \epsilon_{l\nu} = 2m_\mu^2 \frac{Q^2(2E_\nu - \nu) - \nu m_\mu^2}{Q^2\sqrt{Q^2 + \nu^2}} \tag{5.23}$$

$$\tilde{L}_{l0} = -\epsilon_{l\mu}^* T^{\mu\nu} \epsilon_{0\nu} = 2m_\mu^2 \left(1 + \frac{m_\mu^2}{Q^2} \right). \tag{5.24}$$

The minus sign in $\tilde{L}_{l0}$ comes from the mixing of space- and timelike polarization vectors.

Handling the hadronic tensor and its projections is more difficult. Here, we will use the PCAC hypothesis to calculate the needed matrix element $\langle \Delta^{++} | \mathcal{A}_\mu^+ | p \rangle$ for the production of the delta resonance. We introduce the PCAC relations according to [168, 169]. As the axial current produces the pion we identify the divergence of the current with the pion field ϕ_π:

$$\partial^\mu \mathcal{A}_\mu^+ = f_\pi m_\pi^2 \phi_\pi \tag{5.25}$$

with the couling constant $f_\pi = 93\,\mathrm{MeV}$. The current is partially conserved because the divergence differs from zero only by the relatively small pion mass. In this case we obtain useful results as $q^2 \to 0$.

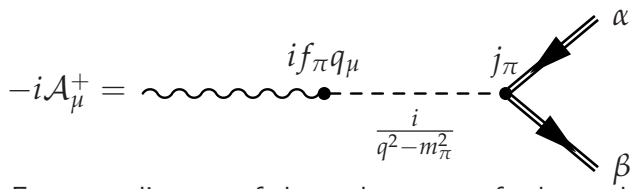

Figure 5.4: Feynman diagram of the replacement of a boson by a pion scattering on external hadronic states.

In applications we need the pion source j_π, which we obtain by using the Klein-Gordon equation in momentum space:

$$\left(-q^2 + m_\pi^2\right) \phi_\pi(q) = j_\pi(q). \tag{5.26}$$

We rewrite next equation (5.25):

$$\partial^\mu \mathcal{A}_\mu^+ = -f_\pi \frac{m_\pi^2}{q^2 - m_\pi^2} j_\pi(q). \tag{5.27}$$

For small Q^2 the Feynman diagram depicted in figure 5.4 leads to the following matrix element of the axial current:

$$-i \left\langle \beta \left| \mathcal{A}_\mu^+ \right| \alpha \right\rangle = \left(i f_\pi q_\mu\right) \left(\frac{i}{q^2 - m_\pi^2}\right) \langle \beta \,|\, j_\pi(q) \,|\, \alpha \rangle + \left\langle \beta \left| \mathcal{R}_\mu \right| \alpha \right\rangle. \tag{5.28}$$

Here $\mathcal{R}_\mu$ is the additional smooth contribution beyond the dominating pion pole. The divergence of the matrix element of an axial current between two arbitrary external states (α and β) can be replaced by the product of the four-momentum-transfer q^μ with the matrix element of the current:

$$\left\langle \beta \left| \partial^\mu \mathcal{A}_\mu^+ \right| \alpha \right\rangle = -i q^\mu \left\langle \beta \left| \mathcal{A}_\mu^+ \right| \alpha \right\rangle. \tag{5.29}$$

Taking the divergence of equation (5.28) and using equation (5.27) for the left-hand side we obtain an Adler-like relation:

$$-f_\pi \frac{m_\pi^2}{q^2 - m_\pi^2} \langle \beta \,|\, j_\pi(q) \,|\, \alpha \rangle = -f_\pi \frac{q^2}{q^2 - m_\pi^2} \langle \beta \,|\, j_\pi(q) \,|\, \alpha \rangle + q^\mu \left\langle \beta \left| \mathcal{R}_\mu \right| \alpha \right\rangle \tag{5.30}$$

$$\Leftrightarrow \qquad q^\mu \left\langle \beta \left| \mathcal{R}_\mu \right| \alpha \right\rangle = f_\pi \langle \beta \,|\, j_\pi(q) \,|\, \alpha \rangle. \tag{5.31}$$

With these equations we project next the hadronic current onto the polarization vectors:

$$\epsilon_0^\mu \left\langle \beta \left| \mathcal{A}_\mu^+ \right| \alpha \right\rangle = i \epsilon_0^\mu \left\langle \beta \left| \mathcal{R}_\mu \right| \alpha \right\rangle \tag{5.32}$$

$$\approx \frac{i}{\sqrt{Q^2}} q^\mu \left\langle \beta \left| \mathcal{R}_\mu \right| \alpha \right\rangle + \mathcal{O}\left(\frac{Q^2}{\nu^2}\right) \tag{5.33}$$

$$= \frac{i f_\pi}{\sqrt{Q^2}} \langle \beta \,|\, j_\pi(q) \,|\, \alpha \rangle. \tag{5.34}$$

Note, that the pion pole in equation (5.32) vanishes exactly due to the orthogonality of ϵ_0^μ and q^μ. Then we approximate in equation (5.33) the polarization vector ϵ_0^μ with $q_\mu/\sqrt{Q^2}$, which is satisfied for $\nu^2 \gg Q^2$. In the last step we used equation (5.31).

Because the remaining polarization vector ϵ_l^μ is proportional to q^μ we use equations (5.27) and (5.29) and obtain the exact relation

$$\epsilon_l^\mu \left\langle \beta \left| \mathcal{A}_\mu^+ \right| \alpha \right\rangle = -\frac{i f_\pi}{\sqrt{Q^2}} \frac{m_\pi^2}{q^2 - m_\pi^2} \left\langle \beta \left| j_\pi(q) \right| \alpha \right\rangle . \tag{5.35}$$

Since we separated the pion pole in equations (5.28) and (5.30) we expect that the remaining amplitudes will vary smoothly with Q^2 for $Q^2 \approx m_\pi^2$.

With these equations we are able to calculate the contribution of the axial current to the cross section:

$$\frac{\mathrm{d}\sigma^A}{\mathrm{d}Q^2\mathrm{d}\nu} = \frac{G_F^2 |V_{ud}|^2}{8\pi^2} \frac{\nu}{E_\nu^2} \frac{f_\pi^2}{Q^2} \left\{ \tilde{L}_{00} + 2\tilde{L}_{l0} \frac{m_\pi^2}{Q^2 + m_\pi^2} + \tilde{L}_{ll} \left(\frac{m_\pi^2}{Q^2 + m_\pi^2} \right)^2 \right\} \sigma\left(\pi^+ \alpha \to \beta\right) . \tag{5.36}$$

As the pion source yields the cross section $\sigma\left(\pi^+ \alpha \to \beta\right)$, the neutrino production cross section is a reflection of pion-target scattering. Note, that the pion energy has to be identified with the invariant mass W. The contributions of $\tilde{L}_{ll}$ and $\tilde{L}_{l0}$ are proportional to the m_μ^2 and will therefore be neglected when calculating the axial contribution of the pion energy spectra in section 5.6. However, for all differential cross sections $\mathrm{d}\sigma/\mathrm{d}Q^2$ we apply the full cross section including all terms.

Now we turn to the production of the delta resonance on a proton:

$$\frac{\mathrm{d}\sigma^A(\nu_\mu p \to \mu^- \Delta^{++})}{\mathrm{d}Q^2\mathrm{d}\nu} = \frac{G_F^2 |V_{ud}|^2}{8\pi^2} \frac{\nu}{E_\nu^2} \frac{f_\pi^2}{Q^2} \tilde{L}_{00} \sigma\left(\pi^+ p \to \Delta^{++}\right) . \tag{5.37}$$

Here we will use experimental data [170] because the pion cross section $\sigma\left(\pi^+ p \to \Delta^{++}\right)$ has been measured with high accuracy. Later, for calculating charge exchange processes we will use data [171] for the cross sections $\pi^- p \to \pi^0 n \;\Leftrightarrow\; \pi^+ n \to \pi^0 p$ which already includes nonresonant background for this channel.

Next we compare the PCAC result with the traditional form factor approach for the delta resonance. Thus we use the definition of the current given in equations (2.7) and (2.8) of [157] and keep only the axial terms that

do not vanish when projected onto ϵ_0^μ:

$$\left\langle \Delta^{++} \,\middle|\, \mathcal{A}_\mu^+ \,\middle|\, p \right\rangle = \sqrt{3}\overline{\psi}_\mu(p')u(p)C_5^A(Q^2) + \sqrt{3}\overline{\psi}_\lambda q^\lambda u(p) q_\mu \frac{C_6^A(Q^2)}{m_N^2} \tag{5.38}$$

$$= \sqrt{3}\overline{\psi}_\mu(p')u(p)C_5^A(Q^2) + \sqrt{3}\overline{\psi}_\lambda(p')q^\lambda u(p)\left[\frac{-if_\pi q_\mu}{q^2 - m_\pi^2}\left\langle \Delta^{++} \,\middle|\, j_\pi \,\middle|\, p \right\rangle + q_\mu g(q^2)\right]. \tag{5.39}$$

Here we have written the pion pole explicitly and denoted the smooth background by the function $g(q^2)$. Comparing this with equation (5.28) we identify the remainder:

$$\left\langle \Delta^{++} \,\middle|\, \mathcal{R}_\mu \,\middle|\, p \right\rangle = -i\sqrt{3}\overline{\psi}_\mu(p')u(p)C_5^A(Q^2) - i\sqrt{3}\overline{\psi}_\lambda(p')q^\lambda u(p) q_\mu g(q^2). \tag{5.40}$$

The relevant contribution according to equation (5.31) for the cross section comes from

$$q^\mu \left\langle \Delta^{++} \,\middle|\, \mathcal{R}_\mu \,\middle|\, p \right\rangle = f_\pi \left\langle \Delta^{++} \,\middle|\, j_\mu \,\middle|\, p \right\rangle \tag{5.41}$$

$$= -i\sqrt{3}\overline{\psi}_\mu(p')q^\mu u(p)\left[C_5^A(Q^2) + q^2 g(q^2)\right] \tag{5.42}$$

and consequently contains both terms from $C_5^A(Q^2)$ and part of $C_6^A(Q^2)$. For $q^2 \approx \mathcal{O}(m_\pi^2)$ the term $q^2 g(q^2)$ will be small and vanishes for $Q^2 \to 0$. This shows that in this limit $C_5^A(0)$ is determined by PCAC. This is known as the off-diagonal Goldberger-Treiman relation [160].

We have shown the equivalence of the PCAC based cross section equation (5.37) and the form factor ansatz of equation (5.11) within the PCAC domain. As PCAC is valid for $\nu^2 \gg Q^2$ and energies $E_\nu \sim \mathcal{O}(1\,\mathrm{GeV})$ the validity is restricted to the low momentum transfer region

$$Q^2 \lesssim 0.2\,\mathrm{GeV}^2. \tag{5.43}$$

5.3 Adler sum rule

A crucial test of neutrino-nucleon scattering reactions is the Adler sum rule [172,173] that follows from current algebra and is valid for all momentum transfers:

$$\left[g_A(Q^2)\right]^2 + \int_{\nu_{\mathrm{th}}}^{\infty} \mathrm{d}\nu \left[\mathcal{W}_{2,\nu n}^A - \mathcal{W}_{2,\nu p}^A\right] = 1. \tag{5.44}$$

The subscript of structure functions denotes whether the neutrino scatters off a proton or neutron. The quantity $g_A(Q^2)$ is the $\langle p|\mathcal{A}_\mu^+|n\rangle$ vertex and is

given by

$$g_A(Q^2) = \frac{-1.26}{\left(1 + \frac{Q^2}{M_A^2}\right)^2} \tag{5.45}$$

with the axial mass $M_A = 1.0\,\mathrm{GeV}$.

By comparing the PCAC cross section equation (5.37) with the parametrized cross section equation (5.11) we find in for $m_\mu \to 0$:

$$\mathcal{W}^A_{2,\nu p/n} = \frac{2f_\pi^2}{\pi} \frac{\nu}{Q^2 + \nu^2} \sigma\left(\pi^+ p/n \to X^{++}\right). \tag{5.46}$$

Thus the Adler sum rule reads

$$\left[g_A(Q^2)\right]^2 + \frac{2f_\pi^2}{\pi} \int_{\nu_{\mathrm{th}}}^{\infty} \mathrm{d}\nu \frac{\nu}{Q^2 + \nu^2} \left[\sigma_{\pi^- p}(\nu) - \sigma_{\pi^+ p}(\nu)\right] = 1. \tag{5.47}$$

For $Q^2 \to 0$ this equation reduces to the Adler-Weisberger relation [172, 174].

As data we use the large compilation given by the PDG [170]. As there is no direct measurement of $\pi^+ n$ scattering as requested in equation (5.46) we use $\pi^- p$ scattering data which are identical by isospin rotation.

The limits of the integration are

$$\nu_{\mathrm{th}} = \frac{m_\pi^2 + 2m_N m_\pi + q^2}{2m_N} < \nu < 1.6\,\mathrm{GeV}, \tag{5.48}$$

where we have truncated the integral to restrict ourselves to the delta resonance. The numerical results of each term of equation (5.47) are shown in figure 5.5. At higher values of Q^2 the contributions defined in equation (5.47) do not match the sum rule due to increasing contributions from high energy processes (HE) like multipion production. In addition to resonance production (RES) and quasi-elastic scattering (QE) the remaining difference gives an insight into the Q^2 dependence of HE contribution.

However, in an independent approach the HE part was determined by interpolating the quark distribution functions to the small Q^2 region [175].

The suggested formula for the HE contributions is [176]:

$$\delta\mathcal{W}_2^A = \mathrm{HE} = 2\frac{Q^2 + 0.19}{Q^2 + 0.29} - \frac{Q^2 + 0.25}{Q^2 + 0.20}, \tag{5.49}$$

where Q^2 is given in GeV. As seen in figure 5.5 this model matches the sum rule with remarkable accuracy. For low momentum-transfers it is negligible and the value of the Adler sum of 1.016 at $Q^2 = 0$ states the precision of our PCAC ansatz.

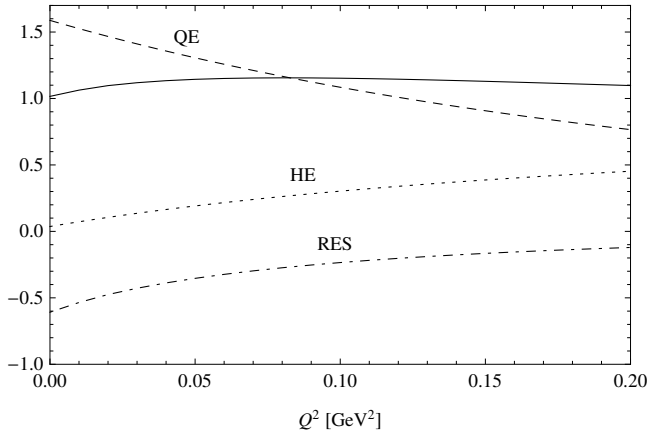

Figure 5.5: Solid line: Sum of the contributions to the Adler sum rule; dashed line: form factor g_A contribution; dotted-dashed line: integrated resonance contribution; dotted line: high energy contributions (Bodek-Yang interpolation).

5.4 Differential cross section

Having the axial part of the cross section for the neutrino production of the delta resonance in form of equation (5.37) at hand we are now able to calculate the differential cross section $\mathrm{d}\sigma/\mathrm{d}Q^2$. For that purpose we combine both the form factor and the PCAC approach to obtain a full description. However, we are still restricted to the low Q^2 region. Following the idea to use the best theory (for example with less free parameters and more accurate input data) for each part of the cross section, we declare our procedure as follows:

1. Use for the axial current the PCAC relation of equation (5.37) with the appropriate data as input.

2. For all vector and the additional axial contributions use the form factor approach of equation (5.11) with the form factors given in equations (5.12-5.16) except the contribution of $(C_5^A)^2$ to avoid double counting the PCAC cross section.

3. Extract the values $C_5^A(Q^2)$ from the PCAC formula and then use it as an input for the vector-axialvector interference terms in equation (5.11).

This way we avoid the uncertainty of the C_5^A functional form and parameters by using experimental inputs with high statistics. The vector form factors have been sufficiently determined. Thus the final step is to extract numerical values of the axial form factor C_5^A from the PCAC formula equation (5.37).

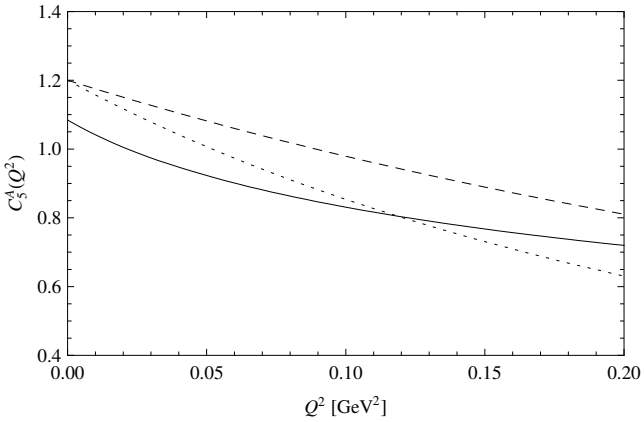

Figure 5.6: Comparison of different $C_5^A(Q^2)$ shapes. Solid line: extracted from PCAC formalism, dashed: as defined in equation (5.15), dotted: as used in [157]: $C_5^A(Q^2) = 1.2(1 + {}^{Q^2}/_{M_A^2})^{-2}(1 + {}^{2Q^2}/_{M_A^2})^{-1}$.

Therefore, we start by keeping solely the axial contribution of $\mathcal{W}_2$ from equation (A.2) from [157]

$$\mathcal{W}_2^A = 2\frac{m_N^2}{M_R^2}\left(C_5^A\right)^2 [\nu + m_N + M_R]\,\delta\left(W^2 - M_R^2\right) \tag{5.50}$$

where M_R is the mass of the resonance. For the delta function we use the Breit-Wiegner form (equation (2.6) of [157])

$$\delta\left(W^2 - M_R^2\right) = \frac{M_R\Gamma_R}{\pi}\frac{1}{(W^2 - M_R^2)^2 + M_R^2\Gamma_R^2} \tag{5.51}$$

where Γ_R the decay width given by equation (2.13) of [157]:

$$\Gamma_R = \Gamma_0\left(\frac{p_\pi(W)}{p_\pi(M_R)}\right)^3 \tag{5.52}$$

with Γ_0 the experimental decay width of the resonance. The pion momentum is given by

$$p_\pi(W) = \frac{1}{2W}\sqrt{\left(W^2 - m_N^2 - m_\pi^2\right) - 4m_N^2 m_\pi^2}. \tag{5.53}$$

With these definitions we integrate the structure function of equation (5.50) over ν in the same range as at the Adler sum and equating this with the same integral over the PCAC relation equation (5.46) we obtain numerical values of $C_5^A(Q^2)$ as shown in figure 5.6. Here two additional common functional forms of C_5^A have been plotted for comparison.

Again we use data for the cross section $\pi^+ p \to \Delta^{++}$ as the non-resonant background of this reaction is small. This is confirmed by a phase-shift

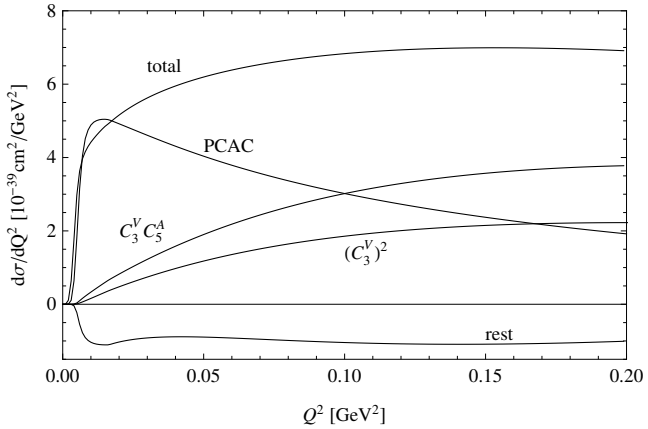

Figure 5.7: Contributions to the total cross section at $E_\nu = 1\,\mathrm{GeV}$ with no cuts.

analysis of pion nucleon scattering [177] (see table IV and figure 2 of this reference). Additional $I = 3/2$ resonances next to the $P_{33}(1232)$ delta resonance are $P_{33}(1600)$, $S_{31}(1620)$ and $D_{33}(1700)$ whose masses are separated from the delta resonance resulting in negligible contributions in our energy domain.

Note, that the $Q^2 = 0$ value

$$C_5^A(Q^2 = 0) = 1.08 \tag{5.54}$$

is in good agreement with the predicted value 1.2 of the off-diagonal Goldberger-Treiman relation. Many groups [178–182] rely on this relation using the value 1.2 while some [162, 163] prefer smaller values down to 0.87 due to calculations from experimental data. This small value has been corrected to a larger value $C_5^A(0) = 1.10 \pm 0.08$ after studies of backgrounds and a simultaneous fit of both BNL and ANL data [179, 180].

Compiling all parts we are now able to calculate the differential cross section $\mathrm{d}\sigma/\mathrm{d}Q^2$. This is shown exemplarily in figure 5.7 for a fixed neutrino energy $E_\nu = 1\,\mathrm{GeV}$. Here the three major contributions are shown separately, together with minor contributions from the remaining terms, and they add up to the total cross section.

As the cross section has been calculated only for neutrinos scattering on protons we can compare it to experimental measurements from old bubble chamber experiments [183, 184] where the data is directly given per nucleon. In contrast, later experiments use complex nuclear targets for which our calculation has to be extended by isospin rotations (see section 5.5) and nuclear corrections for pion rescattering (see section 5.7). In figure 5.8 we compare the measurement [183] of the Argonne experiment (ANL). Here we weighted the theoretical prediction with the ANL flux and performed a $W < 1.4\,\mathrm{GeV}$ cut as this was done in the experimental analysis as well. Figure 5.9 shows a similar comparison with the Brookhaven (BNL) experiment. We calculated the measured cross section from the event rates given

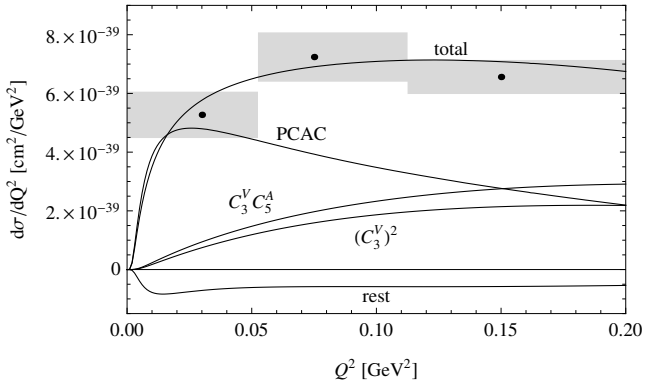

Figure 5.8: Contributions to the total cross section for the reaction $\nu_\mu p \to \mu^- p\pi^+$ with the ANL flux with $W < 1.4\,\mathrm{GeV}$.

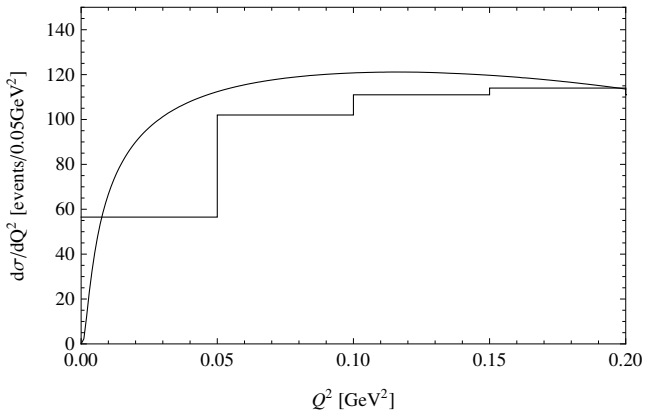

Figure 5.9: Contributions to the total cross section for the BNL flux with $W < 1.4\,\mathrm{GeV}$.

in [184] by using the transformation coefficient derived in [163]. Both predictions are close to the experimental data. Note, that we did not include nonresonant background in our calculations for the channel $\nu_\mu p \to \mu^- p\pi^+$ because in electroproduction the analyses [185, 186] found in comparison of the channels $ep \to ep\pi^0$ and $ep \to en\pi^+$ the nonresonant background is less than 10%. In our case there is only the $I = 3/2$ amplitude.

Finally, we compare our prediction with the high energy neutrino beam of the Fermilab (FNAL) 15-ft bubble chamber measurement [187] at $E_\nu = 25\,\mathrm{GeV}$. Again the prediction is in good agreement with the experimental data as shown in figure 5.10.

5.5 Isospin relations

In the previous section we have discussed the cross section of neutrinos scattering off protons. Today's experiments are sensitive to various reactions such as the scattering of both neutrinos and anti-neutrinos via

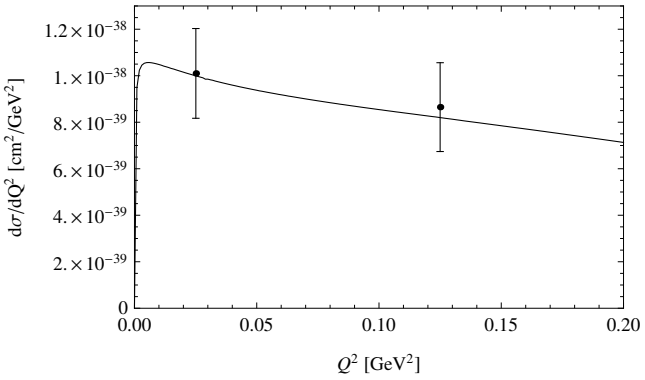

Figure 5.10: Total cross section for the FNAL 15-ft experiment with $W < 1.4\,\mathrm{GeV}$. The neutrino energy is fixed at $E_\nu = 25\,\mathrm{GeV}$.

charged (CC) as well as neutral currents (NC). Furthermore, the target consists of more complex nuclear materials, for example mineral oil, where also neutrons contribute. In this section we will derive estimates of these cross sections from isospin rotations of the particle and gauge multiplets. We use the multiplets in the following form:

$$I = \frac{1}{2}: \qquad \begin{pmatrix} p \\ n \end{pmatrix} \qquad \begin{matrix} I_3 = +1/2 \\ I_3 = -1/2 \end{matrix} \tag{5.55}$$

$$I = 1: \qquad \begin{pmatrix} W^+ \\ W^0 \\ W^- \end{pmatrix} \qquad \begin{matrix} I_3 = +1 \\ I_3 = 0 \\ I_3 = -1 \end{matrix} . \tag{5.56}$$

We start by defining our reference amplitude of the neutrino proton CC production of any $I = 3/2$ resonance X with the definition $J^+ = J^1 + iJ^2$:

$$\left\langle X^{++} \,\middle|\, J^+ \,\middle|\, p \right\rangle = \sqrt{2} \left\langle X^+ + \left| \frac{1}{\sqrt{2}} \left(J^1 + iJ^2 \right) \right| p \right\rangle \tag{5.57}$$

$$= \sqrt{2} a_{\frac{3}{2}} \equiv \text{ ref.} \tag{5.58}$$

For the reaction with anti-neutrinos $\overline{\nu}_\mu p \to \mu^+ X^0$ we get

$$\left\langle X^+ \,\middle|\, J^- \,\middle|\, p \right\rangle = \sqrt{2} \left[\frac{1}{\sqrt{3}} a_{\frac{3}{2}} - \sqrt{\frac{2}{3}} a_{\frac{1}{2}} \right] \tag{5.59}$$

$$= \frac{1}{\sqrt{3}} \text{ ref} - \frac{2}{\sqrt{3}} a_{\frac{1}{2}}. \tag{5.60}$$

We will keep only the $I = 3/2$ amplitudes leading to an overall factor of $\frac{1}{\sqrt{3}}$ to the amplitudes derived in the previous section regarding the reaction

$\nu_\mu p \to \mu^- X^{++}$. Furthermore, the sign of $\mathcal{W}_3$ must be inverted for all anti-neutrino induced reaction due to its interference nature.

Turning to the neutron amplitudes we get by rotation for $\nu_\mu n \to \mu^- X^+$:

$$\left\langle X^+ \,\middle|\, J^+ \,\middle|\, n \right\rangle = \sqrt{2}\left[\frac{1}{\sqrt{3}} a_{\frac{3}{2}} + \sqrt{\frac{2}{3}} a_{\frac{1}{2}}\right] \tag{5.61}$$

$$= \frac{1}{\sqrt{3}}\,\text{ref} + \frac{2}{\sqrt{3}} a_{\frac{1}{2}}, \tag{5.62}$$

and for $\overline{\nu}_\mu n \to \mu^+ X^-$

$$\left\langle X^- \,\middle|\, J^- \,\middle|\, n \right\rangle = \sqrt{2} a_{\frac{3}{2}} = \text{ ref}, \tag{5.63}$$

where, again, the sign of $\mathcal{W}_3$ has to be inverted.

Before relating the NC cross sections to the reference amplitude, the currents must be treated differently, raising from the NC Hamiltonian

$$\mathcal{H}_{\text{eff.}} = \frac{G_F}{\sqrt{2}} \overline{\nu} \gamma^\mu \left(1 - \gamma_5\right) \nu \left[x V_\mu^3 + y A_\mu^3 + \gamma V_\mu^0\right], \tag{5.64}$$

where $x = 1 - 2\sin^2\theta_W$, $y = -1$ and $\gamma = -\frac{2}{3}\sin^2\theta_W$ with θ_W being the Weinberg angle. Consequently, the vector and axial-vector parts, for example form factors, must be scaled accordingly:

$$\left\langle X^+ \,\middle|\, J_\mu^{NC} \,\middle|\, p \right\rangle = x \left\langle X^+ \,\middle|\, V_\mu^3 \,\middle|\, p \right\rangle + y \left\langle X^+ \,\middle|\, A_\mu^3 \,\middle|\, p \right\rangle + \gamma \left\langle X^+ \,\middle|\, V_\mu^0 \,\middle|\, p \right\rangle. \tag{5.65}$$

This leads to the following Clebsch-Gordan coefficients (CGC) for proton scattering

$$\left\langle X^+ \,\middle|\, V_\mu^3 \,\middle|\, p \right\rangle = \left\langle X^+ \,\middle|\, A_\mu^3 \,\middle|\, p \right\rangle = \sqrt{\frac{2}{3}} a_{\frac{3}{2}\mu} - \frac{1}{\sqrt{3}} a_{\frac{1}{2}\mu} \tag{5.66}$$

$$= \frac{1}{\sqrt{3}}\,\text{ref} - \frac{1}{\sqrt{3}} a_{\frac{1}{2}\mu} \tag{5.67}$$

and for neutron scattering

$$\left\langle X^0 \,\middle|\, V_\mu^3 \,\middle|\, n \right\rangle = \sqrt{\frac{2}{3}} a_{\frac{3}{2}\mu} + \frac{1}{\sqrt{3}} a_{\frac{1}{2}\mu} \tag{5.68}$$

$$= \frac{1}{\sqrt{3}}\,\text{ref} + \frac{1}{\sqrt{3}} a_{\frac{1}{2}\mu}. \tag{5.69}$$

Neglecting $I = 1/2$ contributions the cross section for NC on proton and neutron are equal. As the NC is its own isospin rotated counterpart, the cross section for anti-neutrinos contains the same coefficients as for neutrinos. However, the sign of $\mathcal{W}_3$ is inverted for anti-neutrinos. Note also,

reaction	current	$\mathcal{W}_3\times$	m_ℓ	CGC	$C_i^A\times$	$C_i^V\times$
$\nu_\mu p \to \mu^- X^{++}$	CC	+1	m_μ	1	1	1
$\overline{\nu}_\mu p \to \mu^+ X^0$	CC	-1	m_μ	$1/\sqrt{3}$	1	1
$\nu_\mu n \to \mu^- X^+$	CC	+1	m_μ	$1/\sqrt{3}$	1	1
$\overline{\nu}_\mu n \to \mu^+ X^-$	CC	-1	m_μ	1	1	1
$\nu_\mu p \to \nu_\mu X^+$	NC	+1	0	$1/\sqrt{3}$	y	x
$\overline{\nu}_\mu p \to \overline{\nu}_\mu X^+$	NC	-1	0	$1/\sqrt{3}$	y	x
$\nu_\mu n \to \nu_\mu X^0$	NC	+1	0	$1/\sqrt{3}$	y	x
$\overline{\nu}_\mu n \to \overline{\nu}_\mu X^0$	NC	-1	0	$1/\sqrt{3}$	y	x

Table 5.1: Summary of changes for various reactions regarding to neutrino proton scattering as derived in section 5.4. CGC denotes the overall factor given by the Clebsch-Gordan coefficients derived in the text and $C_i^{A(V)}\times$ the factors for each axial (vector) form factor.

that for NC reactions the outgoing lepton mass m_ℓ is vanishing because the neutrino remains a neutrino whereas in CC reactions it turns into a charged lepton.

These CGCs, form factor scaling factors and other properties are summarized in table 5.1. As in experiments only the decay products of the produced resonances are measured, the additional CGCs for the subsequent reactions have to be included. They are listed in table 5.2 and will be discussed in section 5.7 .

For comparison of the various differential cross sections $\mathrm{d}\sigma/\mathrm{d}Q^2$ for pion productions, figure 5.11 shows the charged current and figure 5.12 the neutral current reactions for an exemplary neutrino energy of $E_\mu = 1\,\mathrm{GeV}$.

As shown in figure 5.7 the vector and the axial-vector-vector interference contributions are of comparable size. Thus for anti-neutrino reactions, where the interference term is inverted, they cancel each other with only a small remainder. As a consequence, these reactions are dominated by the axial contribution offering tests for various axial models including our PCAC approach. By choosing the corresponding input data for charge-exchange cross sections, nonresonant background is already included in the PCAC contribution avoiding tedious additional calculations, as needed in other approaches.

5.6 Pion spectra

In order to experimentally identify and measure the reactions considered, it is necessary to calculate the energy spectrum and the angular distribution of the produced pions. These quantities – pion energy and angle – are measured in the laboratory frame. As our cross section in the form of

reaction	CGC
$\Delta^{++} \to p\pi^+$	1
$\Delta^{+} \to p\pi^0$	$\sqrt{2/3}$
$\Delta^{+} \to n\pi^+$	$\sqrt{1/3}$
$\Delta^{0} \to p\pi^-$	$\sqrt{1/3}$
$\Delta^{0} \to n\pi^0$	$\sqrt{2/3}$
$\Delta^{-} \to n\pi^-$	1

Table 5.2: Decays of the delta resonances and their Clebsch-Gordan coeffcients.

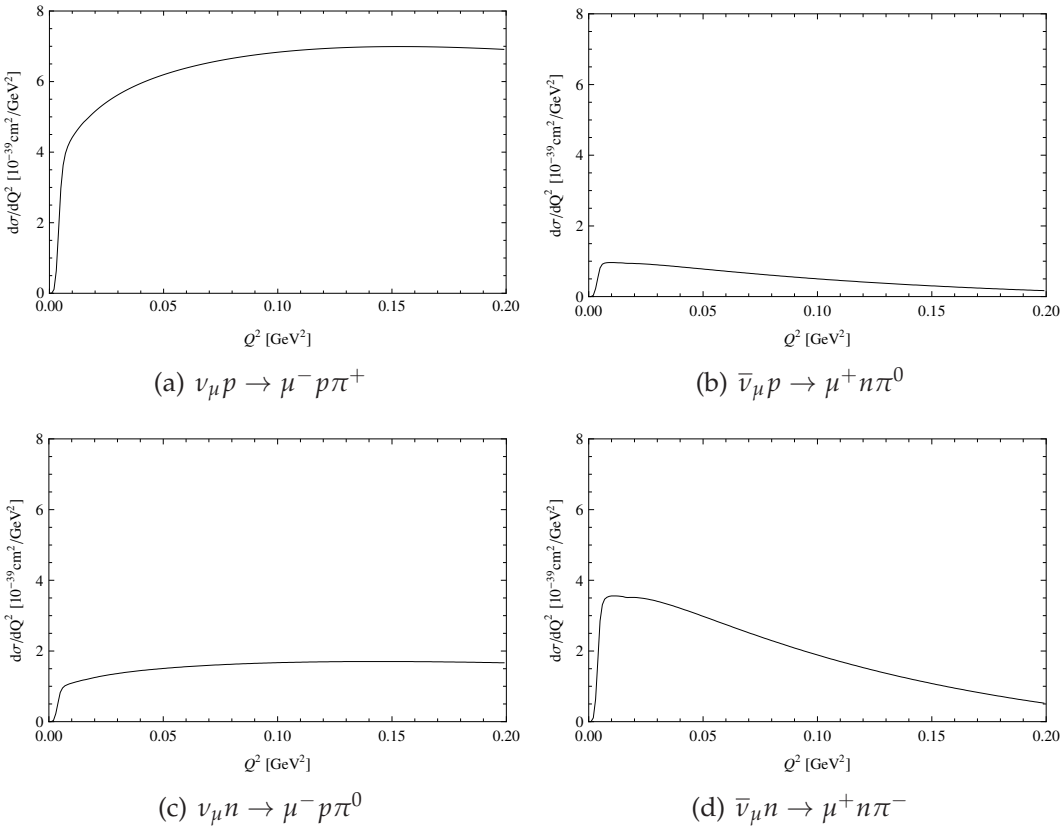

(a) $\nu_\mu p \to \mu^- p\pi^+$ (b) $\overline{\nu}_\mu p \to \mu^+ n\pi^0$

(c) $\nu_\mu n \to \mu^- p\pi^0$ (d) $\overline{\nu}_\mu n \to \mu^+ n\pi^-$

Figure 5.11: Charged current differential cross sections for $E_\nu = 1\,\mathrm{GeV}$.

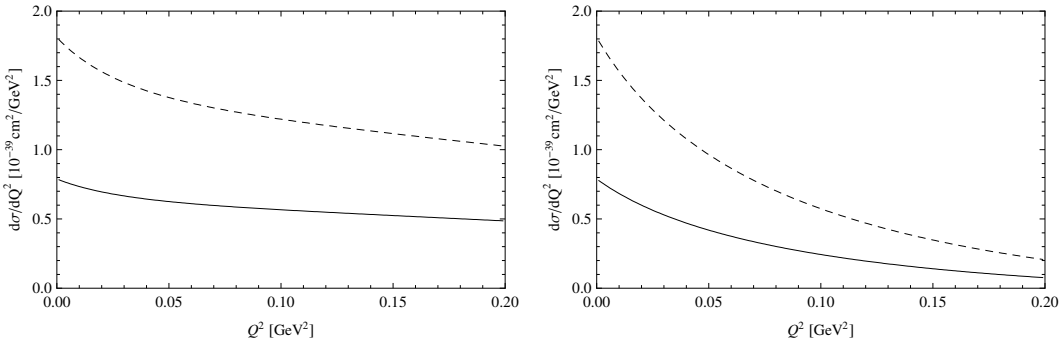

(a) $\nu_\mu p(n) \to \nu_\mu n\pi^+(p\pi^-)$ (solid)
$\nu_\mu p(n) \to \nu_\mu p\pi^0(n\pi^0)$ (dashed)

(b) $\overline{\nu}_\mu p(n) \to \overline{\nu}_\mu n\pi^+(p\pi^-)$ (solid)
$\overline{\nu}_\mu p(n) \to \overline{\nu}_\mu p\pi^0(n\pi^0)$ (dashed)

Figure 5.12: Neutral current reactions at $E_\nu = 1\,\mathrm{GeV}$.

equation (5.37) factorizes the leptonic and the hadronic part in terms of the cross section $\sigma_{\pi^+ p}$ we first have to derive the pion spectrum for this part.

The angular distribution is given by [188]:

$$\frac{\mathrm{d}\sigma}{\mathrm{d}\Omega_{\mathrm{cm}}} = \sigma_{\pi^+ p}(W)\frac{1+3\cos^2\theta_{\mathrm{cm}}}{8\pi} \tag{5.70}$$

where the subscript cm denotes that the differential cross section is in the center of mass frame. To obtain the corresponding observables and cross sections in the laboratory frame (lab) we calculated the corresponding Lorentz boost (see appendix). The cross section $\sigma_{\pi^+ p}(W)$ is, again, given by experimental data [170].

Including the differential form of the pion cross section we can write down the axial part of the triple differential cross section

$$\frac{\mathrm{d}\sigma^A\left(E_\nu, Q^2, W, E_\pi^{\mathrm{lab}}\right)}{\mathrm{d}Q^2\mathrm{d}W\mathrm{d}E_\pi^{\mathrm{lab}}} = \frac{G_F^2|V_{ud}|^2}{8\pi^2}\frac{W}{m_N}\left(\frac{\nu}{E_\nu^2}\frac{\tilde{L}_{00}}{Q^2}f_\pi^2\right)\frac{\mathrm{d}\sigma_{\pi^+ p}(W)}{\mathrm{d}E_\pi^{\mathrm{lab}}}. \tag{5.71}$$

This cross section is shown in figure 5.13 for some fixed values as a function of W. Note, that the irregular form reflects the experimental data as the invariant mass is directly related to the pion energy as indicated in equation (5.53).

First, we integrate over W. The integration limits are given by

$$W^2 = m_N^2 - m_\pi^2 + 2(m_N+\nu)E_\pi^{\mathrm{lab}} - 2\sqrt{Q^2+\nu^2}\,p_\pi^{\mathrm{lab}}\cos\theta_{\mathrm{lab}}. \tag{5.72}$$

considering forward-/backward scattering. The resulting double differential cross sections are given in figure 5.14 as a function of pion energy E_π^{lab} and in figure 5.15 as a function of Q^2.

An interesting question is the difference between muon and electron neutrino induced cross sections. Now having a formalism for the cross

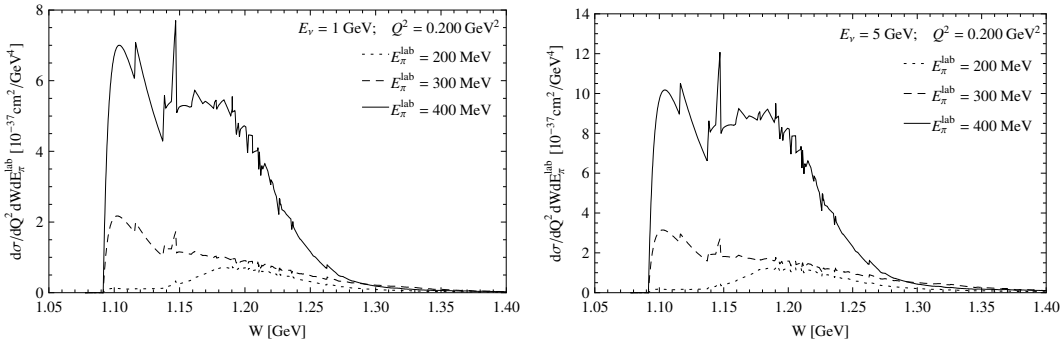

(a) $E_\nu = 1$ GeV (b) $E_\nu = 5$ GeV

Figure 5.13: Differential cross section.

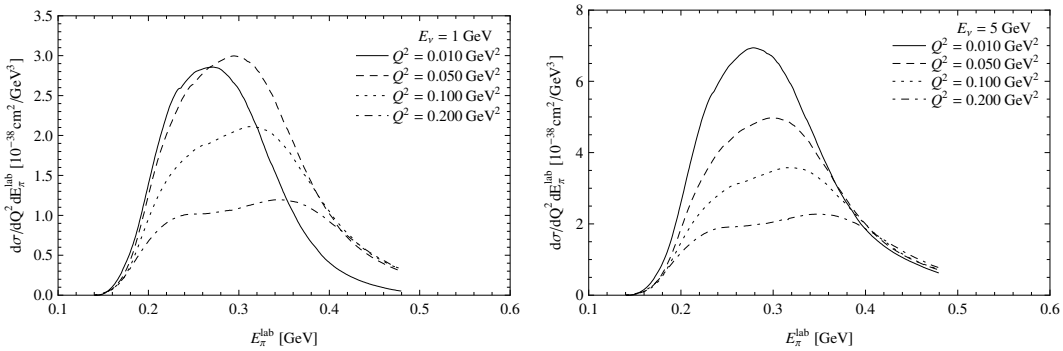

(a) $E_\nu = 1$ GeV (b) $E_\nu = 5$ GeV

Figure 5.14: Differential cross section after W-integration for fixed momentum transfers Q^2

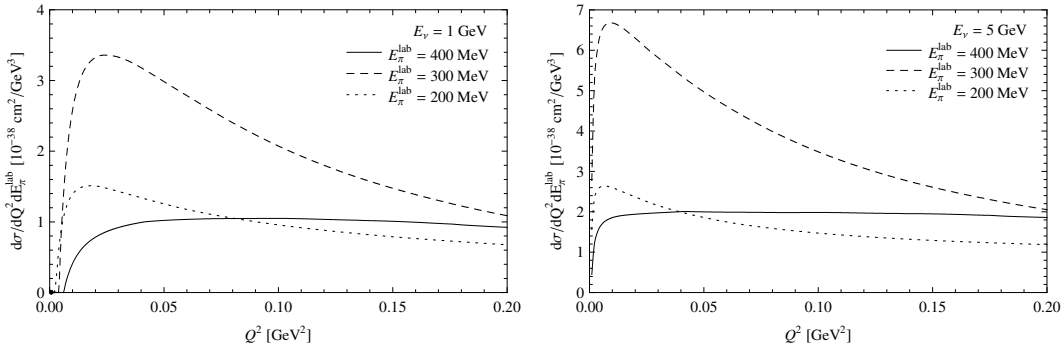

(a) $E_\nu = 1$ GeV (b) $E_\nu = 5$ GeV

Figure 5.15: Differential cross section after W-integration for fixed pion energies E_π^{lab}.

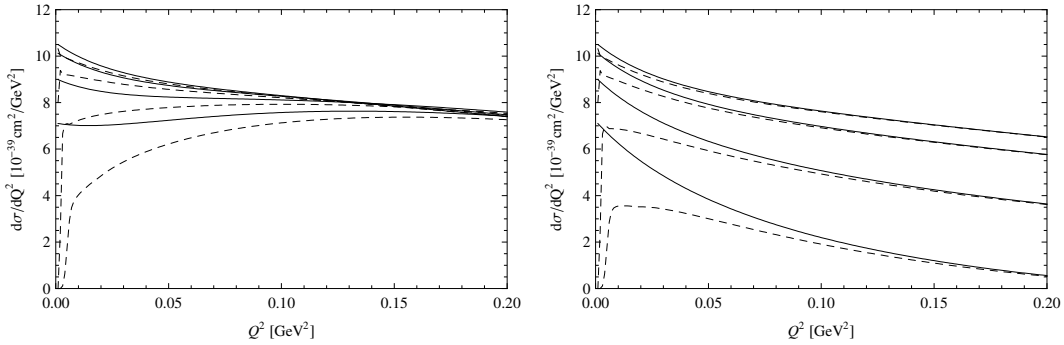

(a) $\nu_\ell p \to \ell^- \Delta^{++}$ (b) $\overline{\nu}_\ell n \to \ell^+ \Delta^-$

Figure 5.16: Comparison of muon (solid) and electron (dashed) neutrino or antineutrino cross section for various energies $E_{\nu,\overline{\nu}} = 1, 2, 5, 10\,\text{GeV}$ (bottom to top).

sections at hands, we can use the full cross section given by equation (5.36) and the contributions from all terms – vector, axial and interference – in order to calculate $\mathrm{d}\sigma/\mathrm{d}Q^2$ for the two cases. The results are shown in figure 5.16. The impact of the neutrino mass is, as expected, smaller for larger momentum transfers and neutrino energies. Furthermore, the neutrino and antineutrino cross sections merge together for $Q^2 \to 0$.

5.7 Nuclear corrections

For calculating the cross section of pion production by neutrinos scattering off complex nuclei, for example carbon CH_2 at MiniBooNE, one has to consider each process that occurs. The dominant channel is the pion production via the delta resonance. Thus we can divide our treatment in the following subsequent steps:

1. The neutrino interacts with a proton or neutron of the nucleus and produces the delta resonance.

2. The resonance decays into pions.
3. The pions may rescatter on other constituents of the nucleus and get emitted.

The MiniBooNE collaboration measured the production of charged pions (π^+) [189] and neutral pions [190] via CC neutrino interactions. The first step, obtaining the cross sections on protons and neutrons, has been computed in the previous sections. Next we consider the decay of the produced delta resonances. For this we introduce the particle multiplets

$$I = \frac{3}{2}: \qquad \begin{pmatrix} \Delta^{++} \\ \Delta^{+} \\ \Delta^{0} \\ \Delta^{-} \end{pmatrix} \qquad \begin{matrix} I_3 = +3/2 \\ I_3 = +1/2 \\ I_3 = -1/2 \\ I_3 = -3/2 \end{matrix} \tag{5.73}$$

$$I = 1: \qquad \begin{pmatrix} \pi^{+} \\ \pi^{0} \\ \pi^{-} \end{pmatrix} \qquad \begin{matrix} I_3 = +1 \\ I_3 = 0 \\ I_3 = -1 \end{matrix} . \tag{5.74}$$

There are three reactions that produce pions:

$$\nu_\mu p \to \mu^- \Delta^{++} \to \mu^- p \pi^+ \tag{5.75}$$

$$\nu_\mu n \to \mu^- \Delta^{+} \to \mu^- p \pi^0 \tag{5.76}$$

$$\nu_\mu n \to \mu^- \Delta^{+} \to \mu^- n \pi^+. \tag{5.77}$$

As mentioned earlier, table 5.2 shows all the decays of the delta resonance and their Clebsch-Gordan coefficients.

Without nuclear corrections one could, in principle, build the incoherent sum of all nucleons of the CH_2 molecule. However, most of the pions are produced within the large carbon nucleus and might rescatter before leaving it. Thus the the pions produced in the decay of the resonances, the initial pions π_i, partially produce in subsequent reactions different pions π_f with altered quantum numbers (for example I_3). We will follow the model of Adler, Nussinov and Paschos (ANP) [191] that is based on an idea of Fermi [192] for neutron diffusion. It solves the problem of rescattering by a stochastic consideration, as described in [193]. Within the nucleus, the pion is considered to be able to move one scattering mean free path l_f in a random direction. If, after this length, it is still located within the nucleus, it has a probability $1/N$ of being captured. If this is not the case, this pattern repeats as long as either the pion left the nucleus or it is finally captured. In a one-dimensional toy model with only one direction z the probability $P_f(z)$ of escaping the nucleus is then given by the differential equation [193]

$$P_f(z) = \frac{1}{2} \mathrm{e}^{-\frac{-z}{l_f}} + \frac{N-1}{2N l_f} \int_0^a P_f(z') \mathrm{e}^{-\frac{|z-z'|}{l_f}} \mathrm{d}z', \tag{5.78}$$

where the first term is the direct escape of the pion and the last term contains the rescattering probability. However, the ANP model [191] employs elaborate assumptions on scatterings and three-dimensional nuclei for calculating the nuclear corrections. Note, that the ANP model follows the assumption that the rescattering can be separated from the leptonic part, making the nuclear corrections only dependent on the kinematics of the produced pions and the properties of the target material. Then the initially produced pions can be altered by either scattering within the nucleus or being absorbed. The detected pions π_f are therefore reduced by absorption by Pauli blocking, expressed by the absorption coefficient A and the charges twisted, expressed by the material dependent rotation matrix M. The analysis showed the following ansatz for the nuclear corrections and values for the charge-exchange matrix for carbon [194]:

$$\begin{pmatrix} \pi_f^+ \\ \pi_f^0 \\ \pi_f^- \end{pmatrix} = M(C_6^{12}) \begin{pmatrix} \pi_i^+ \\ \pi_i^0 \\ \pi_i^- \end{pmatrix} = A(Q^2) \begin{pmatrix} 0.83 & 0.14 & 0.04 \\ 0.14 & 0.73 & 0.14 \\ 0.04 & 0.14 & 0.83 \end{pmatrix} \begin{pmatrix} \pi_i^+ \\ \pi_i^0 \\ \pi_i^- \end{pmatrix}. \quad (5.79)$$

The absorption A is difficult to determine and depend on Q^2:

$$A(Q^2 = 0.05\,\mathrm{GeV}^2) = 0.71 \quad (5.80)$$

$$A(Q^2 = 0.20\,\mathrm{GeV}^2) = 0.79 \quad (5.81)$$

$$A(Q^2 = 0.40\,\mathrm{GeV}^2) = 0.81. \quad (5.82)$$

Due to nondiagonal elements of the matrix M also reactions producing initial π^0 particles, see equation (5.76), contribute to the total π^+ cross section on carbon. The final yield of π^+ for the CH_2 molecule is indicated by $\Sigma^f_{\pi^+}$ and is obtained from

$$\Sigma^f_{\pi^+} = A(Q^2)\left\{0.83\left[\Sigma^p_{\pi^+} + \Sigma^n_{\pi^+}\right] + 0.14\Sigma^n_{\pi^0}\right\}6 + 2\Sigma^p_{\pi^+} \quad (5.83)$$

$$. \quad (5.84)$$

The last term $2\Sigma^p_{\pi^+}$ includes the scattering on H_2 which, for the scales of the problems, is far away from the carbon. The cross sections within the brackets are defined as

$$\Sigma^p_{\pi^+} = \frac{\mathrm{d}\overline{\sigma}}{\mathrm{d}Q^2}\left(\nu_\mu p \to \mu^- p\pi^+\right) \quad (5.85)$$

$$\Sigma^n_{\pi^+} = \frac{\mathrm{d}\overline{\sigma}}{\mathrm{d}Q^2}\left(\nu_\mu n \to \mu^- n\pi^+\right) \quad (5.86)$$

$$\Sigma^n_{\pi^0} = \frac{\mathrm{d}\overline{\sigma}}{\mathrm{d}Q^2}\left(\nu_\mu n \to \mu^- p\pi^0\right) \quad (5.87)$$

which we call the initial or primitive cross sections. The bars over the cross sections indicate averaging over the flux for $0.50\,\mathrm{GeV} \leq E_\nu \leq 2.00\,\mathrm{GeV}$ as indicated in the experimental analysis [189].

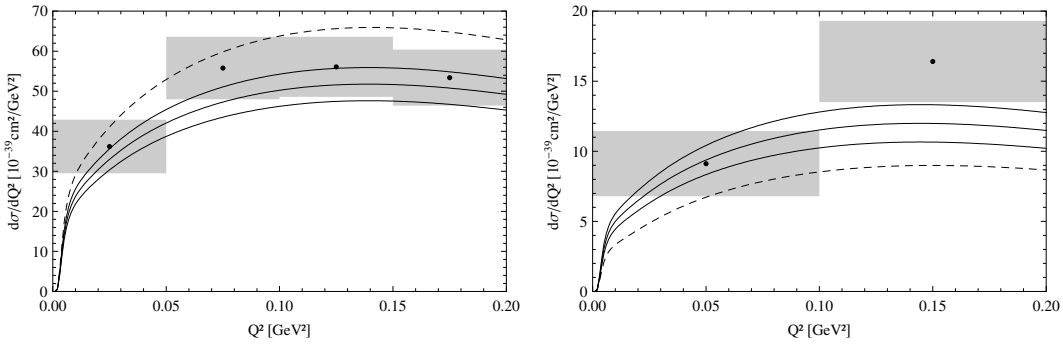

(a) π^+ yield (b) π^0 yield

Figure 5.17: Total flux weighted charged and neutral pion cross sections for the MiniBooNE experiment with $W < 1.4\,\mathrm{GeV}$. Nuclear corrections with $A = 1.0$, 0.9 and 0.8 (top to bottom). The dashed curve represents the cross section without nuclear corrections.

We are now able to calculate the cross section for charged current neutrino induced π^+ production on CH_2. The result is shown in figure 5.17(a) for different absorption coefficients and also without nuclear corrections. The corrections lower the cross section but still keeping them in agreement with the experimental measurement [189]. To take into account the $I = 1/2$ background for the vector current, we augmented the C_3^V form factor by 5% in these plots, which is a rather conservative estimate [185].

With the same method we calculate the cross section and nuclear corrections to the MiniBooNE measurement of neutral pion production [190]. Here the final yield $\Sigma^f_{\pi^0}$ of π^0:

$$\Sigma^f_{\pi^0} = A(Q^2)\left\{0.73\Sigma^n_{\pi^0} + 0.14\left[\Sigma^p_{\pi^+} + \Sigma^n_{\pi^+}\right]\right\} 6. \tag{5.88}$$

The primitive cross sections are identical to the ones in the charged pion yield. The flux averaged cross section for π^0 production at MiniBooNE is presented in figure 5.17(b) in comparison to the experimental data [190].

The curves indicating the cross sections without nuclear corrections are obtained by choosing the transport matrix in equation (5.79) as the unity matrix. Although the neutral pion cross section does not agree with the data as accurate as the charged pion cross section does, it still remains in close agreement, considering the larger errors and kinematic bins. Note, that for the charged pion cross section, the nuclear corrections decrease the yields, whereas for neutral pions the yields are increased. This is understood from figures 5.11. The π^+ cross sections themselves are larger than the π^0 cross sections resulting in this feature by the composition of the final yields. This feeding of the neutral pion yield by initial charged pions is essential.

Interestingly, the most frequently used event generator GiBUU [195] contradicts this feature [196–199] leading to predictions well below the experimental data. In both charged and neutral pion production their uncorrected cross sections match better with the data than the corrected ones, which, in both cases, are too small.

5.8 CP searches

The relations and yields of pions in neutrino oscillation experiments can help to determine the rather unknown CP phase of the PMNS matrix. To see the impact of such a CP violating phase we first examine the structure of the PMNS matrix.

The neutrino mixing matrix matrix U is constructed considering the charged current Lagrangian

$$\mathcal{L}_{\mathrm{cc}} = \frac{g}{\sqrt{2}} \sum_{\ell} \sum_{\alpha} U_{\ell\alpha} \bar{\ell}_L \gamma^{\mu} \nu_{\alpha L} W_{\mu}^{-} + \text{ h. c.}. \tag{5.89}$$

Following the argumentation of [111, 200, 201], we assume, for now, n generations of neutrinos. Then the unitary matrix U has n^2 entries, namely $\frac{1}{2}n(n-1)$ mixing angles and $\frac{1}{2}n(n+1)$ phases. However, as for Dirac neutrinos the Lagrangian (5.89) is invariant under the transformations

$$\nu_{\alpha L} \to \mathrm{e}^{i\theta_\alpha} \nu_{\alpha L} \qquad\qquad U_{\ell\alpha} \to \mathrm{e}^{-i\theta_\alpha} U_{\ell\alpha} \tag{5.90}$$

so that n phases of the mixing matrix can be absorbed by neutrino fields. Additionally, n phases can be absorbed by the charged lepton fields by the rephasings

$$\ell_L \to \mathrm{e}^{i\phi_\ell} \ell_L \qquad\qquad U_{\ell\alpha} \to \mathrm{e}^{i\phi_\ell} U_{\ell\alpha}. \tag{5.91}$$

Considering the constraint $\theta_\alpha = \phi_\ell$ these redefinitions eliminate $2n-1$ unphysical phases leaving

$$\frac{1}{2}(n-1)(n-2) \tag{5.92}$$

physical phases for Dirac neutrinos. Therefore, CP violation is only possible for $n > 2$.

In the case of Majorana neutrinos the phases cannot be absorbed into the neutrino fields, as done in equation (5.90) for Dirac neutrinos, because Majorana fields are self-conjugate. Therefore, the number of phases for Majorana neutrinos is

$$\frac{1}{2}n(n-1). \tag{5.93}$$

As a consequence, CP violation is already possible for $n > 1$.

However, in neutrino oscillation parameters the only exists one CP phase δ which is the Dirac phase. The Majorana phases are only present in LNV processes, such as $0\nu\beta\beta$. The common parametrization of the PMNS matrix is as follows:

$$U = \begin{pmatrix} 1 & 0 & 0 \\ 0 & c_{23} & s_{23} \\ 0 & -s_{23} & c_{23} \end{pmatrix} \begin{pmatrix} c_{13} & 0 & s_{13}e^{-i\delta} \\ 0 & 1 & 0 \\ -s_{13}e^{i\delta} & 0 & c_{13} \end{pmatrix} \begin{pmatrix} c_{12} & s_{13} & 0 \\ -s_{12} & c_{12} & 0 \\ 0 & 0 & 1 \end{pmatrix} \tag{5.94}$$

$$= \begin{pmatrix} c_{12}c_{13} & s_{12}c_{13} & s_{13}e^{-i\delta} \\ -s_{12}c_{23} - c_{12}s_{23}s_{13}e^{i\delta} & c_{12}c_{23} - s_{12}s_{23}s_{13}e^{i\delta} & s_{23}c_{13} \\ s_{12}s_{23} - c_{12}c_{23}s_{13}e^{i\delta} & -c_{12}s_{23} - s_{12}c_{23}s_{13}e^{i\delta} & c_{23}c_{13} \end{pmatrix}, \tag{5.95}$$

where $s_{ij} = \sin\theta_{ij}$ and $c_{ij} = \cos\theta_{ij}$.

The most recent fits of the mixing angles and mass differences (assuming normal hierarchy) are [202]:

$$\sin^2\theta_{12} = 0.30 \pm 0.013 \tag{5.96}$$

$$\sin^2\theta_{23} = 0.41^{+0.037}_{-0.025} \tag{5.97}$$

$$\sin^2\theta_{13} = 0.023 \pm 0.0023 \tag{5.98}$$

$$\Delta m^2_{21} = (7.50 \pm 0.185) \cdot 10^{-5}\,\mathrm{eV}^2 \tag{5.99}$$

$$\Delta m^2_{31} = 2.47^{+0.069}_{-0.067} \cdot 10^{-3}\,\mathrm{eV}^2. \tag{5.100}$$

The CP phase δ remains unconstrained within its errors.

With these definitions and the values at hand the oscillation probability of a neutrino of flavor α to flavor β is given by

$$P(\nu_\alpha \to \nu_\beta) = \left| \sum_j U^*_{\alpha j} U_{\beta j} e^{-i\frac{m_j^2}{2E}L} \right|^2 \tag{5.101}$$

$$= \delta_{\alpha\beta} - 4\sum_{i>j} \Re\left[U^*_{\alpha i}U_{\alpha j}U_{\beta i}U^*_{\beta j}\right] \sin^2\left(\frac{\Delta m^2_{ij}}{4E}L\right) + 2\sum_{i>j} \Im\left[U^*_{\alpha i}U_{\alpha j}U_{\beta i}U^*_{\beta j}\right] \sin\left(\frac{\Delta m^2_{ij}}{2E}L\right). \tag{5.102}$$

Here the mass squared difference is defined as $\Delta m^2_{ij} \equiv m^2_i - m^2_j$. Its baseline dependence for a maximal CP phase is shown in figure 5.18(a).

To measure CP violation with fixed detectors one can use the difference of neutrino and antineutrino oscillation originating from the CP phase. This difference is defined and given by [203]:

$$\Delta P_{\nu\bar{\nu}\alpha\beta} \equiv P(\nu_\alpha \to \nu_\beta) - P(\overline{\nu}_\alpha \to \overline{\nu}_\beta) \tag{5.103}$$

$$= -16 J_{\alpha\beta} \sin\Delta_{12} \sin\Delta_{23} \sin\Delta_{31}, \tag{5.104}$$

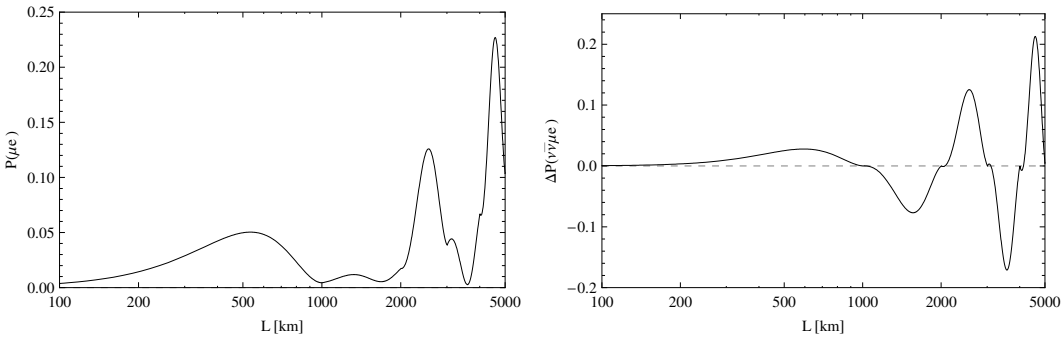

(a) $P(\nu_\mu \to \nu_e)$ (b) $\Delta P_{\nu\bar{\nu}}(\mu e)$

Figure 5.18: Baseline dependence of probabilities at a beam energy of $E_\nu = 1\,\mathrm{GeV}$ assuming a maximal CP phase $\delta = \frac{\pi}{2}$.

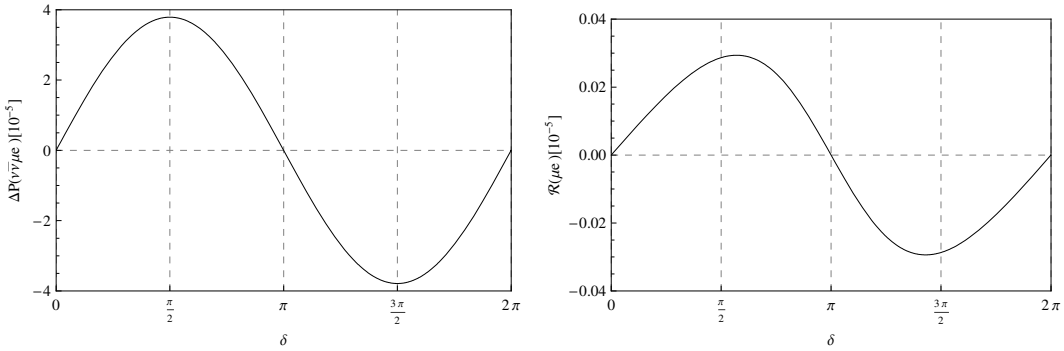

(a) $\Delta P_{\nu\bar{\nu}}(\mu e)$ (b) $\mathcal{R} = \frac{\Delta P_{\nu\bar{\nu}}(\mu e)}{P(\nu_\mu \to \nu_e) + P(\bar{\nu}_\mu \to \overline{\nu u}_e)}$.

Figure 5.19: Probabilities at the MINOS average beam energy of $E_\nu = 17\,\mathrm{GeV}$ with a baseline of $L = 731\,\mathrm{km}$ depending on δ.

where $\Delta_{ij} \equiv \frac{\Delta m^2_{ij} L}{4E}$ and $J_{\alpha\beta} = \pm J$ with positive sign for cyclic and negative sign for anticyclic permutation of flavors and

$$J \equiv s_{12} c_{12} s_{23} c_{23} s_{13} c^2_{13} \sin\delta. \tag{5.105}$$

This difference of neutrino and antineutrinos is shown in figure 5.18(b). To exemplify the impact of varying δ we show this quantity in figure 5.19 with the MINOS experiment specifications.

Next, we will develop a way to help determining the CP phase δ. We will make use of the charge symmetries derived in the previous chapter 5.7 and extend them to antineutrinos in order to calculate the yields of pions from neutrino and antineutrinos.

To calculate the yields of final state pions we collect the appropriate CGCs from tables 5.1 and 5.2 and obtain, for instance, the π^+ production

reactions	yields π^+	π^0	π^-	standard cross section
charged currents				
$\nu_\mu(p+n)$	0.953	0.318	0.075	$\sigma(\nu_\mu p \to \mu^- \Delta^{++})$
$\overline{\nu}_\mu(p+n)$	0.075	0.318	0.953	$\sigma(\overline{\nu}_\mu n \to \mu^+ \Delta^-)$
neutral currents				
$\nu_\mu(p+n)$	0.473	1.06	0.473	$\sigma(\nu_\mu p \to \nu_\mu \Delta^+)$
$\overline{\nu}_\mu(p+n)$	0.473	1.06	0.473	$\sigma(\overline{\nu}_\mu p \to \overline{\nu}_\mu \Delta^+)$

Table 5.3: Yields for neutrinos and antineutrinos including nuclear corrections.

cross section in terms of our standard cross section:

$$\sigma(\nu_\mu n \to \mu^- \Delta^+ \to \mu^- n \pi^+) = \frac{1}{9}\sigma(\nu_\mu p \to \mu^- \Delta^{++}). \tag{5.106}$$

Similarly, we collect the yields taking all reaction into account:

$$\begin{pmatrix} \pi_i^+ \\ \pi_i^0 \\ \pi_i^- \end{pmatrix}_{(p+n)} = \begin{pmatrix} \frac{10}{9} \\ \frac{2}{9} \\ 0 \end{pmatrix} \sigma(\nu_\mu p \to \mu^- \Delta^{++}). \tag{5.107}$$

This we use as the initial vector of equation 5.79 and, calculating the product with the transition matrix, we arrive at:

$$\begin{pmatrix} \pi_f^+ \\ \pi_f^0 \\ \pi_f^- \end{pmatrix}_{(p+n)} = A \begin{pmatrix} 0.953 \\ 0.318 \\ 0.075 \end{pmatrix} \sigma(\nu_\mu p \to \mu^- \Delta^{++}). \tag{5.108}$$

For antineutrinos we obtain initial pion vector:

$$\begin{pmatrix} \pi_i^+ \\ \pi_i^0 \\ \pi_i^- \end{pmatrix}^{\text{anti}}_{(p+n)} = \begin{pmatrix} 0 \\ \frac{2}{9} \\ \frac{10}{9} \end{pmatrix} \sigma(\overline{\nu}_\mu n \to \mu^+ \Delta^-) \tag{5.109}$$

yielding

$$\begin{pmatrix} \pi_f^+ \\ \pi_f^0 \\ \pi_f^- \end{pmatrix}^{\text{anti}}_{(p+n)} = A \begin{pmatrix} 0.075 \\ 0.318 \\ 0.953 \end{pmatrix} \sigma(\overline{\nu}_\mu n \to \mu^+ \Delta^-), \tag{5.110}$$

where the standard cross section is chosen to be $\overline{\nu}_\mu n \to \mu^+ \Delta^-$. We summarize these yields in table 5.3.

Interestingly, the yields of neutrinos and antineutrinos are inverted. This fact, which is a consequence of charge symmetry, leads to

$$\left(\frac{\pi^+}{\pi^0}\right)_\nu = \left(\frac{\pi^-}{\pi^0}\right)_{\overline{\nu}}, \tag{5.111}$$

which does hold beyond the domain of our PCAC calculation, as it follows from a general statement originating from charge symmetry. A deviation from this would be a hint of CP violation. The advantage of the quantity in equation (5.111) is that the standard cross section is canceled out minimizing theoretical uncertainties. Furthermore, we find that this relation holds for all isoscalar target for which the nuclear corrections of neutrinos and antineutrinos are the same and the yields factorize into nuclear correction times standard cross section.

In the following we sketch a procedure to track CP violation in long baseline oscillation experiments:

- Measure various reactions at the nearby detector and determine the neutrino and antineutrino fluxes as well as the pion yields.
- Measure charge related processes at the far away detector and check ratios à la equation (5.111).
- Use the determined fluxes of muon neutrino and antineutrinos from the nearby detector and match the measured electron neutrino and antineutrino flxues at the far away detector by varying the CP phase δ as indicated in figure 5.19.

5.9 Summary

In this chapter we calculated the cross section for hadron production by neutrino scattering. In section 5.1 we revisited the common Lorentz invariant ansatz of expressing the hadronic tensor in terms of form factors. Their functional forms are still rather unknown and are determined by comparison with experimental data. As in the case of the axial form factors the statistics of the experiments is too limited to make strong statements. Albeit good agreement with measurements of the cross sections, except in the low Q^2 region, they remain artificially constructed and lack of deeper physical motivation.

Therefore, we used a different approach for the axial part of the cross section in section 5.2. Here we decomposed the currents to polarization vectors finding the $\lambda = 0$ helicity vector to be dominating. For the projections of the hadronic currents onto these polarization vectors we made use of the PCAC hypothesis. This way we avoided the necessity of modeling the hadronic processes by relating them to well measured pion proton amplitudes. As a consequence, the axial cross section in equation (5.37) turned out to be the product of a leptonic factor and the explicit pion-proton cross section for which we use statistically accurate experimental data as input.

Section 5.3 provided a test of our PCAC formalism. The Adler sum rule requires the constancy of a defined integral over the axial structure

function which is valid for all Q^2. Thus using a model for these structure functions one can check its validity by calculating the Adler sum. It is found to be well satisfied for low Q^2 where PCAC is valid. For larger values of Q^2 the impact of uncertainty of high energy contributions rises. Using the Bodek-Yang interpolation for the high energy part again leads to a good agreement with the Adler sum rule, pointing to the validity of both the PCAC relations and the high energy interpolation.

Using the PCAC model for the axial part of the cross section and the form factor parametrization for the remaining contributions we calculated the differential cross section in section 5.4. For the vector-axial-vector interference we extracted values for the axial form factor $C_5^A(Q^2)$ from the PCAC formula. The resulting predictions show good agreement with the experimental measurements.

For comparisons with other experiments we calculated related cross sections for anti-neutrinos and neutrons targets in both charged and neutral currents in section 5.5. Here we made extensive use of Isospin rotations of the currents leading to simple relations among the cross sections derived in the previous section.

In section 5.7 nuclear corrections in the ANP model were introduced that are needed in complex nuclear targets. The pions produced by the decay of the nucleon resonances partly rescatter within the nucleus, distorting the initial pions to the measured final pions. The final cross section for neutrinos production charged pions on CH_2 measured at MiniBooNE is in agreement with our prediction.

Finally, we presented an application of the pion cross sections and nuclear corrections to *CP* searches in section 5.8. After introducting the concept of *CP* violation in neutrino oscillation experiments we showed that specific charge symmetry relations help to determine the *CP* phase.

6. Conclusions

The four fermion generation scenario is at a crossroads. With the LHC taking more and more data its fate will be sealed sooner or later. However, this time has not yet come and as the parameters get less space, new alternatives will be considered, which has already begun by turning from the simple one Higgs model to two Higgs or multi Higgs models due to the discovery of the potentially Higgs boson with small mass.

In chapter 3 of this thesis we scrutinized the contribution of the additional Majorana neutrino within the SM4 to neutrinoless double beta decay with the assumption of a nonzero PMNS matrix element U_{e4} as indicated by [102]. We find that, considering existing bounds on the 4G mass spectrum described in chapter 2, it should have already revealed itself in experiment even if relative phases to the first three generation neutrinos are taken into account. As this is not the case, we showed that this does not strictly rule out the 4G scenario or the Majorana nature of neutrinos but constrains the latter one. Therefore, we found the neutrino to be a pseudo-Dirac particle and constrained its Majorana mass resulting in figure 3.3. Furthermore, we exemplified the impact of this result on other LNV processes by finding the cross section of like-sign dilepton production heavily suppressed. Next, we showed that the dominant suppression of the PMNS matrix element rise from radiative charged lepton decays. As the small Majorana mass contradicts the common seesaw picture we proposed an extradimensional setup that significantly softens the involved coupling hierarchies and preserves the seesaw approach for the first three generations.

A very similar bound on the Majorana mass of additional neutrino species was derived in chapter 4 by investigating the potential washout by its LNV processes. Without specifying the specific model of baryogenesis we showed that a pre-existing baryon or lepton asymmetry can be preserved from erasure by light Majorana neutrinos if the Majorana mass is small enough to keep the interactions out of equilibrium for the time of the universe cooling from the GUT scale down to the EWPT. The Majorana mass is found to be less than 10 keV for an order one generic coupling. This feature does agree with the result obtained earlier. This result is also valid for sterile neutrinos such as warm dark matter candidates considering appropriate couplings.

Chapter 5 deals with neutrino-nucleus interactions, namely resonant pion production by neutrinos. This channel is of interest for oscillation experiments and still suffers from poor theoretical understanding. Therefore, we developed a new approach for calculating the dominant axial contribution by applying the PCAC hypothesis. Although this ansatz is only valid in a limited kinematic region ($Q^2 \lesssim 0.20\,\mathrm{GeV}^2$), it covers the important part of the axial contribution and may help to develop a broader model that links our approach with the common form factor ansatz. The latter one is a heuristic and artificial ansatz for this problem and suffers, in contrast to our PCAC based approach, from its number of free parameters and uncertainty of the functional forms of the form factors. We find the PCAC relation confirmed by validating the Adler sum rule for small momentum transfers. We calculated various differential cross sections that agree with available experimental data. Moreover, we presented cross sections for scatterings of neutrinos and antineutrinos on protons and neutrons with charged and neutral currents by applying isospin rotations. Then we calculated the energy spectrum of the produced pions to be tested experimentally. As modern oscillation experiments use more complex nuclear structures as targets we applied the ANP model for nuclear corrections in order to present a prediction for the cross section of neutrinos scattering off carbon nuclei. Here we found intriguing relations originating from charge symmetry that may circumvent uncertainties of neutrino cross sections by giving specific pion production ratios. These may help to determine the CP phase in the leptonic sector as it is related to deviations from these ratios.

Acknowledgments

First of all, I wish to thank my family Barbara, Günter and Rabea for their constant support, love and encouragement in every imaginable way. Not less I am grateful to Viola for being with me and for continuing to bring so much joy into my life.

My second thanks are due to my advisor Prof. H. Päs for giving me the opportunity to work in this particularly appealing field of particle theory and giving me the freedom to choose the course of my research as well as allowing me to present my results on various occasions, introducing me to the scientific community.

Furthermore, I would like to thank Prof. E. A. Paschos for giving me the opportunity to continue our work that started way back as my diploma thesis. His great experience has given me many insights in both physical issues themselves and the way of thinking in physics in general.

Last but not least I would give thanks to all other members and companions of our chair for a pleasant and delightful atmosphere and D. Pidt for helping me improve part of this thesis.

Lorentz transformation of cross sections

We define as center of mass system the frame where the resonance is at rest. In the laboratory the four-momentum of the excited resonance after the collision is

$$p'_\mu = (\nu + m_N, |\vec{q}|). \tag{1}$$

We can bring the resonance to rest by the transformation parameter

$$\beta = \frac{|\vec{q}|}{\nu + m_N} \tag{2}$$

and the corresponding

$$\gamma = \frac{1}{\sqrt{1-\beta^2}} = \frac{\nu + m_N}{W}. \tag{3}$$

In the rest frame of the resonance with its invariant mass within its width by W, the energy of the pion is

$$E_\pi^{\mathrm{cm}} = \frac{W^2 - m_N^2 + m_\pi^2}{2W}. \tag{4}$$

With this information we can relate various quantities in the two frames.

The scattering angles of the pion satisfy

$$\tan\theta_{\mathrm{lab}} = \frac{\sin\theta_{\mathrm{cm}}}{\gamma\left(\cos\theta_{\mathrm{cm}} + \gamma\frac{E_\pi^{\mathrm{cm}}}{p_\pi^{\mathrm{cm}}}\right)}. \tag{5}$$

The differential cross sections are related by

$$\frac{\mathrm{d}\sigma}{\mathrm{d}\Omega_{\mathrm{lab}}} = \frac{\mathrm{d}\sigma}{\mathrm{d}\Omega_{\mathrm{cm}}}\frac{1}{J} \tag{6}$$

and

$$\frac{\mathrm{d}\sigma}{\mathrm{d}E_\pi^{\mathrm{lab}}} = 2\pi\frac{\mathrm{d}\sigma}{\mathrm{d}\Omega_{\mathrm{lab}}}\left[\frac{(m_N+\nu)p_\pi^{\mathrm{lab}} - |\vec{q}|E_\pi^{\mathrm{lab}}\cos\theta_{\mathrm{lab}}}{|\vec{q}|(p_\pi^{\mathrm{lab}})^2}\right] \tag{7}$$

with the Jacobian J derived from the above equation

$$J = \frac{\mathrm{d}\cos\theta_{\mathrm{lab}}}{\mathrm{d}\cos\theta_{\mathrm{cm}}} = \frac{\gamma\left(1 + \frac{E_\pi^{\mathrm{cm}}}{p_\pi^{\mathrm{cm}}}\cos\theta_{\mathrm{cm}}\right)}{\left(\sin^2\theta_{\mathrm{cm}} + \gamma^2\left(\cos\theta_{\mathrm{cm}} + \frac{\beta E_\pi^{\mathrm{cm}}}{p_\pi^{\mathrm{cm}}}\right)^2\right)^{3/2}}. \tag{8}$$

Finally, we obtain

$$\frac{\mathrm{d}\cos\theta_{\mathrm{lab}}}{\mathrm{d}E_\pi^{\mathrm{lab}}} = \frac{(m_N + \nu)p_\pi^{\mathrm{lab}} - |\vec{q}|E_\pi^{\mathrm{lab}}\cos\theta_{\mathrm{lab}}}{|\vec{q}|(p_\pi^{\mathrm{lab}})^2}. \tag{9}$$

Bibliography

[1] J. Page and R. A. Plant, *Dazed and Confused*, album: *Led Zeppelin*, copyright: 1969 Atlantic Recording Corporation, publisher: Flames Of Albion Music Inc., Inspired by *J. Holmes*.

[2] J. Chadwick, *The intensity distribution in the magnetic spectrum of beta particles from radium (B + C)*, *Verh.Phys.Gesell.* **16** (1914) 383–391.

[3] W. Pauli, *Wissenschaftlicher Briefwechsel mit Bohr, Einstein, Heisenberg, u. a., Vol. II: 1930 - 1939*. Springer-Verlag, Berlin, 1985.

[4] W. Pauli, *Dear radioactive ladies and gentlemen*, *Phys.Today* **31N9** (1978) 27.

[5] E. Fermi, *Trends to a Theory of beta Radiation. (In Italian)*, *Nuovo Cim.* **11** (1934) 1–19.

[6] E. Fermi, *An attempt of a theory of beta radiation. 1.*, *Z.Phys.* **88** (1934) 161–177.

[7] J. Chadwick, *Possible existence of a neutron*, *Nature* **129** (1932) 312.

[8] J. Chadwick, *The existence of a neutron*, *Proceedings of the Royal Society of London. Series A* **136** (1932), no. 830 692–708.

[9] C. L. Cowan, F. Reines, F. B. Harrison, H. W. Kruse, and A. D. McGuire, *Detection of the free neutrino: a confirmation*, *Science* **124** (1956), no. 3212 103–104.

[10] B. Pontecorvo, *Electron and muon neutrinos*, *Sov.Phys.JETP* **10** (1960) 1236–1240.

[11] G. Danby, J. Gaillard, K. A. Goulianos, L. Lederman, N. B. Mistry, *et. al.*, *Observation of High-Energy Neutrino Reactions and the Existence of Two Kinds of Neutrinos*, *Phys.Rev.Lett.* **9** (1962) 36–44.

[12] M. L. Perl, G. Abrams, A. Boyarski, M. Breidenbach, D. Briggs, *et. al.*, *Evidence for Anomalous Lepton Production in $e^+ - e^-$ Annihilation*, *Phys.Rev.Lett.* **35** (1975) 1489–1492.

[13] **DONUT** Collaboration, K. Kodama *et. al.*, *Observation of tau neutrino interactions*, [hep-ex/0012035].

[14] **Super-Kamiokande Collaboration** Collaboration, Y. Fukuda *et. al.*, *Evidence for oscillation of atmospheric neutrinos*, *Phys.Rev.Lett.* **81** (1998) 1562–1567, [hep-ex/9807003].

[15] **Super-Kamiokande Collaboration** Collaboration, S. Fukuda *et. al.*, *Tau neutrinos favored over sterile neutrinos in atmospheric muon-neutrino oscillations*, *Phys.Rev.Lett.* **85** (2000) 3999–4003, [hep-ex/0009001].

[16] **SNO Collaboration** Collaboration, Q. Ahmad *et. al.*, *Measurement of the rate of $\nu_e + d \to p + p + e^-$ interactions produced by B-8 solar neutrinos at the Sudbury Neutrino Observatory*, *Phys.Rev.Lett.* **87** (2001) 071301, [nucl-ex/0106015].

[17] **SNO Collaboration** Collaboration, Q. Ahmad *et. al.*, *Direct evidence for neutrino flavor transformation from neutral current interactions in the Sudbury Neutrino Observatory*, *Phys.Rev.Lett.* **89** (2002) 011301, [nucl-ex/0204008].

[18] **SNO Collaboration** Collaboration, Q. Ahmad *et. al.*, *Measurement of day and night neutrino energy spectra at SNO and constraints on neutrino mixing parameters*, *Phys.Rev.Lett.* **89** (2002) 011302, [nucl-ex/0204009].

[19] **KamLAND Collaboration** Collaboration, T. Araki *et. al.*, *Measurement of neutrino oscillation with KamLAND: Evidence of spectral distortion*, *Phys.Rev.Lett.* **94** (2005) 081801, [hep-ex/0406035].

[20] **DAYA-BAY Collaboration** Collaboration, F. An *et. al.*, *Observation of electron-antineutrino disappearance at Daya Bay*, *Phys.Rev.Lett.* **108** (2012) 171803, [arXiv:1203.1669].

[21] **RENO collaboration** Collaboration, J. Ahn *et. al.*, *Observation of Reactor Electron Antineutrino Disappearance in the RENO Experiment*, *Phys.Rev.Lett.* **108** (2012) 191802, [arXiv:1204.0626].

[22] S. Weinberg, *A Model of Leptons*, *Phys.Rev.Lett.* **19** (1967) 1264–1266.

[23] P. H. Frampton, P. Q. Hung, and M. Sher, *Quarks and leptons beyond the third generation*, *Phys. Rept.* **330** (2000) 263, [hep-ph/9903387].

[24] B. Holdom *et. al.*, *Four Statements about the Fourth Generation*, *PMC Phys.* **A3** (2009) 4, [arXiv:0904.4698].

[25] S. Cetin, G. Hou, V. Ozcan, A. Rozanov, and S. Sultansoy, *Status of the Fourth Generation: A Brief Summary of B3SM-III Workshop in Four Parts*, [arXiv:1112.2907].

[26] A. Soni, *The "4th generation", $B - CP$ anomalies & the LHC*, [arXiv:0907.2057].

[27] A. Soni, A. K. Alok, A. Giri, R. Mohanta, and S. Nandi, *The Fourth family: A Natural explanation for the observed pattern of anomalies in B^-CP asymmetries*, *Phys. Lett.* **B683** (2010) 302–305, [arXiv:0807.1971].

[28] W.-S. Hou, M. Nagashima, and A. Soddu, *Large time-dependent CP violation in B_s^0 system and finite D^0 - $\bar{D}^0$ mass difference in four generation standard model*, *Phys. Rev.* **D76** (2007) 016004, [hep-ph/0610385].

[29] A. Arhrib and W.-S. Hou, *Flavor changing neutral currents involving heavy quarks with four generations*, *JHEP* **07** (2006) 009, [hep-ph/0602035].

[30] W.-S. Hou, M. Nagashima, and A. Soddu, *Difference in B^+ and B^0 direct CP asymmetry as effect of a fourth generation*, *Phys. Rev. Lett.* **95** (2005) 141601, [hep-ph/0503072].

[31] D. Choudhury and D. K. Ghosh, *A fourth generation, anomalous like-sign dimuon charge asymmetry and the LHC*, *JHEP* **02** (2011) 033, [arXiv:1006.2171].

[32] W.-S. Hou, R. S. Willey, and A. Soni, *Implications of a Heavy Top Quark and a Fourth Generation on the Decays $B \to Kl^+l^-$, $K\nu\bar{\nu}$*, *Phys. Rev. Lett.* **58** (1987) 1608.

[33] W.-S. Hou, A. Soni, and H. Steger, *Charmless decays of bottom mesons and a fourth generation*, *Phys. Rev. Lett.* **59** (1987) 1521.

[34] A. Lenz *et. al.*, *Anatomy of New Physics in B-Bbar mixing*, *Phys. Rev.* **D83** (2011) 036004, [arXiv:1008.1593].

[35] N. Cabibbo, *Unitary Symmetry and Leptonic Decays*, *Phys. Rev. Lett.* **10** (1963) 531–533.

[36] M. Kobayashi and T. Maskawa, *CP Violation in the Renormalizable Theory of Weak Interaction*, *Prog. Theor. Phys.* **49** (1973) 652–657.

[37] **D0** Collaboration, V. M. Abazov *et. al.*, *Evidence for an anomalous like-sign dimuon charge asymmetry*, *Phys. Rev.* **D82** (2010) 032001, [arXiv:1005.2757].

[38] **D0** Collaboration, V. M. Abazov *et. al.*, *Evidence for an anomalous like-sign dimuon charge asymmetry*, *Phys. Rev. Lett.* **105** (2010) 081801, [arXiv:1007.0395].

[39] A. Lenz and U. Nierste, *Theoretical update of $B_s - \bar{B}_s$ mixing*, *JHEP* **06** (2007) 072, [hep-ph/0612167].

[40] A. Lenz and U. Nierste, *Numerical Updates of Lifetimes and Mixing Parameters of B Mesons*, [arXiv:1102.4274].

[41] **ALEPH Collaboration, DELPHI Collaboration, L3 Collaboration, OPAL Collaboration, SLD Collaboration, LEP Electroweak Working Group, SLD Electroweak Group, SLD Heavy Flavour Group** Collaboration, *Precision electroweak measurements on the Z resonance*, *Phys.Rept.* **427** (2006) 257–454, [hep-ex/0509008].

[42] **ATLAS Collaboration** Collaboration, G. Aad *et. al.*, *Observation of a new particle in the search for the Standard Model Higgs boson with the ATLAS detector at the LHC*, *Phys.Lett.* **B716** (2012) 1–29, [arXiv:1207.7214].

[43] **CMS Collaboration** Collaboration, S. Chatrchyan *et. al.*, *Observation of a new boson at a mass of 125 GeV with the CMS experiment at the LHC*, *Phys.Lett.* **B716** (2012) 30–61, [arXiv:1207.7235].

[44] G. D. Kribs, T. Plehn, M. Spannowsky, and T. M. P. Tait, *Four generations and Higgs physics*, *Phys. Rev.* **D76** (2007) 075016, [arXiv:0706.3718].

[45] V. A. Novikov, A. N. Rozanov, and M. I. Vysotsky, *Once more on extra quark-lepton generations and precision measurements*, *Phys. Atom. Nucl.* **73** (2010) 636–642, [arXiv:0904.4570].

[46] V. A. Novikov, L. B. Okun, A. N. Rozanov, and M. I. Vysotsky, *Mass of the Higgs versus fourth generation masses*, *JETP Lett.* **76** (2002) 127–130, [hep-ph/0203132].

[47] J. M. Frere, A. N. Rozanov, and M. I. Vysotsky, *Mass and decays of Brout-Englert-Higgs scalar with extra generations*, *Phys. Atom. Nucl.* **69** (2006) 355–359, [hep-ph/0412080].

[48] M. Hashimoto, *Constraints on Mass Spectrum of Fourth Generation Fermions and Higgs Bosons*, *Phys. Rev.* **D81** (2010) 075023, [arXiv:1001.4335].

[49] O. Eberhardt, A. Lenz, A. Menzel, U. Nierste, and M. Wiebusch, *Status of the fourth fermion generation before ICHEP2012: Higgs data and electroweak precision observables*, arXiv:1207.0438.

[50] S. Bar-Shalom, M. Geller, S. Nandi, and A. Soni, *Two Higgs doublets, a 4th generation and a 125 GeV Higgs*, [arXiv:1208.3195].

[51] B. Holdom, *Heavy quarks and electroweak symmetry breaking*, *Phys.Rev.Lett.* **57** (1986) 2496.

[52] C. T. Hill, M. A. Luty, and E. A. Paschos, *Electroweak symmetry breaking by fourth generation condensates and the neutrino spectrum*, *Phys.Rev.* **D43** (1991) 3011–3025.

[53] M. Hashimoto and V. Miransky, *Dynamics of Mass Quark Hierarchy*, *Phys.Rev.* **D80** (2009) 013004, [arXiv:0901.4354].

[54] M. Hashimoto and V. A. Miransky, *Dynamical electroweak symmetry breaking with superheavy quarks and 2+1 composite Higgs model*, *Phys. Rev.* **D81** (2010) 055014, [arXiv:0912.4453].

[55] J. F. Gunion and H. E. Haber, *The CP conserving two Higgs doublet model: The Approach to the decoupling limit*, *Phys.Rev.* **D67** (2003) 075019, [hep-ph/0207010].

[56] P. Q. Hung and C. Xiong, *Renormalization Group Fixed Point with a Fourth Generation: Higgs-induced Bound States and Condensates*, *Nucl. Phys.* **B847** (2011) 160, [arXiv:0911.3890].

[57] P. Q. Hung and C. Xiong, *Implication of a Quasi Fixed Point with a Heavy Fourth Generation: The emergence of a TeV-scale physical cutoff*, *Phys. Lett.* **B694** (2011) 430–434, [arXiv:0911.3892].

[58] P. Q. Hung and G. Isidori, *Anatomy of the Higgs mass spectrum*, *Phys. Lett.* **B402** (1997) 122–129, [hep-ph/9609518].

[59] B. Holdom, *The discovery of the fourth family at the LHC: What if?*, *JHEP* **08** (2006) 076, [hep-ph/0606146].

[60] G. Burdman, L. Da Rold, O. Eboli, and R. D. Matheus, *A Strongly Coupled Fourth Generation at the LHC*, *Phys. Rev.* **D79** (2009) 075026, [arXiv:0812.0368].

[61] O. Antipin, M. Heikinheimo, and K. Tuominen, *The Next Generation*, *JHEP* **07** (2010) 052, [arXiv:1002.1872].

[62] D. Delepine, M. Napsuciale, and C. A. Vaquera-Araujo, *Dynamical symmetry breaking with a fourth generation*, *Phys. Rev.* **D84** (2011) 033008, [arXiv:1003.3267].

[63] Y. A. Simonov, *Coherent mixing in three and four quark generations*, [arXiv:1004.2672].

[64] H. S. Fukano and K. Tuominen, *Topcolor-like dynamics and new matter generations*, [arXiv:1102.1254].

[65] P. Q. Hung and C. Xiong, *Dynamical Electroweak Symmetry Breaking with a Heavy Fourth Generation*, [arXiv:1012.4479].

[66] B. Holdom, *Negative T?*, *Phys. Rev.* **D54** (1996) 721–724, [hep-ph/9602248].

[67] M. Maltoni, V. A. Novikov, L. B. Okun, A. N. Rozanov, and M. I. Vysotsky, *Extra quark-lepton generations and precision measurements*, *Phys. Lett.* **B476** (2000) 107–115, [hep-ph/9911535].

[68] H.-J. He, N. Polonsky, and S.-f. Su, *Extra families, Higgs spectrum and oblique corrections*, *Phys. Rev.* **D64** (2001) 053004, [hep-ph/0102144].

[69] V. A. Novikov, L. B. Okun, A. N. Rozanov, and M. I. Vysotsky, *Extra generations and discrepancies of electroweak precision data*, *Phys. Lett.* **B529** (2002) 111–116, [hep-ph/0111028].

[70] J. Erler and P. Langacker, *Precision Constraints on Extra Fermion Generations*, *Phys. Rev. Lett.* **105** (2010) 031801, [arXiv:1003.3211].

[71] O. Eberhardt, A. Lenz, and J. Rohrwild, *Less space for a new family of fermions*, *Phys. Rev.* **D82** (2010) 095006, [arXiv:1005.3505].

[72] M. S. Chanowitz, *Higgs Mass Constraints on a Fourth Family: Upper and Lower Limits on CKM Mixing*, *Phys. Rev.* **D82** (2010) 035018, [arXiv:1007.0043].

[73] M. Bobrowski, A. Lenz, J. Riedl, and J. Rohrwild, *How much space is left for a new family of fermions?*, *Phys. Rev.* **D79** (2009) 113006, [arXiv:0902.4883].

[74] A. Soni, A. K. Alok, A. Giri, R. Mohanta, and S. Nandi, *SM with four generations: Selected implications for rare B and K decays*, *Phys. Rev.* **D82** (2010) 033009, [arXiv:1002.0595].

[75] A. J. Buras *et. al.*, *Patterns of Flavour Violation in the Presence of a Fourth Generation of Quarks and Leptons*, *JHEP* **09** (2010) 106, [arXiv:1002.2126].

[76] W.-S. Hou and C.-Y. Ma, *Flavor and CP Violation with Fourth Generations Revisited*, *Phys. Rev.* **D82** (2010) 036002, [arXiv:1004.2186].

[77] S. Nandi and A. Soni, *Constraining the mixing matrix for Standard Model with four generations: time dependent and semi-leptonic CP asymmetries in B^0_d, B_s and D^0*, [arXiv:1011.6091].

[78] A. K. Alok, A. Dighe, and D. London, *Constraints on the Four-Generation Quark Mixing Matrix from a Fit to Flavor-Physics Data*, [arXiv:1011.2634].

[79] M. E. Peskin and T. Takeuchi, *A New constraint on a strongly interacting Higgs sector*, *Phys. Rev. Lett.* **65** (1990) 964–967.

[80] M. E. Peskin and T. Takeuchi, *Estimation of oblique electroweak corrections*, *Phys. Rev.* **D46** (1992) 381–409.

[81] L. Bellantoni, J. Erler, J. J. Heckman, and E. Ramirez-Homs, *Masses of a Fourth Generation with Two Higgs Doublets*, *Phys.Rev.* **D86** (2012) 034022, [arXiv:1205.5580].

[82] W.-S. Hou, *CP Violation and Baryogenesis from New Heavy Quarks*, *Chin. J. Phys.* **47** (2009) 134, [arXiv:0803.1234].

[83] W.-S. Hou, Y.-Y. Mao, and C.-H. Shen, *Leading Effect of CP Violation with Four Generations*, *Phys. Rev.* **D82** (2010) 036005, [arXiv:1003.4361].

[84] M. S. Carena, A. Megevand, M. Quiros, and C. E. M. Wagner, *Electroweak baryogenesis and new TeV fermions*, *Nucl. Phys.* **B716** (2005) 319–351, [hep-ph/0410352].

[85] R. Fok and G. D. Kribs, *Four Generations, the Electroweak Phase Transition, and Supersymmetry*, *Phys. Rev.* **D78** (2008) 075023, [arXiv:0803.4207].

[86] Y. Kikukawa, M. Kohda, and J. Yasuda, *The strongly coupled fourth family and a first-order electroweak phase transition (I) quark sector*, *Prog. Theor. Phys.* **122** (2009) 401–426, [arXiv:0901.1962].

[87] P. Q. Hung, *Minimal SU(5) resuscitated by long-lived quarks and leptons*, *Phys. Rev. Lett.* **80** (1998) 3000–3003, [hep-ph/9712338].

[88] L. M. Carpenter, *Fourth Generation Lepton Sectors with Stable Majorana Neutrinos: From LEP to LHC*, [arXiv:1010.5502].

[89] A. J. Buras, B. Duling, T. Feldmann, T. Heidsieck, and C. Promberger, *Lepton Flavour Violation in the Presence of a Fourth Generation of Quarks and Leptons*, *JHEP* **09** (2010) 104, [arXiv:1006.5356].

[90] G. Burdman, L. Da Rold, and R. D. Matheus, *The Lepton Sector of a Fourth Generation*, *Phys. Rev.* **D82** (2010) 055015, [arXiv:0912.5219].

[91] M. Blennow, E. Fernandez-Martinez, J. Lopez-Pavon, and J. Menendez, *Neutrinoless double beta decay in seesaw models*, *JHEP* **1007** (2010) 096, [arXiv:1005.3240].

[92] S. Antusch, J. P. Baumann, and E. Fernandez-Martinez, *Non-Standard Neutrino Interactions with Matter from Physics Beyond the Standard Model*, *Nucl. Phys.* **B810** (2009) 369–388, [arXiv:0807.1003].

[93] S. Antusch, C. Biggio, E. Fernandez-Martinez, M. B. Gavela, and J. Lopez-Pavon, *Unitarity of the Leptonic Mixing Matrix*, *JHEP* **10** (2006) 084, [hep-ph/0607020].

[94] M. T. Frandsen, I. Masina, and F. Sannino, *Fourth Lepton Family is Natural in Technicolor*, *Phys. Rev.* **D81** (2010) 035010, [arXiv:0905.1331].

[95] S. K. Garg and S. K. Vempati, *Bounds on fourth generation induced double insertions in Supersymmetry*, [arXiv:1103.1011].

[96] A. Aparici, J. Herrero-Garcia, N. Rius, and A. Santamaria, *Neutrino masses from new generations*, *JHEP* **1107** (2011) 122, [arXiv:1104.4068].

[97] A. Aparici, J. Herrero-Garcia, N. Rius, and A. Santamaria, *On the nature of the fourth generation neutrino and its implications*, *JHEP* **1207** (2012) 030, [arXiv:1204.1021].

[98] **Particle Data Group** Collaboration, J. Beringer *et. al.*, *Review of Particle Physics (RPP)*, *Phys.Rev.* **D86** (2012) 010001.

[99] S. T. Petcov and S. T. Toshev, *Conservation od lepton charges, massive Majorana and massless neutrinos*, *Phys. Lett.* **B143** (1984) 175.

[100] K. S. Babu and E. Ma, *Natural hierarchy pf radiatively induced Majorana neutrino masses*, *Phys. Rev. Lett.* **61** (1988) 674.

[101] M. A. Schmidt and A. Y. Smirnov, *Neutrino Masses and a Fourth Generation of Fermions*, *Nucl.Phys.* **B857** (2012) 1–27, [arXiv:1110.0874].

[102] H. Lacker and A. Menzel, *Simultaneous Extraction of the Fermi constant and PMNS matrix elements in the presence of a fourth generation*, *JHEP* **1007** (2010) 006, [arXiv:1003.4532].

[103] A. Menzel *et. al.*, *Simultaneously extracting g_f and constraining the pmns matrix in sm4*, Presented at the "Flavor and the Fourth Family" workshop, Durham, UK, 2011.

[104] A. Lenz, H. Päs, and D. Schalla, *Fourth Generation Majorana Neutrinos*, *Phys. Rev. D 85,* **075025** (2012) [arXiv:1104.2465].

[105] A. Lenz, H. Päs, and D. Schalla, *Constraints on fourth generation Majorana neutrinos*, *J. Phys. Conf. Ser.* **259** (2010) 012096, [arXiv:1010.3883].

[106] **EXO-200 Collaboration** Collaboration, N. Ackerman *et. al.*, *Observation of Two-Neutrino Double-Beta Decay in ^{136}Xe with EXO-200*, *Phys.Rev.Lett.* **107** (2011) 212501, [arXiv:1108.4193].

[107] F. Simkovic, A. Faessler, V. Rodin, P. Vogel, and J. Engel, *Anatomy of nuclear matrix elements for neutrinoless double-beta decay*, *Phys.Rev.* **C77** (2008) 045503, [arXiv:0710.2055].

[108] F. Simkovic, R. Hodak, A. Faessler, and P. Vogel, *Relation between the $0\nu\beta\beta$ and $2\nu\beta\beta$ nuclear matrix elements revisited*, *Phys.Rev.* **C83** (2011) 015502, [arXiv:1012.0512].

[109] J. Schechter and J. Valle, *Neutrinoless Double beta Decay in $SU(2) \times U(1)$ Theories*, *Phys.Rev.* **D25** (1982) 2951.

[110] **IGEX** Collaboration, C. E. Aalseth *et. al.*, *The Igex ^{7}6Ge Neutrinoless Double-Beta Decay Experiment: Prospects for Next Generation Experiments*, *Phys. Rev.* **D65** (2002) 092007, [hep-ex/0202026].

[111] R. Mohapatra and P. Pal, *Massive neutrinos in physics and astrophysics. Second edition*, *World Sci.Lect.Notes Phys.* **60** (1998) 1–397.

[112] M. Hirsch, H. V. Klapdor-Kleingrothaus, and O. Panella, *Double beta decay in left-right symmetric models*, *Phys. Lett.* **B374** (1996) 7–12, [hep-ph/9602306].

[113] M. Hirsch and H. V. Klapdor-Kleingrothaus, *Constraints on left-right symmetric models from neutrinoless double beta decay*, . Prepared for International Workshop on Neutrinoless Double Beta Decay and Related Topics, Trento, Italy, 24 Apr - 5 May 1995.

[114] K. Muto and H. V. Klapdor, *double beta decay, neutrino mass and nuclear structure*, . IN *KLAPDOR, H.V. (ED.): NEUTRINOS* 183-237.

[115] K. Zuber, *MeV neutrinos in double beta decay*, *Phys.Rev.* **D56** (1997) 1816–1819, [hep-ph/9605405]. 7 pages, 6 uudecoded EPS-figures.

[116] **WMAP** Collaboration, D. N. Spergel *et. al.*, *Wilkinson Microwave Anisotropy Probe (WMAP) three year results: Implications for cosmology*, *Astrophys. J. Suppl.* **170** (2007) 377, [astro-ph/0603449].

[117] M. Gonzalez-Garcia, M. Maltoni, and J. Salvado, *Updated global fit to three neutrino mixing: status of the hints of $\theta_{13} > 0$*, *JHEP* **1004** (2010) 056, [arXiv:1001.4524].

[118] L. Wolfenstein, *Different Varieties of Massive Dirac Neutrinos*, *Nucl.Phys.* **B186** (1981) 147.

[119] S. Petcov, *On Pseudodirac Neutrinos, Neutrino Oscillations and Neutrinoless Double beta Decay*, *Phys.Lett.* **B110** (1982) 245–249.

[120] T. Tomoda, *Double beta decay*, *Rept.Prog.Phys.* **54** (1991) 53–126.

[121] P. Minkowski, *$\mu \to e\gamma$ at a Rate of One Out of 10^9 Muon Decays?*, *Phys.Lett.* **B67** (1977) 421.

[122] M. Gell-Mann, P. Ramond, and R. Slansky, *Complex spinors and unified theories*, *Conf.Proc.* **C790927** (1979) 315–321. To be published in Supergravity, P. van Nieuwenhuizen & D.Z. Freedman (eds.), North Holland Publ. Co., 1979.

[123] T. Yanagida, *Horizontal Symmetry and Masses of Neutrinos*, *Conf.Proc.* **C7902131** (1979) 95.

[124] R. N. Mohapatra and G. Senjanovic, *Neutrino Mass and Spontaneous Parity Violation*, *Phys.Rev.Lett.* **44** (1980) 912.

[125] A. Ali, A. V. Borisov, and N. B. Zamorin, *Majorana neutrinos and same-sign dilepton production at LHC and in rare meson decays*, *Eur. Phys. J.* **C21** (2001) 123–132, [hep-ph/0104123].

[126] G. Belanger, F. Boudjema, D. London, and H. Nadeau, *Inverse neutrinoless double beta decay revisited*, *Phys. Rev.* **D53** (1996) 6292–6301, [hep-ph/9508317].

[127] A. D. Martin, W. J. Stirlin, R. S. Thorne, and G. Watt, *Parton distributions for the LHC*, *Eur. Phys. J.* **C63** (2009) 189–285, [arXiv:0901.0002].

[128] **MEG collaboration** Collaboration, J. Adam *et. al.*, *New limit on the lepton-flavour violating decay $\mu^+ \to e^+\gamma$*, *Phys.Rev.Lett.* **107** (2011) 171801, [arXiv:1107.5547]. 5 pages, 2 figures, accepted for publication at Phys. Rev. Lett.

[129] **BABAR** Collaboration, B. Aubert *et. al.*, *Searches for Lepton Flavor Violation in the Decays $\tau^\pm \to e^\pm\gamma$ and $\tau^\pm \to \mu^\pm\gamma$*, *Phys. Rev. Lett.* **104** (2010) 021802, [arXiv:0908.2381].

[130] T. P. Cheng and L.-F. Li, $\mu \to e\gamma$ *in theories with Dirac and Majorana neutrino mass terms*, *Phys. Rev. Lett.* **45** (1980) 1908.

[131] N. Arkani-Hamed and S. Dimopoulos, *New origin for approximate symmetries from distant breaking in extra dimensions*, *Phys. Rev.* **D65** (2002) 052003, [hep-ph/9811353].

[132] W.-S. Hou and F.-F. Lee, *An Updated Numerical Analysis of eV Seesaw with Four Generations*, *Int.J.Mod.Phys.* **A25** (2010) 5913–5922, [arXiv:1004.2359].

[133] J. Barry, W. Rodejohann, and H. Zhang, *Light Sterile Neutrinos: Models and Phenomenology*, *JHEP* **1107** (2011) 091, [arXiv:1105.3911].

[134] P. de Holanda and A. Smirnov, *Solar neutrino spectrum, sterile neutrinos and additional radiation in the Universe*, *Phys.Rev.* **D83** (2011) 113011, [arXiv:1012.5627].

[135] J. Kopp, M. Maltoni, and T. Schwetz, *Are there sterile neutrinos at the eV scale?*, *Phys.Rev.Lett.* **107** (2011) 091801, [arXiv:1103.4570].

[136] W.-Y. Keung and P. Schwaller, *Long Lived Fourth Generation and the Higgs*, *JHEP* **1106** (2011) 054, [arXiv:1103.3765].

[137] T. Asaka, S. Blanchet, and M. Shaposhnikov, *The nuMSM, dark matter and neutrino masses*, *Phys.Lett.* **B631** (2005) 151–156, [hep-ph/0503065].

[138] A. Kusenko, *Sterile neutrinos, dark matter, and the pulsar velocities in models with a Higgs singlet*, *Phys.Rev.Lett.* **97** (2006) 241301, [hep-ph/0609081].

[139] S. Hollenberg, H. Päs, and D. Schalla, *Baryon asymmetry of the universe and new neutrino states*, [arXiv:1110.0948].

[140] M. Fukugita and T. Yanagida, *Baryogenesis Without Grand Unification*, *Phys.Lett.* **B174** (1986) 45.

[141] **WMAP Collaboration** Collaboration, E. Komatsu *et. al.*, *Seven-Year Wilkinson Microwave Anisotropy Probe (WMAP) Observations: Cosmological Interpretation*, *Astrophys.J.Suppl.* **192** (2011) 18, [arXiv:1001.4538].

[142] S. Davidson, E. Nardi, and Y. Nir, *Leptogenesis*, *Phys.Rept.* **466** (2008) 105–177, [arXiv:0802.2962].

[143] A. Sakharov, *Violation of CP Invariance, c Asymmetry, and Baryon Asymmetry of the Universe*, *Pisma Zh.Eksp.Teor.Fiz.* **5** (1967) 32–35.

[144] V. Kuzmin, V. Rubakov, and M. Shaposhnikov, *On the Anomalous Electroweak Baryon Number Nonconservation in the Early Universe*, *Phys.Lett.* **B155** (1985) 36.

[145] S. Blanchet, T. Hambye, and F.-X. Josse-Michaux, *Reconciling leptogenesis with observable $\mu \to e\gamma$ rates*, *JHEP* **1004** (2010) 023, [arXiv:0912.3153].

[146] H. Murayama, V. Rentala, J. Shu, and T. T. Yanagida, *Saving fourth generation and baryon number by living long*, *Phys. Lett.* **B705** (2011) 208–2011, [arXiv:1012.0338].

[147] M. Fukugita and T. Yanagida, *Sphaleron induced baryon number nonconservation and a constraint on Majorana neutrino masses*, *Phys. Rev.* **D42** (1990) 1285–1286.

[148] H. Klapdor-Kleingrothaus, S. Kolb, and V. Kuzmin, *Light lepton number violating sneutrinos and the baryon number of the universe*, *Phys.Rev.* **D62** (2000) 035014, [hep-ph/9909546].

[149] H. V. Klapdor-Kleingrothaus, S. Kolb, and U. Sarkar, *Neutrino Majorana mass and baryon number of the universe below the electroweak symmetry breaking scale*, *Phys. Lett.* **B487** (2000) 289–293, [hep-ph/0005268].

[150] E. W. Kolb and M. S. Turner, *The Early universe*, *Front. Phys.* **69** (1990) 1–547.

[151] G. Giudice, A. Notari, M. Raidal, A. Riotto, and A. Strumia, *Towards a complete theory of thermal leptogenesis in the SM and MSSM*, *Nucl.Phys.* **B685** (2004) 89–149, [hep-ph/0310123].

[152] J. G. Morfin, J. Nieves, and J. T. Sobczyk, *Recent Developments in Neutrino/Antineutrino - Nucleus Interactions*, [arXiv:1209.6586].

[153] E. Paschos and D. Schalla, *Neutrino production of hadrons at low energy and in the small Q^2 region*, *Phys.Rev.* **D84** (2011) 013004, [arXiv:1102.4466].

[154] E. Paschos and D. Schalla, *Pion production by neutrinos in the delta resonance region and possible application to CP searches*, [arXiv:1209.4219].

[155] E. Paschos and D. Schalla, *Neutrino-induced pion production at low energies and in the small Q^2 region*, [arXiv:1212.4662].

[156] P. Lipari, *Neutrino oscillation studies and the neutrino cross-section*, *Nucl.Phys.Proc.Suppl.* **112** (2002) 274–287, [hep-ph/0207172].

[157] O. Lalakulich and E. A. Paschos, *Resonance production by neutrinos. I: J = 3/2 resonances*, *Phys. Rev.* **D71** (2005) 074003, [hep-ph/0501109].

[158] P. A. Schreiner and F. Von Hippel, *Neutrino production of the Delta (1236)*, *Nucl. Phys.* **B58** (1973) 333–362.

[159] O. Lalakulich, E. A. Paschos, and G. Piranishvili, *Resonance production by neutrinos: The second resonance region*, *Phys. Rev.* **D74** (2006) 014009, [hep-ph/0602210].

[160] M. Goldberger and S. Treiman, *Decay of the pi meson*, *Phys.Rev.* **110** (1958) 1178–1184.

[161] E. A. Paschos, J.-Y. Yu, and M. Sakuda, *Neutrino production of resonances*, *Phys. Rev.* **D69** (2004) 014013, [hep-ph/0308130].

[162] E. Hernandez, J. Nieves, and M. Valverde, *Weak pion production off the nucleon*, *Phys. Rev.* **D76** (2007) 033005, [hep-ph/0701149].

[163] O. Lalakulich, T. Leitner, O. Buss, and U. Mosel, *One pion production in neutrino reactions: including non- resonant background*, *Phys. Rev.* **D82** (2010) 093001, [arXiv:1007.0925].

[164] K. Furuno *et. al.*, *BNL 7-foot bubble chamber experiment: Neutrino deuterium interactions*, . Prepared for 2nd International Workshop on Neutrino - Nucleus Interactions in the Few GeV Region (NUINT 02), Irvine, California, 12-15 Dec 2002.

[165] G. J. Gounaris, A. Kartavtsev, and E. A. Paschos, *Coherent pion production by neutrinos on nuclei*, *Phys. Rev.* **D74** (2006) 054007, [hep-ph/0512139].

[166] E. A. Paschos and D. Schalla, *Coherent Pion Production*, *Phys. Rev.* **D80** (2009) 033005, [arXiv:0903.0451].

[167] J. Ballam *et. al.*, *Production and decay of A_1 and A_2 resonances in 16-GeV/c $\pi - p$ interactions*, *Phys. Rev. Lett.* **21** (1968) 934–937.

[168] M. Gell-Mann and M. Levy, *The axial vector current in beta decay*, *Nuovo Cim.* **16** (1960) 705.

[169] M. Scadron, *Current Algebra, PCAC and the Quark Model*, *Rept.Prog.Phys.* **44** (1981) 213–292.

[170] **Particle Data Group** Collaboration, K. Nakamura *et. al.*, *Review of particle physics*, *J. Phys.* **G37** (2010) 075021, sec. 41, p. 14.

[171] **Crystal Ball Collaboration** Collaboration, M. Sadler *et. al.*, *Differential cross-section of the charge exchange reaction $\pi^- p \to \pi^0 n$ in the momentum range from 148 to 323-MeV/c*, *Phys.Rev.* **C69** (2004) 055206, [nucl-ex/0403040].

[172] S. L. Adler, *Sum rules giving tests of local current commutation relations in high-energy neutrino reactions*, *Phys. Rev.* **143** (1966) 1144–1155.

[173] S. L. Adler, *Adler sum rule*, [arXiv:0905.2923].

[174] W. I. Weisberger, *Unsubtracted Dispersion Relations and the Renormalization of the Weak Axial Vector Coupling Constants*, *Phys. Rev.* **143** (1966) 1302–1309.

[175] A. Bodek and U.-k. Yang, *Axial and Vector Structure Functions for Electron- and Neutrino- Nucleon Scattering Cross Sections at all Q^2 using Effective Leading order Parton Distribution Functions*, [arXiv:1011.6592].

[176] A. Bodek and U. Yang. (private communications).

[177] R. A. Arndt, I. I. Strakovsky, R. L. Workman, and M. M. Pavan, *Updated analysis of pi N elastic scattering data to 2.1-GeV: The Baryon spectrum*, *Phys.Rev.* **C52** (1995) 2120–2130, [nucl-th/9505040].

[178] T. Leitner, O. Buss, L. Alvarez-Ruso, and U. Mosel, *Electron- and neutrino-nucleus scattering from the quasielastic to the resonance region*, *Phys. Rev.* **C79** (2009) 034601, [arXiv:0812.0587].

[179] K. M. Graczyk, D. Kielczewska, P. Przewlocki, and J. T. Sobczyk, *C_5^A axial form factor from bubble chamber experiments*, *Phys. Rev.* **D80** (2009) 093001, [arXiv:0908.2175].

[180] E. Hernandez, J. Nieves, M. Valverde, and M. J. Vicente Vacas, *$N - \Delta(1232)$ axial form factors from weak pion production*, *Phys. Rev.* **D81** (2010) 085046, [arXiv:1001.4416].

[181] L. Alvarez-Ruso, S. K. Singh, and M. J. Vicente Vacas, *$\nu d \to \mu^- \Delta^{++} n$ reaction and axial vector $N - \Delta$ coupling*, *Phys. Rev.* **C59** (1999) 3386–3392, [nucl-th/9804007].

[182] M. Sajjad Athar, S. Chauhan, and S. K. Singh, *$CC1\pi^+$ to CCQE cross sections ratio at accelerator energies*, *J. Phys.* **G37** (2010) 015005, [arXiv:0908.1442].

[183] G. M. Radecky *et. al.*, *Study of single pion production by weak charged currents including low-energy νd interactions*, *Phys. Rev.* **D25** (1982) 1161–1173.

[184] T. Kitagaki *et. al.*, *Charged current exclusive pion production including neutrino deuterium interactions*, *Phys. Rev.* **D34** (1986) 2554–2565.

[185] S. Galster *et. al.*, *Coincidence experiment on inelastic electron-proton scattering in the region of the* $\Delta(1236)$ *at* $q^2 = -0.35$ *and* -1.0 *(GeV/c)*^{2}, *Phys. Rev.* **D5** (1972) 519–527.

[186] W. Bartel *et. al.*, *Electroproduction of pions near the* $\Delta(1236)$ *isobar and the form-factor of* $G_M^*(q^2)$ *of the* $(\gamma N\Delta)$ *vertex*, *Phys. Lett.* **B28** (1968) 148–151.

[187] J. Bell *et. al.*, *Study of the Reactions* $\nu p \to \mu^- \Delta^{++}$ *at High Energies and Comparisons with Theory*, *Phys. Rev. Lett.* **41** (1978) 1012.

[188] S. Gasiorowicz, *Elementary particle physics*. John Wiley & Sons, Inc., 1966.

[189] **MiniBooNE Collaboration** Collaboration, A. Aguilar-Arevalo *et. al.*, *Measurement of Neutrino-Induced Charged-Current Charged Pion Production Cross Sections on Mineral Oil at* $E_\nu \sim 1$ *GeV*, *Phys.Rev.* **D83** (2011) 052007, [arXiv:1011.3572].

[190] **MiniBooNE Collaboration** Collaboration, A. Aguilar-Arevalo *et. al.*, *Measurement of* ν_μ*-induced charged-current neutral pion production cross sections on mineral oil at* $E_\nu \in 0.5 - 2.0$ *GeV*, *Phys.Rev.* **D83** (2011) 052009, [arXiv:1010.3264].

[191] S. L. Adler, S. Nussinov, and E. Paschos, *Nuclear charge exchange corrections to leptonic pion production in the (3,3) resonance region*, *Phys.Rev.* **D9** (1974) 2125–2143.

[192] E. Fermi *Ric. Sci.* **7** (1936) 13.

[193] E. Amaldi, *Handbuch der Physik*, vol. 38 no. 2, section 122, p. 557, Springer-Verlag, Berlin, 1959, edited by S. Flügge.

[194] E. Paschos, I. Schienbein, and J. Yu, *Pion rescattering in nuclei*, *Nucl.Phys.Proc.Suppl.* **139** (2005) 119–124, [hep-ph/0408148].

[195] O. Buss, T. Gaitanos, K. Gallmeister, H. van Hees, M. Kaskulov, *et. al.*, *Transport-theoretical Description of Nuclear Reactions*, *Phys.Rept.* **512** (2012) 1–124, [arXiv:1106.1344].

[196] O. Lalakulich, K. Gallmeister, and U. Mosel, *Neutrino Nucleus Reactions within the GiBUU Model*, [arXiv:1110.0674].

[197] O. Lalakulich, K. Gallmeister, T. Leitner, and U. Mosel, *Pion production in the MiniBooNE*, *AIP Conf.Proc.* **1405** (2011) 127–133, [arXiv:1107.5947].

[198] O. Lalakulich and U. Mosel, *Pion production in the MiniBooNE experiment*, [arXiv:1210.4717].

[199] U. Mosel and O. Lalakulich, *Neutrino-nucleus interactions*, [arXiv:1211.1977].

[200] M. Fukugita and T. Yanagida, *Physics of neutrinos and applications to astrophysics*, .

[201] H. Nunokawa, S. J. Parke, and J. W. Valle, *CP Violation and Neutrino Oscillations*, *Prog.Part.Nucl.Phys.* **60** (2008) 338–402, [arXiv:0710.0554].

[202] M. Gonzalez-Garcia, M. Maltoni, J. Salvado, and T. Schwetz, *Global fit to three neutrino mixing: critical look at present precision*, [arXiv:1209.3023].

[203] V. D. Barger, K. Whisnant, and R. Phillips, *CP Violation in Three Neutrino Oscillations*, *Phys.Rev.Lett.* **45** (1980) 2084.

Acronyms

$0\nu\beta\beta$	neutrinoless double beta decay
$2\nu\beta\beta$	two neutrino double beta decay
4G	four generation
ANL	Argonne National Laboratory
ANP	Adler-Nussinov-Paschos
ATLAS	A Toroidal LHC Apparatus
BAU	baryon asymmetry of the Universe
BNL	Brookhaven National Laboratory
BSM	beyond the standard model
CC	charged current
CC1π	charged current single pion production
CCQE	charged current quasi-elastic scattering
CGC	Clebsch-Gordan-Coefficient
CKM	Cabibbo-Kobayashi-Maskawa
cm	center of mass
CMS	Compact Muon Solenoid
CP	charge and parity
CVC	conserved vector current
D0	Experiment located at Tevatron section D0
Daya Bay	Daya Bay Reactor Neutrino Experiment
DIS	deep inelastic scattering
DONUT	Direct Observation of the NU Tau
DSB	dynamical symmetry breaking
EWPT	electroweak phase transition
EWSB	electroweak symmetry breaking
EXO	Enriched Xenon Observatory
FCNC	flavor changing neutral current
FNAL	Fermi National Accelerator Laboratory
GERDA	GERmanium Detector Array
GUT	grand unified theory
HE	high energy
IGEX	International Germanium Experiment
K2K	KEK to Kamioka
KamLAND	Kamioka Liquid Scintillator Antineutrino Detector

KATRIN	Karlsruhe Tritium Neutrino Experiment
lab	laboratory
LEP	Large Electron-Positron collider
LHC	Large Hadron Collider
LNV	lepton number violation
LSD	like-sign dilepton production
LSND	Liquid Scintillator Neutrino Detector
LSS	large scale structure
MINERνA	Main Injector Experiment for ν-A
MiniBooNE	Booster Neutrino Experiment
MINOS	Main Injector Neutrino Oscillation Search
MSTW	Martin-Stirling-Thorne-Watt
NC	neutral current
NEMO	Neutrino Ettore Majorana Observatory
NME	nuclear matrix elements
NOνA	NuMI Off-Axis ν_e Appearance
OPERA	Oscillation Project with Emulsion-tRacking Apparatus
PCAC	Partially Conserved Axialvector Current
PDG	particle data group
PMNS	Pontecorvo-Maki-Nakagawa-Sakata
QE	quasi elastic
RENO	Reactor Experiment for Neutrino Oscillation
RES	resonance procution
SciBooNE	Scintillator Bar Booster Neutrino Experiment
SLC	Stanford Linear Accelerator
SM	standard model
SM3	standard model with three generations
SM4	standard model with four generations
SNO	Sudbury Neutrino Observatory
Super-K	Super-Kamiokande
T2K	Tokai to Kamioka